

MINISTRY OF EDUCATION AND TRAINING
HCM CITY UNIVERSITY OF TECHNOLOGY AND EDUCATION

HO NHAT LINH

**DEVELOPMENT AND OPTIMIZATION OF GRIPPERS
FOR CYLINDER SAMPLES USING COMPLIANT
MECHANISMS**

PH.D. DISSERTATION

MAJOR: MECHANICAL ENGINEERING

CODE: 9520103

Ho Chi Minh City, July 2023

MINISTRY OF EDUCATION AND TRAINING
HCM CITY UNIVERSITY OF TECHNOLOGY AND EDUCATION

HO NHAT LINH

**DEVELOPMENT AND OPTIMIZATION OF GRIPPERS
FOR CYLINDER SAMPLES USING COMPLIANT
MECHANISMS**

PH.D. DISSERTATION

MAJOR: MECHANICAL ENGINEERING

CODE: 9520103

Supervisor 1: Assoc. Prof. Dr. Le Hieu Giang

Supervisor 2: Dr. Dao Thanh Phong

Reviewer 1:

Reviewer 2:

Reviewer 3:

Ho Chi Minh City, July 2023

QUYẾT ĐỊNH

Về việc đổi tên luận án cho nghiên cứu sinh khóa 2016

HIỆU TRƯỞNG TRƯỜNG ĐẠI HỌC SƯ PHẠM KỸ THUẬT TP. HỒ CHÍ MINH

Căn cứ Quyết định số 426/TTg ngày 27 tháng 10 năm 1976 của Thủ tướng Chính phủ về một số vấn đề cấp bách trong mạng lưới các trường đại học và Quyết định số 118/2000/QĐ-TTg ngày 10 tháng 10 năm 2000 của Thủ tướng Chính phủ về việc tổ chức lại Đại học Quốc gia Thành Phố Hồ Chí Minh, tách Trường Đại học Sư phạm Kỹ thuật Thành phố Hồ Chí Minh trực thuộc Bộ Giáo dục và Đào tạo;

Căn cứ Quyết định số 70/2014/QĐ-TTg ngày 10 tháng 12 năm 2014 của Thủ tướng Chính phủ về việc ban hành Điều lệ trường Đại học;

Căn cứ Quyết định số 937/QĐ-TTg ngày 30 tháng 6 năm 2017 về việc phê duyệt đề án thí điểm đổi mới cơ chế hoạt động của Trường Đại học Sư phạm Kỹ thuật Tp. Hồ Chí Minh;

Căn cứ Thông tư số 10/2009/TT-BGDĐT ngày 07 tháng 5 năm 2009 của Bộ Giáo dục và Đào tạo về việc Ban hành Quy chế đào tạo trình độ tiến sĩ;

Căn cứ Thông tư số 05/2012/TT-BGDĐT ngày 15 tháng 02 năm 2012 của Bộ Giáo dục và Đào tạo về việc sửa đổi, bổ sung một số điều của Quy chế đào tạo trình độ tiến sĩ ban hành kèm theo Thông tư số 10/2009/TT-BGDĐT ngày 07 tháng 5 năm 2009 của Bộ trưởng Bộ Giáo dục và Đào tạo;

Xét nhu cầu công tác và khả năng cán bộ;

Xét đề nghị của nghiên cứu sinh và Trường phòng Đào tạo,

QUYẾT ĐỊNH

Điều 1: Đổi tên luận án tiến sĩ cho:

Nghiên cứu sinh : **Hồ Nhật Linh**

Ngành : Kỹ thuật cơ khí

Khoá: 2016 – 2019

Tên luận án mới : **Phát triển và tối ưu hóa tay kẹp chi tiết dạng trục sử dụng cơ cấu mềm**

Người HD thứ nhất (HD chính): **PGS.PGS.TS Lê Hiếu Giang**

Người HD thứ hai : **TS. Đào Thanh Phong**

Thời gian thực hiện : **03/10/2016 đến 03/10/2019**

Điều 2: Giao cho Phòng Đào tạo quản lý, thực hiện theo đúng Quy chế đào tạo trình độ tiến sĩ của Bộ Giáo dục & Đào tạo đã ban hành.

Điều 3: Trưởng các đơn vị: phòng Đào tạo, khoa quản ngành, phòng KHTC và các Ông (Bà) có tên ở Điều 1 chịu trách nhiệm thi hành quyết định này.

Quyết định có hiệu lực kể từ ngày ký. ✕

Nơi nhận:

- BGH (để chỉ đạo);
- Như điều 3;
- Lưu: VT, SĐH (3b).



SCIENTIFIC CURRICULUM VITAE

I. Personal information

1. Full name: **HO NHAT LINH**
2. Birthday: 01/01/1982 Place of birth: Long An
3. Nationality: Vietnam Sex: Male
4. Academic degree: Master of Engineering - 2016
5. Contact:

No.		<i>Office</i>	<i>Home</i>
1	Address	2nd Floor, No.63, Xuan Hong street, 12 Ward, Tan Binh District, HCMC, Viet Nam	B69/4, My Hoa 2, Xuan Thoi Dong Ward, Hoc Mon District, HCMC, Viet Nam
2	Phone/ fax	(+84) 944.800.004	(+84) 944.800.004
3	Email	honhatlinh01011982@gmail.com	

6. Education background (latest):

<i>Level</i>	<i>Time</i>	<i>Institution</i>	<i>Major/Specialty</i>
BS.	2005	HCM University of Technology and Education, Viet Nam	Mechanical Engineering
MS.	2016	Ho Chi Minh City University of Technology, Viet Nam	Mechanical Engineering

II. Work experience

<i>Time</i>		<i>Organization</i>	<i>Position</i>
<i>From</i>	<i>to</i>		

06/2005	01/2007	CÔNG TY TNHH VIE-PAN – Việt nam	Mechanical Engineer
01/2007	05/2009	CTY TNHH IKEBA SANGYO – Nhật Bản	Mechanical Engineer
06/2009	10/2012	CTY TNHH SEKO SANGYO – Nhật Bản	Mechanical Engineer
12/2012	09/2013	CTY TNHH NIDEC SEIMITSU VIET NAM	Mechanical Engineer
09/2013	Present	CTY TNHH KOEI VIET NAM	Sales engineer

III. Reference

Dr. Dao Thanh Phong

Office: Institute for Computational Science, Ton Duc Thang University

Email: daothanhphong@tdtu.edu.vn

Assoc.Prof. Dr. Le Hieu Giang

Office: HCMC University of Technology and Education

Email: gianglh@hcmute.edu.vn

Commitment: I hereby guarantee that all the above declaration is the truth and only the truth. I will fully take responsibility if there is any deception.

Ho Chi Minh City, July 2023

Signature and Full name

Ho Nhat Linh

CONTENTS

CONTENTS.....	IV
ORIGINALITY STATEMENT.....	IX
ACKNOWLEDGMENTS.....	X
ABSTRACT.....	XI
LIST OF ABBREVIATIONS.....	XII
LIST OF SYMBOLS.....	XIV
LIST OF FIGURES.....	XVII
LIST OF TABLES.....	XXII
CHAPTER 1 INTRODUCTION.....	1
1.1. Background and motivation.....	1
1.2. Problem description of proposed compliant grippers.....	6
1.3. Objects of the dissertation.....	8
1.4. Objectives of the dissertation.....	8
1.5. Research scopes.....	8
1.6. Research methods.....	9
1.7. The scientific and practical significance of the dissertation.....	9
1.7.1. Scientific significance.....	9
1.7.2. Practical significance.....	9
1.8. Contributions.....	9
1.9. Outline of the dissertation.....	10
CHAPTER 2 LITERATURE REVIEW.....	11
2.1. Overview of compliant mechanism.....	11
2.1.1. Definition of compliant mechanism.....	11

2.1.2. Categories of compliant mechanism	13
2.1.3. Compliant joints or flexure hinges	15
2.2. Actuators	17
2.3. Displacement amplification based on the compliant mechanism	18
2.3.1. Lever mechanism.....	19
2.3.2. The Scott-Russell mechanism	20
2.3.3. Bridge mechanism	22
2.4. Displacement sensors based on compliant mechanisms	25
2.5. Compliant grippers based on embedded displacement sensors	28
2.6. International and domestic research	29
2.6.1. Research works in the field by foreign scientists.....	29
2.6.1.1. Study on compliant mechanisms by foreign scientists.....	29
2.6.1.2. Study on robotic grippers and compliant grippers by foreign scientists ...	30
2.6.2. Research works in the field by domestic scientists	38
2.6.2.1. Research on compliant mechanisms by domestic scientists.....	38
2.6.2.2. Research on robotic grippers and compliant grippers by domestic scientists	39
2.7. Summary	43
CHAPTER 3 THEORETICAL FOUNDATIONS	45
3.1. Design of experiments	45
3.2. Modeling methods and approaches for compliant mechanisms	48
3.2.1. Analytical methods	48
3.2.1.1. Pseudo-rigid-body model.....	49
3.2.1.2. Lagrange-based dynamic modeling approaches	50
3.2.1.3. Finite Element Method	51

3.2.1.4. Graphic method, Vector method, and Mathematical analysis	52
3.2.2. Data-driven modeling methods	52
3.2.3. Statistical methods	55
3.3. Optimization methods.....	56
3.3.1. Metaheuristic algorithms	58
3.3.2. Data-driven optimization	59
3.4. Weighting factors in multi-objective optimization problems	59
3.5. Summary	60
CHAPTER 4 DESIGN, ANALYSIS, AND OPTIMIZATION OF A DISPLACEMENT SENSOR FOR AN ASYMMETRICAL COMPLIANT GRIPPER	61
4.1. Research targets of displacement sensor for compliant gripper	61
4.2. Structural design of proposed displacement sensor	62
4.2.1. Mechanical design and working principle of a proposed displacement sensor.	62
4.2.1.1. Description of structure of displacement sensor	62
4.2.1.2. The working principle of a displacement sensor.....	65
4.2.2. Technical requirements of a proposed displacement sensor.....	68
4.3. Behavior analysis of the displacement sensor.....	68
4.3.1. Strain versus stress.....	68
4.3.2. Stiffness analysis	80
4.3.3. Frequency response	82
4.4. Design optimization of a proposed displacement sensor.....	85
4.4.1. Description of optimization problem of a proposed displacement sensor	85
4.4.1.1. Definition of design variables	88

4.4.1.2. Definition of objective functions.....	89
4.4.1.3. Definition of constraints	90
4.4.1.4. The proposed method for optimizing the displacement sensor	90
4.4.2. Optimal Results and Discussion	95
4.4.2.1. Determining Weight Factor.....	95
4.4.2.2. Optimal results	104
4.4.3. Verifications.....	108
4.5. Summary	111
 CHAPTER 5 COMPUTATIONAL MODELING AND OPTIMIZATION OF A SYMMETRICAL COMPLIANT GRIPPER FOR CYLINDRICAL SAMPLES 113	
5.1. Basic application of symmetrical compliant gripper for cylinder samples .	113
5.2. Research targets of symmetrical compliant gripper	114
5.3. Mechanical design of symmetrical compliant gripper	115
5.3.1. Description of structural design	115
5.3.2. Technical requirements of proposed symmetrical compliant gripper.....	117
5.3.3. Behavior analysis of the proposed compliant gripper	117
5.3.3.1. Kinematic analysis.....	117
5.3.3.2. Stiffness analysis	121
5.3.3.3. Static analysis	124
5.3.3.4. Dynamic analysis.....	125
5.4. Design optimization of the compliant gripper	126
5.4.1. Problem statement of optimization design.....	126
5.4.1.1. Determination of design variables.....	127
5.4.1.2. Determination of objective functions	128
5.4.1.3. Determination of constraints	128

5.4.2. Proposed optimization method for the compliant gripper	129
5.4.3. Optimized results and validations	131
5.4.3.1. Optimized results.....	131
5.4.3.2. Validations	136
5.5. Summary	139
CHAPTER 6 CONCLUSIONS AND FUTURE WORKS	141
6.1. Conclusions	141
6.2. Future works.....	142
REFERENCES.....	143
APPENDIX.....	165

ORIGINALITY STATEMENT

I, Ho Nhat Linh, confirm that this dissertation is the product of my efforts, carried out under the guidance of **Assoc. Prof. Dr. Le Hieu Giang** and **Dr. Dao Thanh Phong**, to the best of my understanding.

The information and findings presented in this dissertation are authentic and have not been previously published.

ACKNOWLEDGMENTS

First of all, I am grateful to my adviser, **Assoc. Prof. Le Hieu Giang** and Dr. **Dao Thanh Phong** have supported me with his knowledge and dedication throughout my Ph.D. studies and provided me with the perspective required to conduct research in the field of Compliant mechanisms.

I would want to thank my compliance team members, who will follow me throughout my research career.

Also, I would like to thank for the financial support from the HCMC University of Technology and Education, Vietnam, under Grant No. T2018-16TĐ, and Vietnam National Foundation for Science and Technology Development (NAFOSTED) under grant No.107.01-2019.14.

To conclude, I extend my heartfelt appreciation to my spouse and parents for their motivation, assistance, and endurance.

Ho Nhat Linh

ABSTRACT

Developing a gripper with accurate grasping and positioning tasks has been a daunting challenge in the assembly industry. To meet these requirements, this thesis aims to develop two new types of compliant grippers. The first gripper with an asymmetrical structure is capable of integrating displacement sensors. The second gripper with a symmetrical structure is served for assembly. The hypothesized grasping objects are small-sized cylinders as the shaft of the vibration motor used in mobile phones or electronic devices (ϕ 0.6mm \times 10mm).

In the first part, a displacement sensor for self-identifying the stroke of an asymmetric compliant gripper is analyzed and optimized. Strain gauges are placed in the flexible beams of the gripper and turn it into the displacement sensor with a resolution of micrometers. In addition, static and dynamic equations of the gripper are built via the pseudo-rigid-body model (PRBM) and Lagrange's principle. To increase the stiffness and frequency, silicone rubber is filled the open cavities of the gripper. Taguchi-coupled teaching learning-based optimization (HTLBO) method is formulated to solve the multi-response optimization for the gripper. Initial populations for the HTLBO are generated using the Taguchi method (TM). The weight factor (WF) for each fitness function is properly computed. The efficiency of the proposed method is superior to other optimizers. The results determined that the displacement is 1924.15 μ m and the frequency is 170.45 Hz.

In the second part, a symmetric compliant gripper consisting of two symmetrical jaws is designed for the assembly industry. The kinematic and dynamic models are analyzed via PRBM and the Lagrange method. An intelligent computational technique, adaptive network-based fuzzy inference system-coupled Jaya algorithm, is proposed to improve the output responses of the gripper. The WF of each cost function is computed. The results achieved a displacement of 3260 μ m. Besides, the frequency was 61.9 Hz. Physical experiments are implemented to evaluate the effectiveness of both compliant grippers. The experimental results are relatively agreed with the theoretical results.

LIST OF ABBREVIATIONS

Abbreviation	Full name
CAD	Computer-aided design
FEM	Finite element method
FEA	Finite element analysis
CG	Compliant gripper
CM	Compliant mechanism
PEA	Piezoelectric actuator
MDS	Micro-displacement sensor
SR	Silicon rubber
TM	Taguchi method
ANOVA	Analysis of variance
<i>S/N</i>	Signal-to-Noise
AVONSNR	Average value of normalized <i>S/N</i> ratios
RSM	Response surface methodology
PRBM	Pseudo-rigid-body model
TLBO	Teaching learning-based optimization
HTLBO	Hybrid teaching learning-based optimization
GA	Genetic algorithm
PSO	Particle swarm optimization

Abbreviation	Full name
AEDE	Adaptive elitist differential evolution
ANFIS	Adaptive neuro-fuzzy inference system technique
WF	Weight factor
DA	Displacement amplification
MOO	Multi-objective optimization
MOOP	Multi-objective optimization problem
NSGA-II	Nondominated sorting genetic algorithm II
WEDM	Wire electrical discharged machining
FH	Flexure hinge

LIST OF SYMBOLS

Abbreviation	Full name
S	Safety factor
σ_y	Yield strength of the material
f	Frequency
E	Young's modulus
ε	Strain
σ	Stress
y	The quality response
i	The number of experiments
q	The number of replicates of experiment 'i'
n_d	The population size
X	The vector of design variables
x_i	Design variable
$U_{L,i}$	Upper limit of the design variable
$U_{L,i}$	Lower limit of the design variable
pop	The population
r	Random value
T_F	The teaching factor

Abbreviation	Full name
$m(\cdot)$	Average value of the data set.
S/N	Signal-to-noise ratio
z_i	Normalized mean S/N
η_i	S/N ratio
m	The number of responses
R	The resistance
G	Gauge factor
V_o	The output of the circuit
V_{ex}	The excitation voltage of the circuit
F_y	Force in the y direction
S	Sensitivity
N	The number of failure cycles
S_{ut}	The ultimate strength
S_e	The endurance strength limit
M	The bending moments
$d\phi/ds$	The differentiation of deflection
W	External work
F_i	Input force

Abbreviation	Full name
F_o	Output force
k_{PEA}	The stiffness of PEA
$F_{preload}$	Preload force of the piezoelectric actuator
M_s	The entire mass of the gripper
K_s	The stiffness of the gripper
l_i	Length of the i^{th} flexure hinge
t_i	Thickness of the i^{th} flexure hinge
W	Width of the positioning platform
L	Length of the positioning platform
H	Hight of the positioning platform

LIST OF FIGURES

Figure 1. 1: Some applications of robotic gripper [2]: a) Medicine/biology, b) Material handling, c) Picking, packaging, and shelling, and d) Machine tending robots.	1
Figure 1.2: Several types of grippers in the industry [3]: a) Vacuum grippers, b) Pneumatic grippers, c) Hydraulic grippers, d) Magnetic grippers, and e) Electric grippers.	2
Figure 1. 3: A miniaturized vibrating motor: a) Mobile phone, b) Vibrating mobile-phone motor, c) Miniaturized motor [13].....	7
Figure 2. 1: a) Traditional rigid-body clamp and b) Compliant clamp [16].....	11
Figure 2. 2: Classification of compliant mechanism based on compliance [18].....	13
Figure 2. 3: Classified based on the static deformation of a structure [18].....	14
Figure 2. 4: A compliant active mechanism with two flexible segments [19].....	14
Figure 2. 5: A passive compliant mechanism with four rigid links and a flexible link [19].....	14
Figure 2. 6: Four types of typical CM : a) Inverter, b) Compliant platform, c) Microgripper, and d) Positioning stage [20].....	15
Figure 2. 7: Three principal categories of FH arrangements: a) Single-axis; b) Multiple-axis; c) Two-axis [28].	16
Figure 2. 8: Complex type of FHs: a) Cross hinge, b) Cartwheel hinge, c) Leaf spring, d) Hyperbolic hinge [28].	16
Figure 2. 9: Flexure hinges with notch shape [29]: a) Circular hinge, b) Filleted leaf hinge, c) Elliptical hinge, d) V shape hinge, e) Hyperbolic hinge, f) Parabolic hinge.	16
Figure 2. 10: Actuators: a) Piezoelectric actuators [34]; b) Electrostrictive actuators [35]; c) Magnetostrictive actuators [36]; d) Shape memory alloy (SMA) actuators [37]; and e) Pneumatic actuators [38].	18
Figure 2. 11: Lever mechanism.....	19

Figure 2. 12: Lever mechanism for in-compliant grippers: a) A hybrid amplifying structure [39]; b) Single lever mechanism [42]; c) Serial lever mechanisms [43]; d) Different lever mechanisms [44].	20
Figure 2. 13: Schematic of Scott-Russell mechanism: a) The principle of operation; b) Analysis of the amplification ratio.	21
Figure 2. 14: Application of Scott-Russell mechanism in gripper design: a) Micro-gripper with Scott-Russell mechanism [46]; b) A large-range micro-gripper with Scott-Russell mechanism [47].	22
Figure 2. 15: Schematic of bridge mechanism: a) Displacement of bridge mechanism; b) Amplification factor analysis of a bridge mechanism. [48].	23
Figure 2. 16: Bridge mechanism for compliant grippers: a) Half of the bridge mechanism [49], b) Serial bridge mechanism [50], c) Two stage-bridge mechanism [52], d) Orthogonal bridge mechanism [53].	24
Figure 2. 17: Commercial displacement sensors: a) Optical displacement sensors [54]; b) Linear proximity sensors [55]; and c) Ultrasonic displacement sensors [56].	25
Figure 2. 18: Some displacement sensors-based mechanisms [57]–[60]: a) Micro-displacement sensors based on cascaded levers, b) A strain-based approach for multimode sensing, c) PVDF-based motion sensing, d) Strain gauge for direct displacement measurement.	26
Figure 2. 19: Gripper applications for assembly systems: a) Multipurpose SPI3 gripper [76]; b) i-Hand [79]; c) 4-DOF gripper [80]; d) a variable-aperture gripper [83]; e) Three-jaw gripper [85].	33
Figure 2. 20: Gripper tips with compliance structures [87]: a) Spring structures, and b) Flexure structures.	34
Figure 2. 21: Robotic Peg-in-hole Assembly [88], [89].	35
Figure 2. 22: Microgripper for optical fiber assembly [44].	36
Figure 2. 23: Micro assembly by compliant piezoelectric micro grippers [90].	36
Figure 2. 24: A few studies on CM were done by Vietnamese scientists: a) A tristable mechanism [98]; b) A damping compliant mechanism [99]; c) A compliant linear mechanism [100]; d) Bistable compliant mechanism [101].	39

Figure 2. 25: Robotic gripper: a) Pineapple harvesting robot [106]; b) Food packaging system [108]; c) A Soft Pneumatic Finger [109]; c) A soft pneumatic hand for manipulating one group of objects [110].	41
Figure 2. 26: Compliant grippers: a) Asymmetric CG [112]; b) Electrothermal CG [113]; c) Constant-force CG [114]; d) A sand crab-inspired CG [115]; e) Compliant CG [116]; f) A CG for advanced manufacturing application [117].	42
Figure 3. 1: Taguchi's experimental procedure [122].	46
Figure 3. 2: Categorization of the kinetostatic and dynamic modeling strategies for CM [123].	48
Figure 3. 3: A cantilever beam [66].	50
Figure 3. 4: PRBM of a cantilever beam [66].	50
Figure 3. 5: Typical FEA procedure by commercial software.	52
Figure 3. 6: Structure of ANFIS [135].	53
Figure 3. 7: Classification of optimization techniques [141].	56
Figure 3. 8: Three main categories of optimization techniques.	57
Figure 4. 1: Design structure: a) Displacement sensor and b) Asymmetrical compliant gripper.	62
Figure 4. 2: Silicon rubber is reinforced along the contour of the cavity.	65
Figure 4. 3: A proposed half-Wheatstone bridge circuit	66
Figure 4. 4: Block diagram of the strain measurement system.	69
Figure 4. 5: Measured strain for displacement sensor platform.	69
Figure 4. 6: Meshed model of the displacement sensor platform.	70
Figure 4. 7: Stress distribution of displacement sensor platform.	70
Figure 4. 8: Strain distribution of displacement sensor platform.	70
Figure 4. 9: Displacement distribution of displacement sensor platform.	70
Figure 4. 10: Relationship between strain and position (7) for group A in situations where SR is filled and where it is absent.	71
Figure 4. 11: Relationship between strain and position (8) for group A in situations where SR is filled and where it is absent.	72
Figure 4. 12: Relationship between strain and position (9) for group A in situations where SR is filled and where it is absent.	72

Figure 4. 13: Relationship between strain and position (10) for group A in situations where SR is filled and where it is absent.....	73
Figure 4. 14: Relationship between strain and position (11) for group A in situations where SR is filled and where it is absent.....	73
Figure 4. 15: Relationship between strain and position (12) for group A in situations where SR is filled and where it is absent.....	74
Figure 4. 16: Relationship between strain and position (S_{1B}) for group B in situations where SR is filled and where it is absent.....	75
Figure 4. 17: Relationship between strain and position (S_{2B}) for group B in situations where SR is filled and where it is absent.....	75
Figure 4. 18: Relationship between strain and position (S_{1E}) for group E in situations where SR is filled and where it is absent.....	76
Figure 4. 19: Relationship between strain and position (S_{2E}) for group E in situations where SR is filled and where it is absent.....	76
Figure 4. 20: Relationship between strain and position (S_{1F}) for group F in situations where SR is filled and where it is absent.....	77
Figure 4. 21: Relationship between strain and position (S_{2F}) for group F in situations where SR is filled and where it is absent.....	77
Figure 4. 22: Strain distributions for positions (11): At flexure hinges A, S_{2B} of B, S_{2E} of E, and S_{2F} of F.....	78
Figure 4. 23: Stress distributions for positions (11): At flexure hinges A, S_{2B} of B, S_{2E} of E, and S_{2F} of F.....	79
Figure 4. 24: Block diagram of the stiffness measurement system.	80
Figure 4. 25: Experiment fort measuring the displacement of displacement sensor.	80
Figure 4. 26: Measurement of stiffness in x-direction of displacement sensor.....	82
Figure 4. 27: Block diagram of measuring frequency by hammer	83
Figure 4. 28: Experiments for measuring frequency by hammer.	83
Figure 4. 29: Block diagram of measuring frequency by PEA.....	84
Figure 4. 30: Experiments for measuring frequency with exerted PEA.	84
Figure 4. 31: Frequency versus displacement for exerted PEA without SR.	84

Figure 4. 32: Frequency versus displacement for exerted PEA with filled SR.	84
Figure 4. 33: PRBM scheme: a) Displacement sensor and b) Model of asymmetrical compliant gripper.....	86
Figure 4. 34: Flowchart of proposed HTLBO	94
Figure 4. 35: Block diagram of displacement measurement system	109
Figure 4. 36: Experimental tests: a) Displacement and b) Frequency.	109
Figure 4. 37: Test of physical strain.	110
Figure 5. 1: Assemble system for the mini vibrating motors: a) Assembling system, b) Details of motor shaft and core.....	114
Figure 5. 2: CAD model: a) Rectangular shape and b) Symmetric compliant gripper.	116
Figure 5. 3: Levers: (a) Lever mechanism, (b) Double lever mechanism.....	116
Figure 5. 4: The reaction force of the left and right jaws.	117
Figure 5. 5: Kinematic model of the symmetrically compliant gripper.....	118
Figure 5. 6: Schematic diagram: (a) Motion vector and (b) Rotational angle changes of the symmetrical compliant gripper.	118
Figure 5. 7: Flexure beam with force at the free end.	122
Figure 5. 8: Flowchart of multi-objective optimization by ANFIS-Jaya.	129
Figure 5. 9: Block diagram of the displacement and frequency measurement system.	137
Figure 5. 10: Experiment setup for the prototype.	137

LIST OF TABLES

Table 1. 1: Five types of gripper and their advantages and disadvantages [4], [5].	3
Table 2. 1: Pros and cons of compliant mechanism [16].	12
Table 3. 1: Blind search algorithms, heuristic search algorithms, and meta-heuristic algorithms.	57
Table 4. 1: Initial design parameters.	63
Table 4. 2: Mechanical characteristics of AL7075.	63
Table 4. 3: Mechanical characteristics of Silicone rubber.	65
Table 4. 4: Stress values at various positions.	79
Table 4. 5: Displacement with various forces.	81
Table 4. 6: Displacement along the x -direction.	82
Table 4. 7: First natural frequency.	85
Table 4. 8: Parameters and their upper and lower limits.	95
Table 4. 9: Numerical experiments using Taguchi technique.	95
Table 4. 10: Results and S/N ratios.	96
Table 4. 11: Mean S/N ratios for the displacement.	98
Table 4. 12: Frequency - mean S/N ratios.	98
Table 4. 13: Gripping effort - mean S/N ratios.	98
Table 4. 14: ANOVA for displacement.	99
Table 4. 15: ANOVA for frequency.	100
Table 4. 16: ANOVA for gripping effort.	101
Table 4. 17: The values of normalized S/N ratios (z_i).	102
Table 4. 18: The WF for the displacement.	103
Table 4. 19: The WF for the frequency.	103
Table 4. 20: The WF for the gripping effort.	104
Table 4. 21: Case 1: The optimal solutions at different weight factors.	105
Table 4.22: Case 1: Comparison of the recommended approach with other optimizers.	106
Table 4. 23: Case 2: The optimal solutions at different weight factors.	106

Table 4.24: Case 2: Comparison of the recommended approach with other optimizers.....	107
Table 4. 25: Case 3: The optimal solutions at different weight factors.....	107
Table 4.26: Case 3: Comparison of the recommended approach with other optimizers.....	108
Table 4. 27: Experimental results.....	110
Table 5. 1: Parameters and their upper and lower limits.	131
Table 5. 2: The results of experiments on displacement and frequency.	131
Table 5. 3: The values of S/N ratios.....	132
Table 5. 4: The normalized S/N ratios (z_i).	133
Table 5. 5: WF of displacement response.....	134
Table 5. 6: WF of frequency response.....	134
Table 5. 7: ANFIS parameters.....	135
Table 5. 8: Comparison of several optimization techniques.....	136
Table 5. 9: The optimum, FEA and experimental outcomes are compared.	138

Chapter 1 introduces several types of common grippers for industrial fields. Advantages, disadvantages, and applicability of the grippers are provided. From the analysis of the existing grippers, the gaps are described and the research motivation is indicated. Then, the research problem, objects, objectives, methods, scientific and practical significance, and contributions are also identified. Finally, the structure of the dissertation is outlined.

1.1. Background and motivation

The original purpose of developing the robotic gripper is to assist or substitute humans in performing monotonous, unclean, or hazardous tasks [1]. Robotic grippers can be found in numerous applications, such as medical, biology, material handling, picking, packaging and shelling, and machine tending, as illustrated in Figure 1. 1.

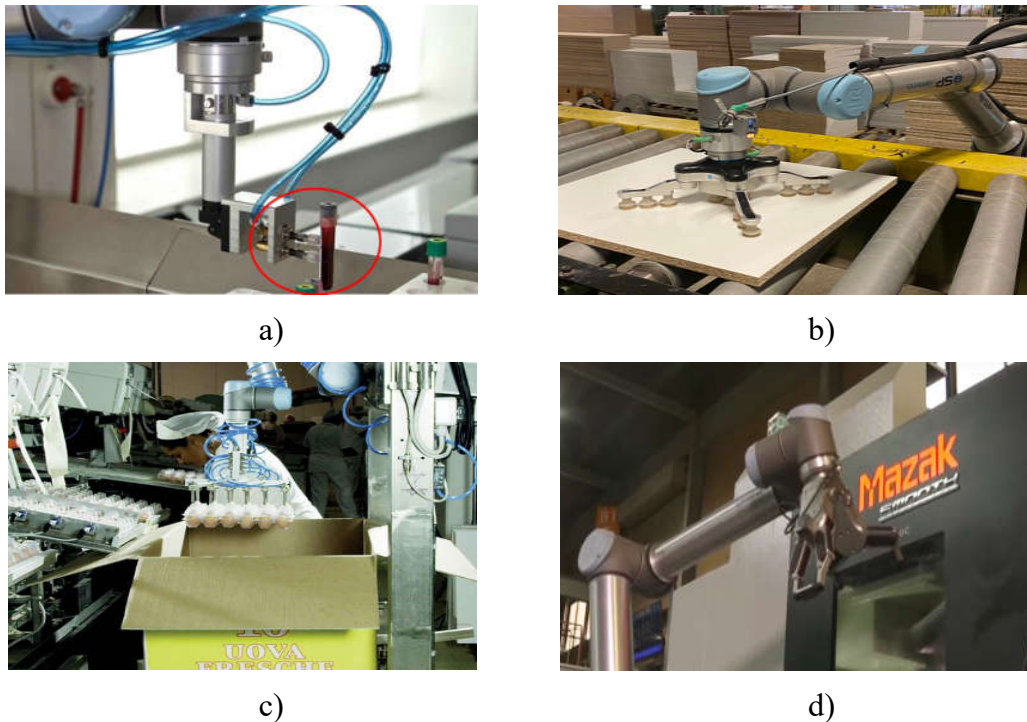


Figure 1. 1: Some applications of robotic gripper [2]: a) Medicine/biology, b) Material handling, c) Picking, packaging, and shelling, and d) Machine tending robots.

To perform multiple-complex assemble tasks, the industrial robotic grippers are

chosen because they are superior to humans. Furthermore, the expense of manual labor is rising, while the cost of robotic grippers is decreasing. As a result, the industry and academia have been motivated to create more sophisticated robotic arms and grippers to overcome the challenging problems of human resources. The function of robotic arms is comparable to that of human arms, while the gripper attached to the arm functions like a human hand. In practice, a gripper is often attached to a robotic arm (universal robot UR3, UR5, and so forth), and it is responsible for interacting with the environment and grasping objects. Depending on the different purposes, grippers are manufactured to a variety of specifications. At present, robotic grippers are usually classified into 5 basic types, including magnetic grippers, electric grippers, pneumatic grippers, hydraulic grippers, and vacuum grippers [3], as depicted in Figure 1.2.

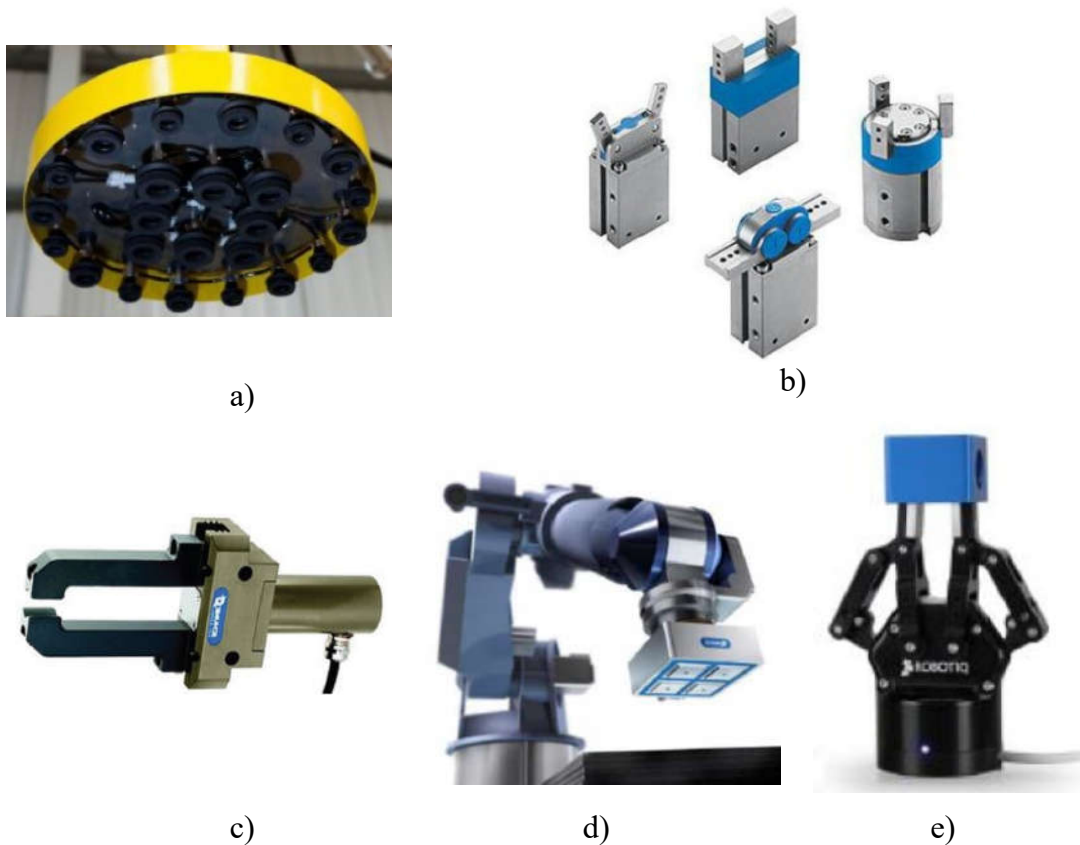


Figure 1.2: Several types of grippers in the industry [3]: a) Vacuum grippers, b) Pneumatic grippers, c) Hydraulic grippers, d) Magnetic grippers, and e) Electric grippers.

Figure 1.2a illustrates the vacuum grippers, by relying on the contrast between the pressure in the atmosphere and in a vacuum, this category of a device can elevate, grasp, and transport items. A miniature electromechanical pump or compressed air-driven pump typically produces the vacuum. To ensure the cobot maintains a secure hold on the item it has grabbed, the vacuum flow must remain uninterrupted. The usage of a vacuum gripper is in automating packaging and palletizing processes. As shown in Figure 1.2b, a pneumatic gripper utilizes compressed air and pistons to manipulate its jaws (also known as fingers). Pneumatic grippers, which are versatile tools suitable for a variety of applications, are typically available in two-finger or three-finger configurations. Hydraulic grippers are designed to rely on the power provided by the hydraulic fluid, and hydraulic clamps (refer to Figure 1.2c). It provides more clamping force than its pneumatic counterparts for heavy-duty applications. Figure 1.2d displays magnetic grippers that can use permanent magnets or electromagnets for configuration. Permanent magnets do not require an external power source for grasping, but a stripper push is needed to release the object. Electromagnets require a controller unit and DC power to grasp magnetic objects. The use of electric grippers in various robotic applications, such as machine tending and pick & place, is widespread, as evidenced in Figure 1.2e. Although electric grippers do not offer the same gripping strength as hydraulic grippers, they are adequate for tasks that demand quickness and light/moderate gripping force. Typically, electric grippers are designed in either two-jaw or three-jaw configurations. When handling cylindrical objects, the three-jaw grippers are often preferred. Table 1. 1 provides the advantages, disadvantages, and applicability of these grippers.

Table 1. 1: Five types of gripper and their advantages and disadvantages [4], [5].

Types of grippers	Advantages	Disadvantages	Application fields
Vacuum Grippers	<ul style="list-style-type: none"> Irrespective of their positions, it is capable of handling 	<ul style="list-style-type: none"> Sensitive to dusty conditions The utilization of 	<ul style="list-style-type: none"> Paper industries Glass industries Other thin and

Types of grippers	Advantages	Disadvantages	Application fields
	<p>different types of objects.</p> <ul style="list-style-type: none"> • Low price compared to others 	<p>extensive electricity results in increased costs.</p>	<p>light items.</p>
Pneumatic Grippers	<ul style="list-style-type: none"> • Can work in confined areas • Possess a wide range of grip force • Have rapid response times • Not expensive 	<ul style="list-style-type: none"> • Can only handle single-part types • Provide limited position and force control 	<ul style="list-style-type: none"> • Robotics field • Manufacturing of medical devices • Injection molding • Processing in the lab • Automated systems
Hydraulic Grippers	<ul style="list-style-type: none"> • Great grasping power. 	<ul style="list-style-type: none"> • Voluminous than other grippers • Require more maintenance 	<ul style="list-style-type: none"> • Heavy-duty industries
Electric Grippers	<ul style="list-style-type: none"> • Allow for variable force and speed of object grasping. • Due to the addition of a force sensor, it is now able to manipulate a variety of components kinds with ease. 	<ul style="list-style-type: none"> • Provide less gripping force • Expensive 	<ul style="list-style-type: none"> • Gripping of parts that are easily deformed or damaged • Measurement • Gripping in a narrow space • Detection or identification

Types of grippers	Advantages	Disadvantages	Application fields
Magnetic grippers	<ul style="list-style-type: none"> • Non-contact handling • High holding force • Speed • Minimal maintenance 	<ul style="list-style-type: none"> • Limited compatibility • Sensitivity to temperature • Safety concerns • Cost 	<ul style="list-style-type: none"> • Material handling • Manufacturing and assembly • Robotics

From the detailed analysis above, it can be seen that these five types of grippers have been developed for numerous applications [6]–[8]. To operate a gripper, the jaws are attached to a robot manipulator. The robotic gripper often includes a manipulator, jaws, actuator, sensor, and controller. Depending on the type of products as well as the needs of the manufacturing industry, the gripper has a wide range of different applications, e.g., assembling, packing, bin picking, vision system, and so forth. Although the benefit of a gripper can handle goods and components at a high speed. Nevertheless, there are still a few common limitations of industrial grippers, e.g., bulky and assembled requirements with many different components. These cause high maintenance costs. Besides, traditional grippers require an assembled system of different components, such as rigid links, kinematic joints, motors, actuators, sensors, and so on. Such assembly systems lead to errors in operation.

To meet a precise grasping requirement in small working spaces, a new type of gripper must be developed. Nowadays, compliant gripper (CG) have been developed to alternative the aforementioned traditional grippers [9]–[11]. The reasons are that the compliant grippers possess excellent benefits of a monolithic structure, reduced manufacture, less component, free friction and lubricant, lightweight, decreased cost, etc. Nevertheless, a key issue of a CG is that it requires extra displacement/force sensors to realize the working stroke, a position as well as acting forces of jaws. To equip commercial sensors, an extra control of displacement sensors would be complex. Therefore, a direct-online observation of stroke and forces of the jaw is a facing challenge in decreasing the working complexity and manufacturing cost.

Especially in an assembly system of DC motors of cell-phone, the placement of a cylinder shaft into a core requires an accurate motion of jaws. In the assembly process of a micro pin in a micro motor, the question is how to accurately position the position of the micro pin. The traditional grippers are not able to perform this difficult task. Especially for a vibrating motor DC assembly system [12], the gripper requires a high-precision operation in grasping, positioning, and releasing the cylinder shaft.

Through reviewing the survey, there has been a lack of studies on the development of displacement sensors for compliant grippers which can direct-online observe stroke and forces. In addition, there has not been any research related to compliant grippers that can be applied to DC motor assembly systems. Therefore, the first motivation of this thesis is to develop an asymmetrical CG whose jaw's stroke can be self-measured by an integrated displacement sensor. The second motivation of this thesis is to develop a symmetrical CG that is responsible for handling the cylinder shaft for DC motor assembly application.

In summary, from reviewing the mentioned-above issues, the research topic entitled "*Development and optimization of grippers for cylinder samples using compliant mechanisms*" is implemented in this dissertation. The results obtained from this study can make a significant contribution to the development of techniques for designing, analyzing, and optimizing compliant grippers for assemble industry.

1.2. Problem description of proposed compliant grippers

Manipulating small objects (e.g., electronic components) is a very challenging task due to some technical characteristics involved in accuracy, especially in the field of assembling small-sized components in game machines or mobile devices [12]. In this dissertation, two compliant grippers are proposed to grip and release cylinder samples for the DC motor assembly line. An application in a vibrating motor assembly system is described and considered as a hypothesis for study. The shaft and core assembly of a vibrating motor which is applicable to mobile phones are considered an object of study (refer to Figure 1. 3).

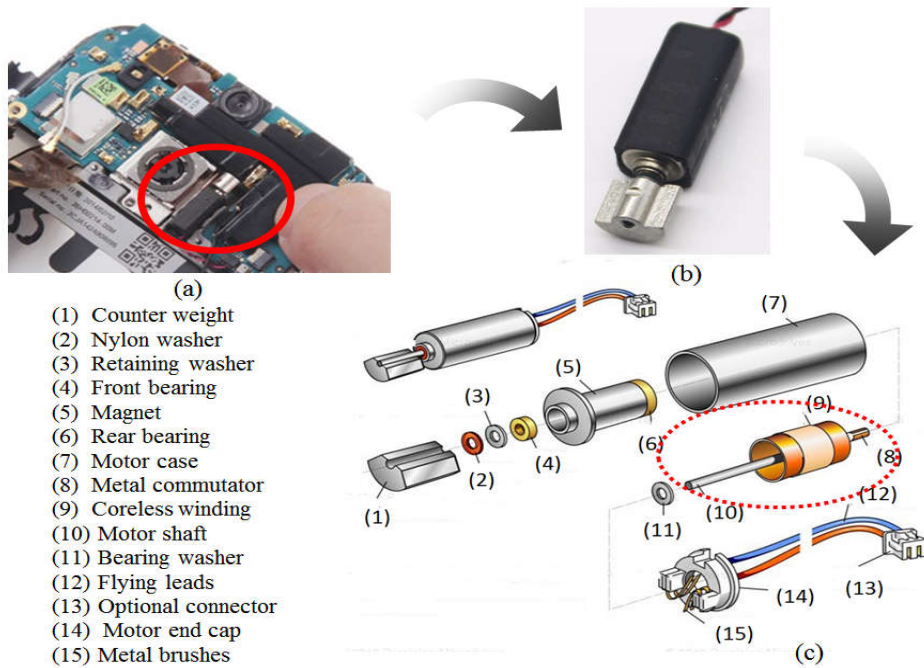


Figure 1. 3: A miniaturized vibrating motor: a) Mobile phone, b) Vibrating mobile-phone motor, c) Miniatured motor [13].

As depicted in Figure 1. 3c, multiple components are brought together to construct a miniaturized vibrating motor. One crucial step in the assembly process is how the shaft and the core are assembled together. According to Ref. [12], [13], the shaft has a size of $\phi 0.6 \text{ mm} \times 10 \text{ mm}$ and the core has a size of $\phi 2.5 \text{ mm} \times 3 \text{ mm}$. To fulfill the assembly task for vibrating DC motors, the following two important issues of compliant grippers are considered in this dissertation. The first problem is how to directly measure the displacement, the so-called working travel of jaws, quickly and precisely. The second problem is how to enhance simultaneously the stroke of jaws and the responding speed (i.e., improvement of natural frequency) of the gripper.

To solve the two stated-above problems, this dissertation focuses on two main parts: (i) A displacement sensor is embedded into the asymmetrical gripper to directly measure the stroke of jaws. (ii) A simultaneous improvement of both the stroke and the first resonant frequency for the symmetrical gripper through reasonable optimization techniques.

In electronics manufacturing, it's important to note that the handle used to hold the object (typically made of plastic or metal and weighing just a few grams) doesn't

require a significant amount of friction. As a result, the gripping force produced by the traditional mechanical gripping module is adequate for this task. Additionally, since the gripper undergoes minimal displacement, hysteresis is not a significant factor to consider [14].

1.3. Objects of the dissertation

This dissertation aims to develop and optimize compliant grippers for cylinder samples using compliant mechanisms. The research objects include as follows:

- (i). An asymmetrical compliant gripper with an integrating displacement sensor.
- (ii). A symmetrical compliant gripper for handling cylinder samples.

1.4. Objectives of the dissertation

This dissertation covers the following objectives:

- (i). To develop an asymmetric compliant gripper with an integrating displacement sensor for direct measurement of jaw stroke.
- (ii). To develop a symmetrical compliant gripper for handling cylinder samples.
- (iii). To develop mathematical equations that describe static and dynamic behaviors of the suggested grippers.
- (iv). To develop new soft-computing-based optimization approaches in improving the performances of proposed compliant grippers.

1.5. Research scopes

In order to meet an assembling task for the vibrating DC motor [12], [13], the scopes of this dissertation are as follows:

- (i). Design a new displacement sensor for directly measuring the stroke of the asymmetrical compliant gripper with a range over 1000 μm , a high frequency of over 60 Hz, and a minimal gripping effort.
- (ii). Design a new symmetrical compliant gripper with a displacement range of over 1000 μm and a high frequency of over 60 Hz.
- (iii). Formulation of the static and kinematic equations of the gripper
- (iv). Development of efficient optimization techniques.

1.6. Research methods

The main methods cover in this dissertation are as follows: (i) Empirical method and expert knowledge; (ii) Numerical simulation method; (iii) Experimental planning; (iv) Analytical modeling and intelligent methods based on artificial intelligence; (v) Optimization method; (vi) Experimental method.

1.7. The scientific and practical significance of the dissertation

1.7.1. Scientific significance

The scientific significances of the thesis include the following points:

- Propose a new design principle of displacement sensor in directly measuring the displacement of the jaw.
- Develop new design approaches for compliant grippers.
- Efficiently analytical and soft-computing approaches are developed for the analysis synthesis of the compliant grippers.
- New hybrid optimization approaches are developed for compliant grippers.

1.7.2. Practical significance

The practical significances of the thesis include the following points:

- The developed displacement sensor can self-measure the stroke of the jaws of compliant grippers.
- The developed compliant grippers can grip and release cylinder shafts for use in the assembling industry.
- The design, analysis, and optimization methods can be employed for compliant grippers as well as related engineering fields.
- The dissertation can be used for referring of post-graduate students.

1.8. Contributions

The thesis has the following contributions as follows:

- ***In terms of sciences:***

- The thesis proposes a novel design principle for a displacement sensor that enables direct measurement of jaw displacement. This contribution advances the field of mechanical engineering and robotics by introducing a new

approach for accurate measurement and control during gripping and fixation processes.

- The thesis develops efficient analytical and soft-computing approaches for the analysis and synthesis of compliant grippers. These methods provide theoretical foundations and computational tools for researching and optimizing the flexible mechanisms of grippers.
 - The thesis introduces new hybrid optimization approaches for improving the performance of compliant grippers. These approaches combine different computational methods and optimization techniques to enhance the efficiency and effectiveness of grippers. This contribution opens up new potential applications for optimizing and improving the performance of compliant grippers.
 - The thesis presents innovative design approaches for compliant grippers. This contributes to the advancement of compliant robotics technology and expands the application possibilities in industries.
- *In terms of applications:*
- Micro-displacement sensors based on a compliant mechanism (CM) may be considered as alternative sensors with a low cost.
 - Symmetric grippers based on a CM can be considered for potential application orientations in assembly lines.

1.9. Outline of the dissertation

Chapter 1: Introduction

Chapter 2: Literature review

Chapter 3: Theoretical foundations

Chapter 4: Design, analysis, and optimization of a displacement sensor for an asymmetrical compliant gripper

Chapter 5: Computational modeling and optimization of a symmetrical compliant gripper for cylindrical samples

Chapter 6: Conclusions and future work

In this chapter, some different concepts are summarized and presented. Specifically, the concepts of compliant mechanisms as well as their classification, and some types of flexure hinges are also provided. In addition, several modules such as displacement amplifiers based on compliant mechanisms, displacement sensors based on compliant mechanisms, and several types of actuators are also introduced. Furthermore, a survey on the state-of-art domestic and international research on the robotic gripper, compliant mechanism, and compliant gripper is carried out.

2.1. Overview of compliant mechanism

2.1.1. Definition of compliant mechanism

In mechanical engineering, a mechanism is utilized for transferring motion, force, torque, or energy. Traditional couplings such as bearings and kinematic joints are commonly used in rigid-link mechanisms. However, traditional mechanisms have disadvantages, e.g., clearance, backlash, and friction that they cannot perform smooth motions and precise positioning requirements. To counteract the drawbacks of traditional mechanisms, the CM has been studied and developed, as shown in Figure 2. 1. Earlier research on compliance mechanisms was pointed out by Burns and Crossley in 1965 [15], Howell in 2001 [16], and Lobontiu in 2002 [17]. Lobontiu has defined a compliant mechanism as a mechanism that connects rigid parts and has at least a deformation member which will be called a flexible hinge (FH) [17].

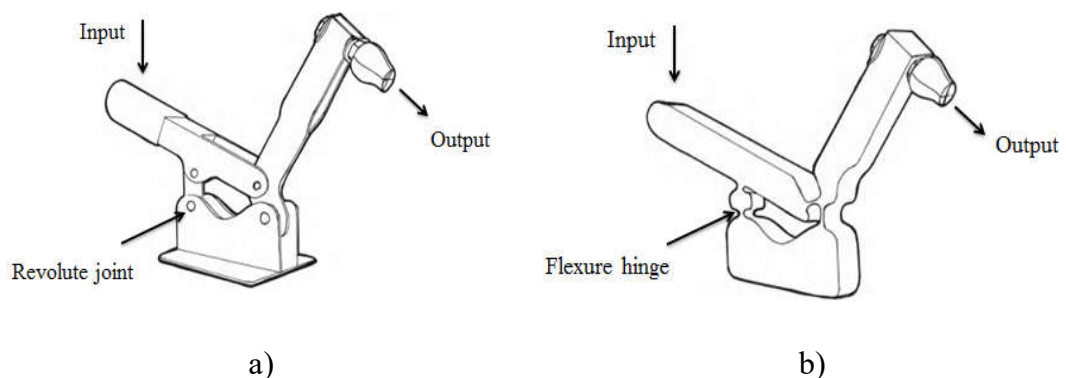


Figure 2. 1: a) Traditional rigid-body clamp and b) Compliant clamp [16].

Similar to traditional rigid mechanisms, flexure hinge-based CM also have the same

function as the transfer force, torque, and motion, but are based on the elastic deformation of flexible members. CM offers unique pros and cons, as provided in Table 2. 1.

Table 2. 1: Pros and cons of compliant mechanism [16].

Pros	Cons
<i>Simplicity:</i> CM can be simpler than traditional rigid-link mechanisms since they require fewer parts and no assembly of joints.	<i>Limited precision:</i> CM can be less precise than traditional mechanisms since they can be more sensitive to manufacturing tolerances and environmental conditions.
<i>Lightweight:</i> Because of their simple construction, CM are often lighter in weight than rigid-link mechanisms.	<i>Limited range of motion:</i> CM has a limited range of motion due to the elasticity of its structural elements.
<i>Flexibility:</i> CM can deform and adapt to different loads and environments, making them more versatile than rigid-link mechanisms.	<i>Limited load capacity:</i> CM may not be able to handle large loads or forces due to the elastic nature of their components.
<i>Lower friction:</i> CM typically have less friction than traditional mechanisms since they rely on elastic deformation rather than sliding or rolling contacts.	<i>Design complexity:</i> The design of CM can be more challenging than rigid-link mechanisms due to their nonlinear behavior and complex stress patterns.
<i>Higher reliability:</i> CM is less prone to mechanical failure since they have no joints that can wear or fail over time.	<i>Limited to simple motions:</i> CM is generally limited to simple motions, such as translation or rotation, and may not be suitable for more complex motions.

2.1.2. Categories of compliant mechanism

Numerous methods of classifying CM have been put forward. Notwithstanding, Zentner and Bohm [18] have organized CM into groups based on their level of compliance and how they deform.

2.1.2.1. Compliance-driven classification

In this categorization, a compliant mechanism was divided into fixed and variable structures. Fixed compliance structures have specific compliance determined by the system's geometry and material characteristics and can take on one or more equilibrium shapes under a given fixed load. In situations where there is only one equilibrium shape, the deformation is directly proportional to the load. However, structures with multiple stable and unstable equilibrium positions for a given load require the user or environmental conditions to determine a particular equilibrium shape. This is referred to as static stability. Figure 2. 2 illustrates this classification.

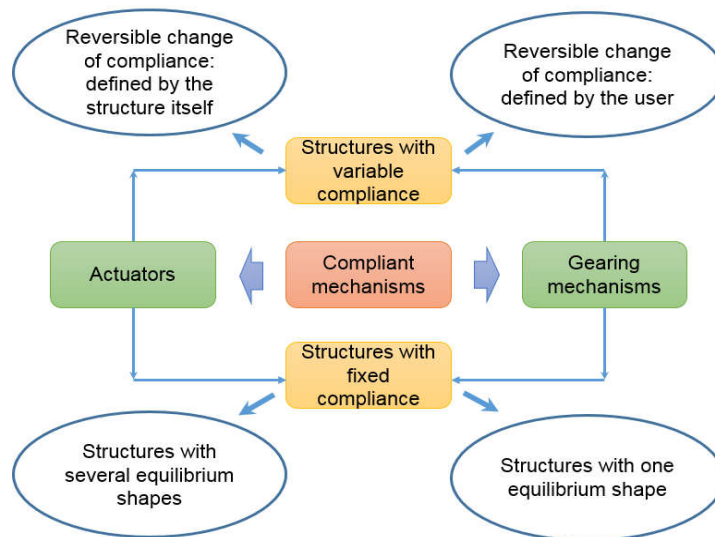


Figure 2. 2: Classification of compliant mechanism based on compliance [18].

2.1.2.2. Deformation-based classification

If deformation behavior is used to categorize compliant structures, there are two subcategories, such as dynamic and static deformation. In this particular case, the focus is on the static deformation behavior of fixed-compliance CM, and therefore inertia and damping are not taken into account.

The static deformation of a structure can be classified as either stable or unstable [18], as demonstrated in Figure 2. 3. Stable deformation behavior involves a

surjective mapping of a particular load, F , onto the deformation, u . This allows for the differentiation between monotonic behavior and behavior with a single, smooth reversal. When a compliant structure exhibits unstable behavior, it can undergo snap-through, which is a form of discontinuous deformation behavior, or bifurcation, which is a type of local bifurcation.

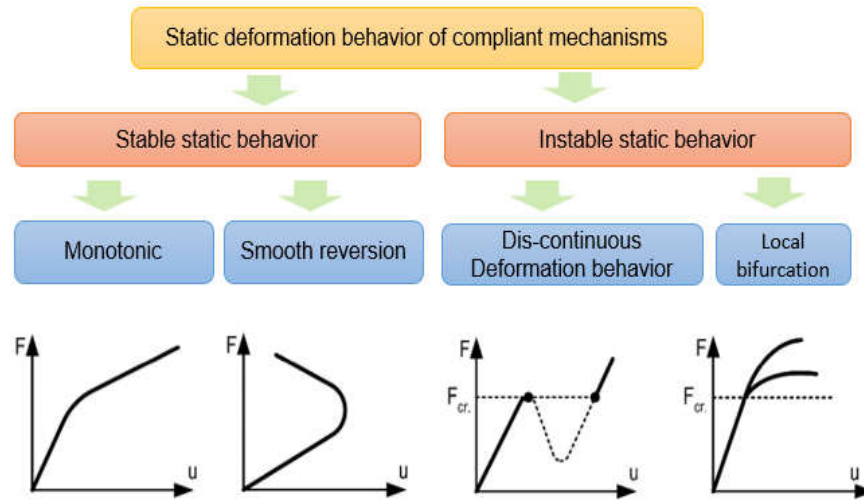


Figure 2. 3: Classified based on the static deformation of a structure [18].

2.1.2.3. Classification based on the association of the compliance and movement segments of the mechanism

Depending on the association of the compliant segments and the mechanism's motion, Prasanna et al. [19] have divided the compliant mechanism into two categories as follows: An Active compliant (refer to Figure 2. 4) and a passive compliant (see in Figure 2. 5).

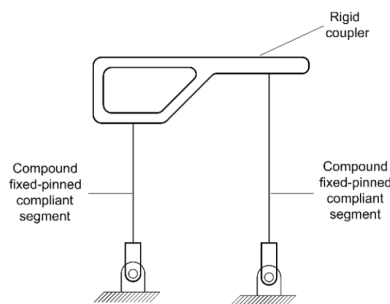


Figure 2. 4: A compliant active mechanism with two flexible segments [19].

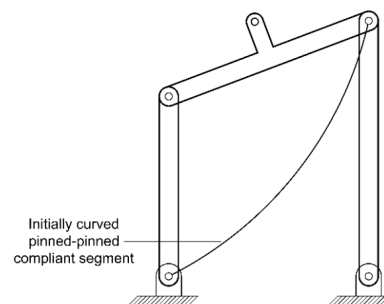


Figure 2. 5: A passive compliant mechanism with four rigid links and a flexible link [19].

2.1.2.4. Classified based on the function

Compliant mechanisms can also be classified based on the function they serve. According to Wu [20], CM can be categorized as inverters, compliant platforms, micro-grippers, positioning stages, and other types, as shown in Figure 2. 6(a-d).

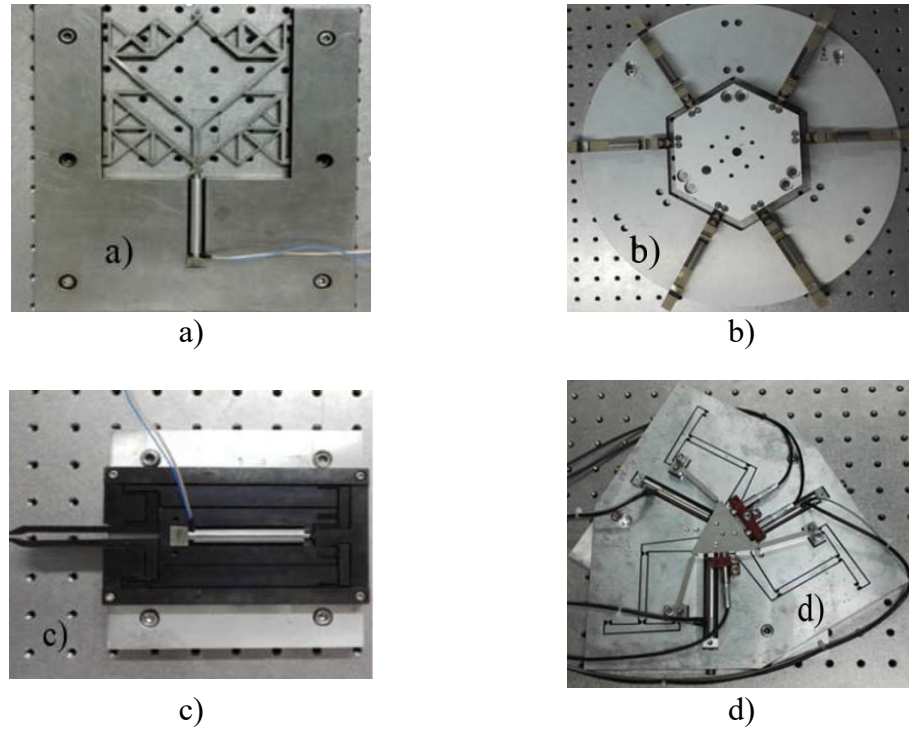


Figure 2. 6: Four types of typical CM : a) Inverter, b) Compliant platform, c) Microgripper, and d) Positioning stage [20].

2.1.3. Compliant joints or flexure hinges

A compliant joint can be named as a flexure hinge of a compliant mechanism. FH is a mechanical element that connects two rigid elements and allows them to rotate relative to each other through its bending ability [21]. In recent years, many types of flexible joints have been studied and developed. Paro et al. [22] built compliance equations and the approximate engineering formulas were proposed for the flexure hinge and right circular hinge. Later on, based on research by Paros et al. [22], the new configuration of flexure has been studied and developed. There are also some other outstanding studies that may be mentioned such as elliptical FH, circular FH [23], and corner-filletted FH [24]. In recent years, numerous studies have been conducted on elliptic-arc FH [25], conical-shaped notch FH [26], hybrid FHs [27],

and so on. Based on the applicability and geometry profile, FHs are classified into two main categories: simple type and complex type. In particular, simple joints are defined as including 1-axis, 2-axis, and multiple axes as shown in Figure 2. 7.

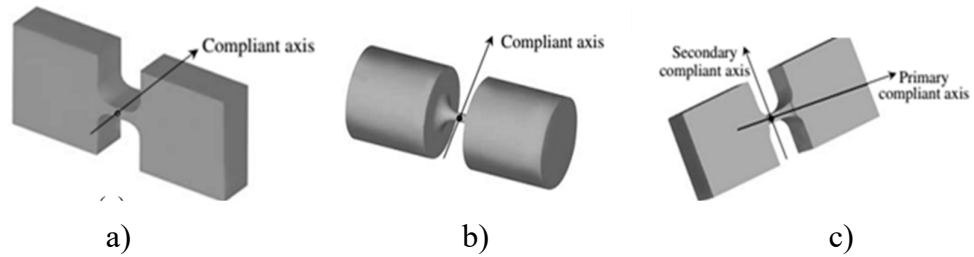


Figure 2. 7: Three principal categories of FH arrangements: a) Single-axis; b) Multiple-axis; c) Two-axis [28].

The complex type is created by a combination of primitive FH as indicated in Figure 2. 8 [28].

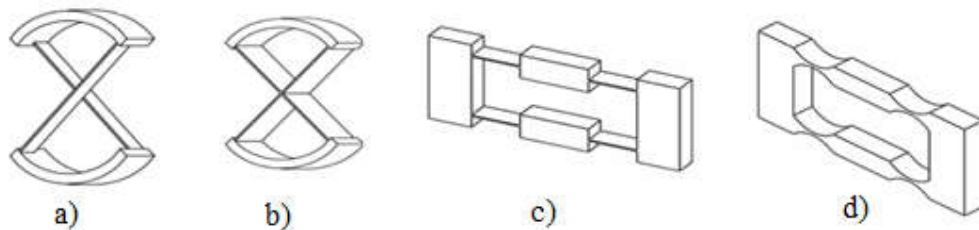


Figure 2. 8: Complex type of FHs: a) Cross hinge, b) Cartwheel hinge, c) Leaf spring, d) Hyperbolic hinge [28].

Each type of FHs has its scope of use, depending on its structure and operating range. However, FH with a simple structure is chosen, as shown in Figure 2. 9.

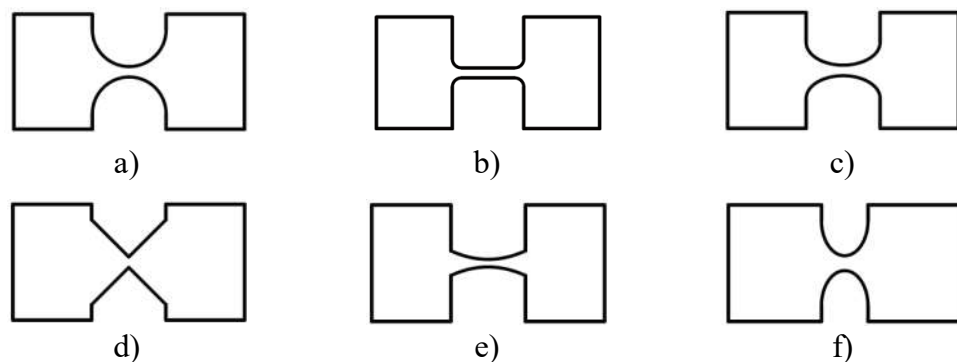


Figure 2. 9: Flexure hinges with notch shape [29]: a) Circular hinge, b) Filleted leaf hinge, c) Elliptical hinge, d) V shape hinge, e) Hyperbolic hinge, f) Parabolic hinge.

In the present dissertation, two types of compliant grippers have been proposed for use in the assembly industry. Operations such as gripping, positioning, and releasing an object are performed repeatedly and repeatedly throughout its lifespan. For the proposed grippers, FHs should be selected appropriately. Based on the research results shown in references [30]–[32], It is remarked that the leaf hinge with a rectangular cross-section is the most suitable choice to build the compliant grippers due to the following reasons:

- It is capable of generating a large deformation. This gives the proposed design a more flexible working range.
- The center of rotation of the leaf hinge is continuously variable and distributed over the length. This feature helps to limit the generation of concentrated stresses. This means that filleted leaf hinges are more durable than other forms.
- It has a simple structure and is easy to be manufactured.

2.2. Actuators

Actuators are employed to generate the CM's motions in precision engineering. CM are flexible structures that are designed to produce motion and force without traditional joints or bearings. Instead, they rely on the deformation of their flexible components to create movement. Actuators are used in CM to control and manipulate this deformation to achieve specific outputs. Some common types of actuators in CM can be listed such as piezoelectric, electrostrictive, magnetostrictive, shape memory alloy, and pneumatic actuators [33]. These actuators provide a means of driving the motion of the compliant mechanism in a controlled and precise manner. The selection of an appropriate actuator depends on the specific requirements of the compliant mechanism, such as the required force, displacement, speed, and frequency. Figure 2. 10 illustrated several types of actuators that are commonly used in the compliant mechanism field.

The choice of the actuator depends on the specific application and the desired performance characteristics, such as force, speed, precision, and durability. It can be seen that actuators such as magnetostrictive actuators, and pneumatic actuators are bulky in structure. Micro-scale CM can incorporate electrostrictive actuators and

SMA actuators using microelectromechanical systems (MEMS) fabrication. However, Piezoelectric actuators (PEA) are commonly used for actuating CM due to their compact size, ability to provide continuous and small motion with high displacement accuracy, and high-frequency response.

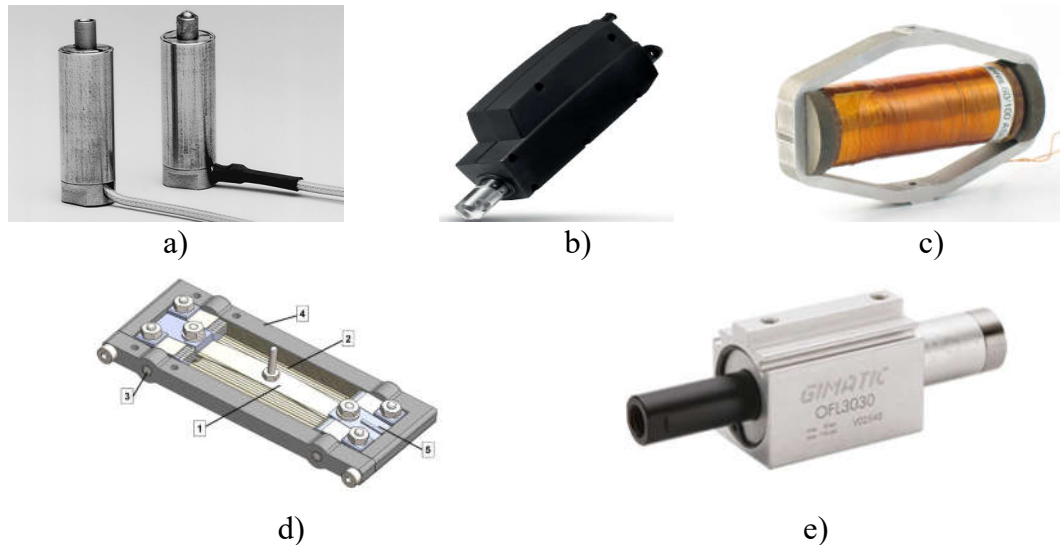


Figure 2. 10: Actuators: a) Piezoelectric actuators [34]; b) Electrostrictive actuators [35]; c) Magnetostrictive actuators [36]; d) Shape memory alloy (SMA) actuators [37]; and e) Pneumatic actuators [38].

2.3. Displacement amplification based on the compliant mechanism

Because FHs are developed based on the principle of deformation of the material. Therefore, its performance is limited by material properties. It can be seen that it is necessary to integrate a displacement amplifier to increase the working range of the device. However, a compliant mechanism is small and often designed to apply in narrow working spaces or harsh environments, so the integration of commercial displacement amplifiers being provided on the market no can be done. In recent years, CM was also used to design displacement amplifiers used for microactuator applications, sensors, MEMS, and especially in potential applications of the gripper to handle cylindrical objects.

Despite the availability of numerous design options for displacement amplifiers, many still rely on conventional structures [39]. This thesis presents some of the notable research studies on amplification structures.

2.3.1. Lever mechanism

A lever consists of a rigid beam that is placed on a fixed hinge or fulcrum [39], [40], as shown in Figure 2. 11.

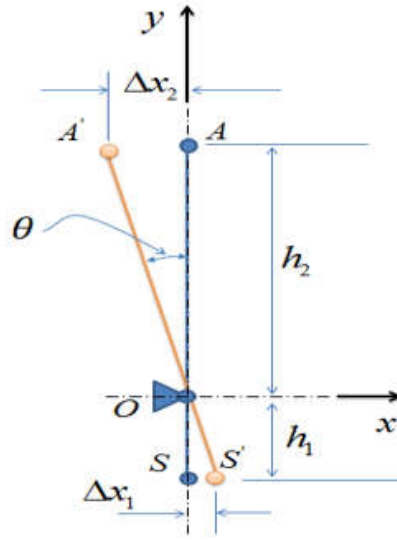


Figure 2. 11: Lever mechanism.

With, point O is a fixed hinge which is considered as the center of rotation of the lever, S is the input point and A is the output point.

The principle of operation of the lever is described as a reference [40] and it is calculated by the following equation:

$$r_{lever} = \frac{\Delta x_2}{\Delta x_1} = \frac{h_2}{h_1} \quad (2. 1)$$

Usually, for simple lever mechanisms, less than ten times magnification is permitted [41]. Thus, to increase the magnification of the mechanism, a compound lever magnification mechanism can be a suitable choice, as shown in Figure 2. 12(a-d) [39], [42]–[44].

Several research findings from recent years may support this view. For example, the research results of Ho et al. [39], the lever structure in this study has an amplification of 7.63, as indicated in Figure 2. 12a. Xing et al. [42] developed an asymmetric gripper that has a displacement amplification ratio of 4.16 by utilizing a flexible parallel four-bar mechanism and a single lever mechanism, as shown in Figure 2. 12b.

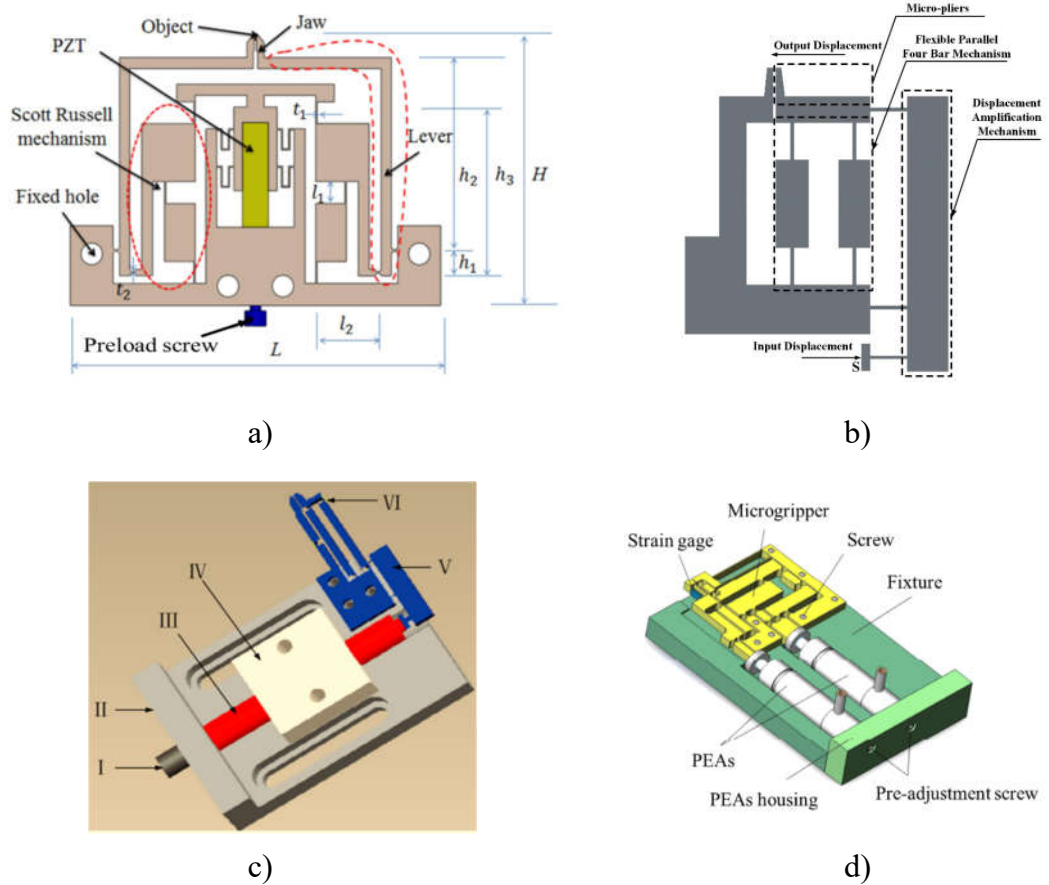


Figure 2. 12: Lever mechanism for in-compliant grippers: a) A hybrid amplifying structure [39]; b) Single lever mechanism [42]; c) Serial lever mechanisms [43]; d) Different lever mechanisms [44].

2.3.2. The Scott-Russell mechanism

The Scott-Russell mechanism is a device that can generate the exact straight motion of a point and is described as consisting of four bars [45], as shown in Figure 2. 13. In which, the length relationship is $DG = FG = EG = l$, $\angle DEF = \beta$, D is a fixed point, E is the input point and F is the output point.

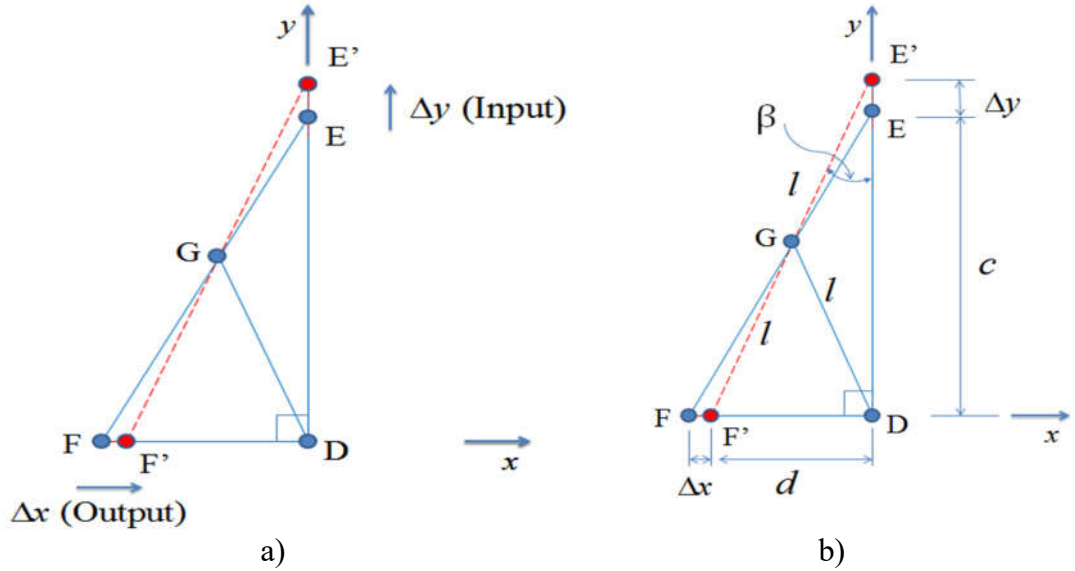


Figure 2. 13: Schematic of Scott-Russell mechanism: a) The principle of operation; b) Analysis of the amplification ratio.

The principle of operation of the Scott-Russell mechanism is determined by the following equation [45]:

$$r_{SR} = \frac{\Delta x_F}{\Delta y_E} \approx \frac{d\Delta x_F}{d\Delta y_E} = x'_F(\Delta y_E) = -\frac{y_E}{\sqrt{4l^2 - y_E^2}} = -\cot \beta \quad (2. 2)$$

or

$$\Delta x_F = -\Delta y_E \cot \beta \quad (2. 3)$$

Equation (2. 3) indicates that output displacement Δx_F is $\cot \beta$ times higher than input displacement Δy_E . And The change of displacement value Δy_E is responsible for the change in the value of Δx_F . In addition, Eq (2. 3) also implies that r_{SR} increases when the length of segment DF is smaller than DE. Signal “-” show a minus direction.

To improve the performance of the amplifier mechanism, this mechanism is also often combined with other magnifying mechanisms. For instance, Figure 2. 14(a) depicts how to create a gripper by combining the Scott-Russell mechanism and lever mechanism in sequence Sun [46]. The results of this study achieved the amplifier ratio of the design is 8 and 15.5 respectively before and after the combination. Similarly, Liu et al. established a connection between the parallel mechanism and the improved Scott-Russell mechanism [47]. They reported that the magnification ratio

of the enhanced Scott-Russell mechanism increased by 3.56 times in comparison to the conventional design. Ho et al have proposed a gripper with a hybrid displacement amplifier of Scott-Russell and a lever mechanism [39]. In this study, the amplifier ratio obtained is 20.6 times compared to the input displacement. Figure 2. 14(a, b) shows the application of the Scott-Russell mechanism in CG design.

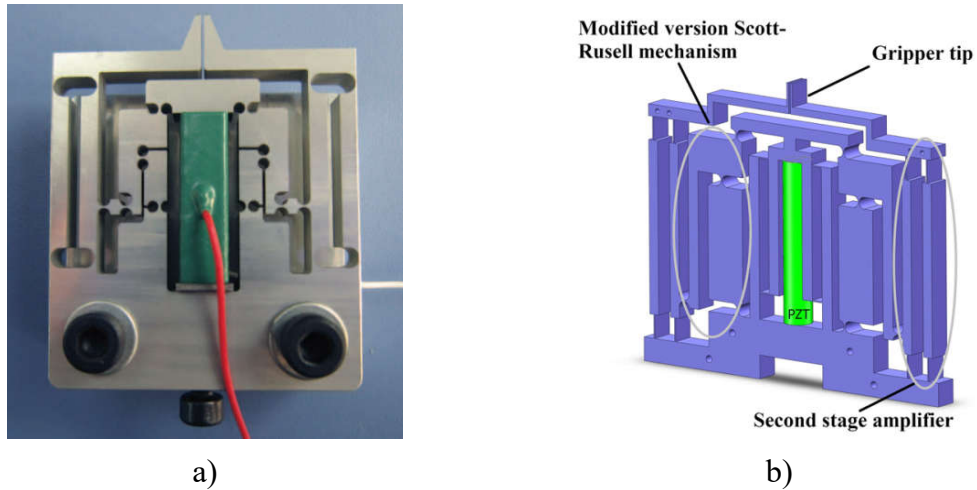


Figure 2. 14: Application of Scott-Russell mechanism in gripper design: a) Micro-gripper with Scott-Russell mechanism [46]; b) A large-range micro-gripper with Scott-Russell mechanism [47].

2.3.3. Bridge mechanism

Besides structures such as a lever or Scott-Russell, the bridge mechanism is also one of several structures that can be applied to displacement amplifier design. Figure 2. 15 show a schematic of a bridge-type mechanism and its analysis diagram [48].

The bridge-type mechanism is based on the instability of compression linkage in materials mechanics. When the input is applied, the flexible hinge deforms to move perpendicular to the input direction. To achieve significant motion amplification, rectangular or circular flexible hinges are typically employed in bridge amplification mechanisms. Compared to the lever mechanism, the bridge mechanism is more space-efficient for obtaining equivalent magnification, but it also involves a more complex displacement analysis model.

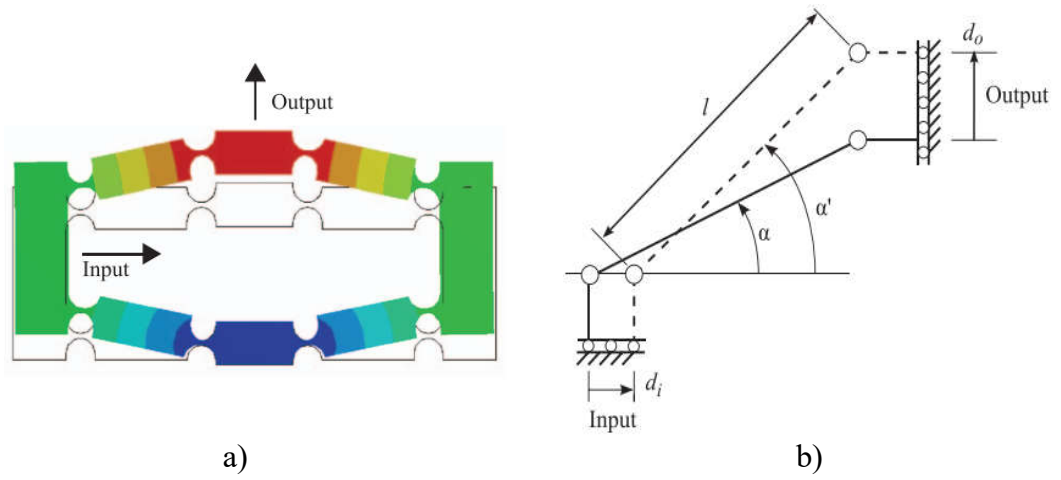


Figure 2. 15: Schematic of bridge mechanism: a) Displacement of bridge mechanism; b) Amplification factor analysis of a bridge mechanism. [48].

The displacement amplifier is determined by equation (2. 4) [48].

$$r_{SR} = \left(\sqrt{l^2 \sin^2 \alpha + d_i (2l \cos \alpha - d_i)} - l \sin \alpha \right) / d_i \quad (2. 4)$$

Besides using the full bridge mechanism, there have been studies that have investigated the use of grippers that utilize only half of the bridge mechanism, which reduces the space they occupy [49], referred to Figure 2. 16a. Additionally, the bridge structure may be joined in parallel or in series to provide a large clamping stroke. The restricted area is utilized by the series bridge mechanism to achieve a higher magnification ratio [50]. To make this clear, Chen and co-authors employed a series of connections of two bridge mechanisms to increase the stroke of the end-effector, as shown in Figure 2. 16b. On the other hand, according to reference [51], parallel bridge mechanisms typically have a common end that is fixed. Furthermore, Das developed a gripper that utilizes a bridge mechanism with double stairs to achieve a magnification of 19.3 for grasping and releasing tasks. Additionally, the bridge mechanism has been used in a multi-dimensional configuration by combining two or three bridges. This information is based on references [52] and [53], sequentially, as depicted in Figure 2. 16c and Figure 2. 16d.

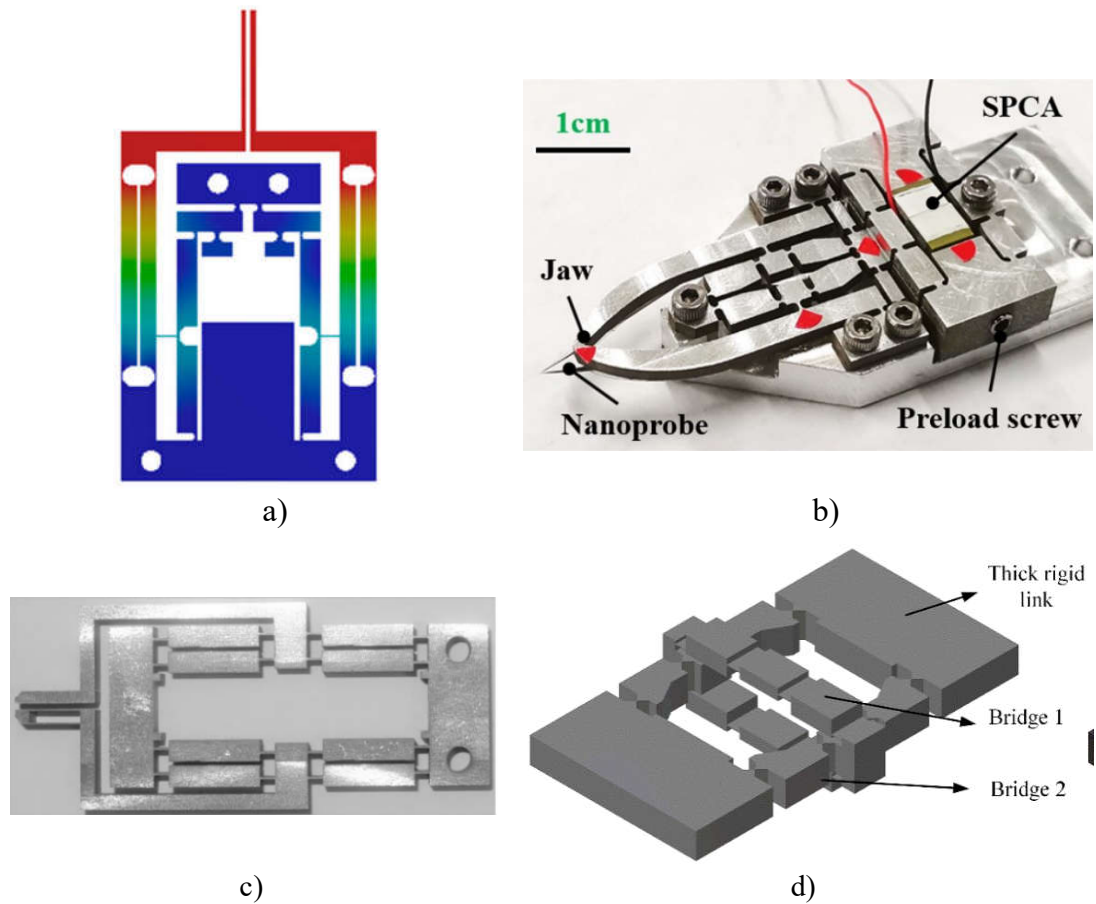


Figure 2. 16: Bridge mechanism for compliant grippers: a) Half of the bridge mechanism [49], b) Serial bridge mechanism [50], c) Two stage-bridge mechanism [52], d) Orthogonal bridge mechanism [53].

Of the mechanism listed above, each mechanism has its strengths and weaknesses. The choice of displacement amplifier depends on the specific needs and requirements of the design engineer. However, in this dissertation, the leverage structure is chosen because of the following outstanding advantages:

- **Amplification ratio:** The lever amplifier is capable of producing a higher amplification ratio than the Scott-Russell mechanism and bridge mechanism. This means that for a given input force, the Lever amplifier can produce a greater output force.
- **Efficiency:** The Lever amplifier is generally considered to be more efficient than the Scott-Russell mechanism and Bridge mechanism. This is because it has fewer moving parts, which reduces friction and energy loss.

- Size: The lever amplifier is typically smaller and more compact than the Scott-Russell mechanism and bridge mechanism. This can be advantageous if you have limited space or need to incorporate the mechanism into a smaller device.
- Cost: The cost of each mechanism will vary depending on the specific design and materials used. In general, the lever amplifier may be less expensive than the Scott-Russell mechanism and Bridge mechanism due to its simpler design and fewer moving parts.

2.4. Displacement sensors based on compliant mechanisms

As mentioned above, CM is commonly used in MEMS devices, precision positioning devices, precision grippers, etc. To limit the risks arising during the operation of devices based on CM, it is necessary to control the behavior of the position changes of the components of the device. A displacement sensor is utilized to identify the position variations of the device and converts them into electrical signals. As a result, the device can operate correctly and reliably hold the item. Some commonly used commercial sensors are presented as shown in Figure 2.17.

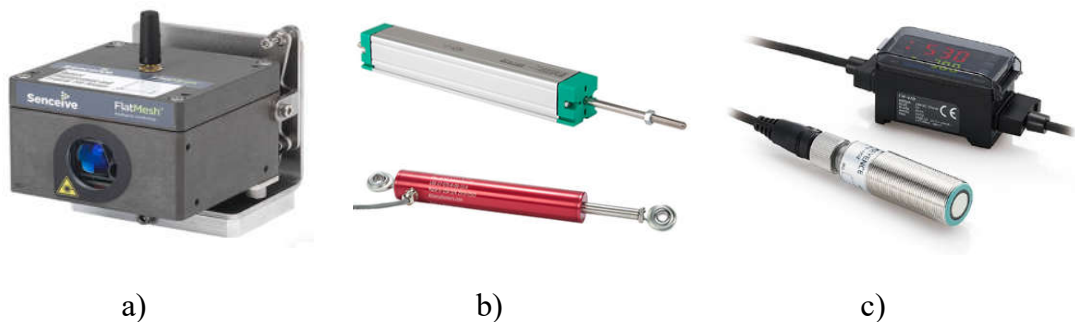


Figure 2.17: Commercial displacement sensors: a) Optical displacement sensors [54]; b) Linear proximity sensors [55]; and c) Ultrasonic displacement sensors [56].

Although commercial sensors have a very good resolution but their costs are high, especially in precision engineering. In recent years, with the great development of science and technology, electronic components are widely produced and supplied in the market. Research on integrating sensors into existing devices is possible. The field of compliant mechanism research is no exception. Up to now, there has been a lot of research on attaching electronic devices to parts of the compliance mechanism to

form an integrated sensor called “sensors based on compliant mechanisms”. Figure 2. 18 illustrates some sensors based on CM.

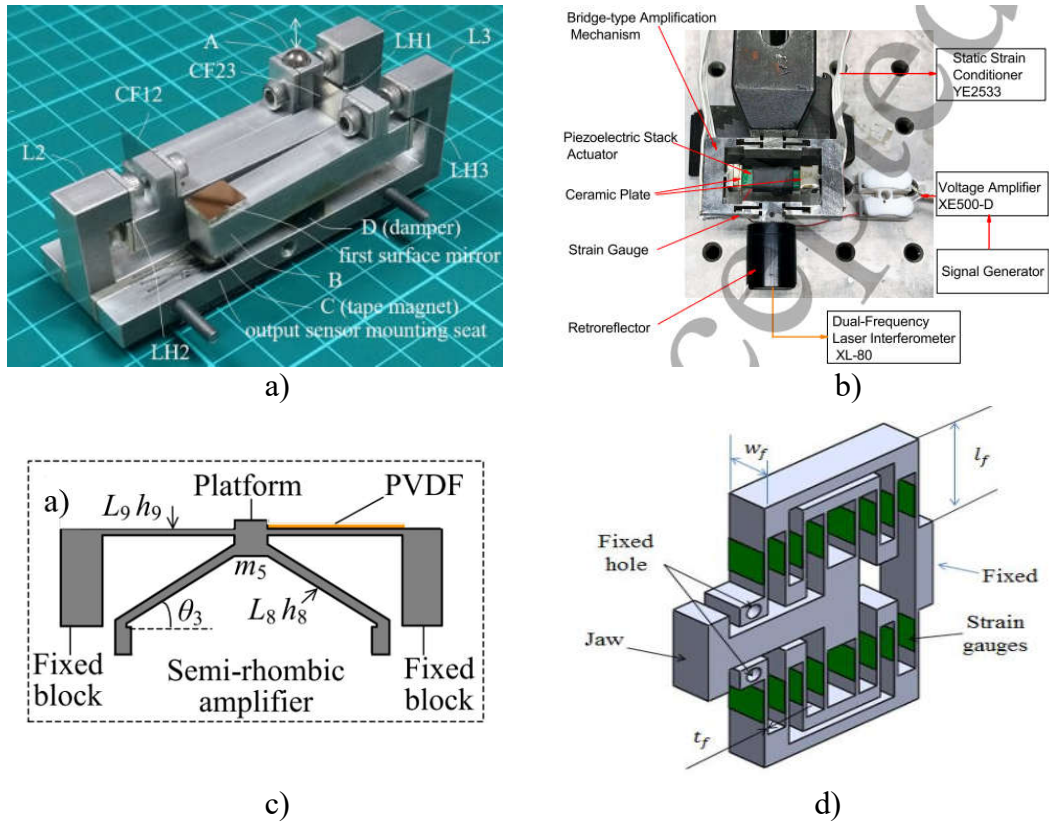


Figure 2. 18: Some displacement sensors-based mechanisms [57]–[60]: a) Micro-displacement sensors based on cascaded levers, b) A strain-based approach for multimode sensing, c) PVDF-based motion sensing, d) Strain gauge for direct displacement measurement

Dao et al. [61] developed a micro-displacement sensor via using strain gauges to measure the displacement. Chen et al. [57] devised a strain-based approach for multimode sensing, which utilizes a compound-compliant bridge-type amplification mechanism that combines multiple sensing units. By employing a consistent strain gauge configuration, this method achieves precise sensing of output displacement, input displacement, and input force across different modes. A compact flexure mechanism for XYZ movement, which employs piezoelectric actuation and includes an integrated displacement sensor based on polyvinylidene fluoride (PVDF), was developed by Ling et al. [58]. The sensing technique involves attaching a shaped

PVDF film onto the flexible guiding beams and utilizing the kinematic relationship of the clamped-sliding flexible beam, which is a commonly utilized approach in CM.

A micro displacement sensor was introduced by Ho et al. [59] in improving the grasping reliability of a CG by measuring directly the displacement or force. Most recently, a new contact-type micro-displacement sensor with sub-micron precision was designed and developed by Tsao et al. [60] at a significantly lower cost compared to commercial devices.

From an examination of previous studies, it can be seen that integrating displacement sensors into the CG can provide several important benefits such as:

- **Working space:** For some applications, the working space with the handle is very narrow or the working environment is harsh. Therefore, the use of commercial sensors is difficult. An integrated sensor is a suitable alternative.
- **Control and Precision:** Displacement sensors can be used to measure the position and movement of the gripper's jaws. This information can be fed back to a control system to ensure that the gripper is moving with the desired precision and accuracy. This can be especially important in applications where the gripper needs to grasp and manipulate delicate or fragile objects.
- **Force Feedback:** Compliant grippers are designed to provide a gentle and adaptable grip on objects, but it can be challenging to precisely control the amount of force being applied. By integrating displacement sensors, it is possible to measure the amount of force being applied to an object and adjust the gripper's motion accordingly. This can help to prevent damage to delicate objects or ensure that the gripper is applying enough force to hold objects securely.
- **Safety:** In some applications, it may be necessary to ensure that the gripper is not applying too much force to an object or that it is not accidentally colliding with other objects in the environment. By integrating displacement sensors, it is possible to monitor the position and movement of the gripper in real time and shut down the system if any abnormal conditions are detected.

Although, there are many advantages when it comes to integrating the

displacement sensors monolithically into the compliant gripper. However, the implementation depends on the structure of the grippers. In this dissertation, both options are applied. In it, the first proposed design, an asymmetric gripper, the technique of developing a monolithically integrated displacement sensor is introduced. The rest of the design is not included.

2.5. Compliant grippers based on embedded displacement sensors

A compliant gripper can be seen as an outstanding application of the compliant mechanism during its formation and development. The CG is widely applied in the biomedical, assembly industry, surgery, and so forth. According to the survey, regulated grippers can be divided into different types depending on their function and characteristics. However, in another aspect, it can also be classified into 2 types, with and without integrated supporting devices such as sensors.

Compliant grippers without built-in displacement sensors, these grippers typically do not have any feedback mechanism to measure the grip force or the position of the object in the gripper. As a result, they are often used in applications where the gripping force and position are not critical. Because, this can easily become the cause of damage to objects such as zebrafish egg cells [62], optical fiber [63], a shaft of a DC motor [12], etc. To meet production requirements, in some cases, sensors or control systems are used in conjunction with these grippers. However, it also has many difficulties. It could be due to an unsuitable environment, limited operating space, or cost issues.

To improve these problems, compliant grippers with integrated displacement/position or force sensors are developed. Unlike a gripper without a sensor, compliant grippers with an integrated displacement sensor have a feedback mechanism to measure the grip force and position of the object in the gripper. These grippers are typically used in applications where the gripping force and position are critical, such as in assembly or manufacturing processes. The integrated displacement sensor can provide precise measurements of the object's position in the gripper.

Economically, compliant grippers without an integrated displacement sensor are simpler and less expensive, but may not provide the level of precision required for

some tasks. Grippers with an integrated displacement sensor offer greater precision and control but are typically more complex and expensive. The choice of gripper will depend on the specific application and the level of precision required.

2.6. International and domestic research

2.6.1. Research works in the field by foreign scientists

2.6.1.1. Study on compliant mechanisms by foreign scientists

The development of compliance mechanisms began in the 1960s. However, it was not until the 1990s that the growth flourished with case studies.

In 1994, a method was introduced by Howell and Midha [64] to assist in the design of a certain type of compliant mechanism that features relatively rigid sections and small-length flexible sections, known as flexural pivots. In 2003, Lu and colleagues [65] described a systematic technique for synthesizing CM that transforms a specified curve or profiles into a target curve utilizing a minimal number of actuators. By utilizing the PRBM, Yu et al. [66] created a novel dynamic model of CM in 2005. In 2010, Awtar et al. [67] proposed a closed-form parametric model that accurately captures load-displacement relationships in two-dimensional beam flexures. This highly adaptable model accounts for the nonlinearities resulting from load equilibrium applied to a deformed arrangement. Ma et al. [68] put forth a novel approach for simulating significant deflections known as the chained beam-constraint model in 2016. This method involves dividing a flexible beam into multiple elements and modeling each element utilizing the beam-constraint model. A method for creating compliant mechanism topologies for spatial design cases based on the compliance ellipsoid was introduced by Nijssen et al. [69] in 2018. A survey conducted by Linß et al. [30] in 2019 offers various techniques for the general and simplified modeling of the elastic-kinematic properties of FHs and CM, covering four hinge contours. In their work, Chen and colleagues [70] introduced a versatile technique that effectively models significant planar deformations in uniform cross-sectional curved beams. This approach can be conveniently customized for use with curved beams of diverse geometries while maintaining a high degree of precision.

Wang et al. [71] developed compliant mechanism FHs for bridge-type structures in 2021. These hinges employ a flexure joint and are designed to offer a high

magnification ratio, minimal stress, and frictionless bending. Chen et al. [72] introduced a new compliant planar parallelogram mechanism in 2023 that utilizes 8 initially curved to achieve high-precision translational motion.

The above are just a few typical studies carried out by international scientists in the process of formation and development of CM. More information can be found in Refs. [7], [73].

2.6.1.2. Study on robotic grippers and compliant grippers by foreign scientists

Throughout the history of the robotics industry, there have been many types of grippers developed for application and application orientation in various fields such as agricultural harvest, biomedical, product sorting, packaging, and so on. In this section, some typical studies are introduced.

In 1998, Hujic et al. [74] integrated proximity sensors into grippers and created a dynamic system for predicting, planning, and executing the interception of objects. This method negates the need to constantly track the object's motion, a requirement of traditional tracking-based techniques that demand a steady reduction in the distance between the robot's end-effector and the object. By 2002, a robot system for harvesting lettuce plants was developed by Cho et al. [75]. They utilized Fuzzy logic control to determine the ideal grip force to be applied to lettuce plants. The input variables used were leaf area index and height, while voltage was used as the output variable for the fuzzy logic controller. In 2006, Molfino et al. [76] focused on how electro-mechanical products in the white industry can be assembled and disassembled more flexibly. They proposed an alternative approach for assembling and disassembling washing-machine components, using high-degree-of-freedom assembly cells with reconfigurable grippers capable of handling different components. Their study introduced a low-cost, multifunctional gripper designed for cylindrical and prismatic-shaped parts commonly found in washing machines (refer to Figure 2. 19a). While the gripper offers flexibility, it has limitations such as a complex structure with 4 degrees of freedom, noisy pneumatic actuators, and requiring a large operating space. Vacuum gripper research was carried out by Mantriota [77] in 2007, where they proposed a mathematical model to determine the contact forces between the suction cup and the object.

In 2010, Zahraee et al. [78] created a robotic hand-held surgical tool that improves the dexterity of laparoscopic interventions. This device provides two separate degrees of freedom (DoFs), which is adequate for performing minimally invasive surgery suturing procedures in living organisms. In 2012, Chen et al. conducted a study on an intelligent robotic gripper called i-Hand, which uses multiple small sensors (as shown in Figure 2. 19b). The gripper was designed for successful assembly tasks in an electronic manufacturing system. The research has several strengths: First, it overcomes the limitations of traditional robotic hands by effectively detecting the condition of assembled parts during assembly. The second, an online Fault Detection and Diagnosis (FDD) algorithm is proposed. Finally, different assembly situations are considered and handled based on an event-driven workflow. The proposed model and algorithm were proven effective through experiments. However, it can easily be seen that using the gripper with multiple sensors within a narrow range leads to system bloat and increased costs [79]. Traditional robotic hands face limitations in capturing cylindrical assemblies with precise posture in electronic manufacturing systems. To address this, in 2013, Cannella et al introduced a 4 DOF clamp design inspired by human hands. The gripper utilizes four DC motors, a control board, and a power supply, as illustrated in Figure 2. 19c. This gripper offers precise positioning, online twisting, and maintains a constant gripping force. However, the positioning of the main objects is highly dependent on the operator due to the complex structure of the complex structure with many mechanical components. The interaction of these moving parts can lead to operational problems [80]. In 2014, Tortora et al. [81] created a miniaturized robotic gripper to perform retraction tasks during minimally invasive surgeries. In 2017, Zhu et al. [82] presented a soft-bodied gripper design that incorporates curvature sensors for shape control. The soft gripper features three identical fingers, which are driven by fluid elastomer actuators. At the same time, Rosati et al. developed a cost-effective gripper with a variable aperture that can adapt to different handling needs without impacting the production system's cycle time as shown in Figure 2. 19d. The gripper incorporates an electrically-actuated mechanism for adjusting the aperture and a pneumatically-actuated mechanism for efficient open/close operations. Although designed with a complex structure with many

mechanical parts, gears, motors, and cylinders, the accuracy is less than 0.1mm when picking and locating objects from 5 to 105 mm in size. Simulations and initial tests demonstrated that this design enhances flexibility in robotized work cells without extending the cycle time [83].

In the early 2020s, The TWISTER Hand, a novel cable-driven underactuated robotic gripper, is introduced by Lee et al. [84]. It is specially designed to handle objects with different shapes, weights, sizes, and textures by utilizing each finger of the gripper, which consists of a compliant and continuum mechanism based on an origami design. In Wen et al.'s study, a dual robotic arm was employed in a smart factory to automate the assembly process of screws and nuts on a conveyor belt, as shown in Figure 2. 19e. They used mutual visual tracking and positioning technology to track the screw and nut assembly. The robotic arm was controlled in real-time using a geometric method based on a single-lens charge-coupled device. Fuzzy visual tracking control was utilized to grab the screw and nut. Despite an 8% tracking and positioning error, the dual robotic arms successfully completed the assembly. This study's establishment of mutual visual tracking and positioning technology for dual robotic arms can lead to efficient completion of assembly tasks in related fields in the future [85] (2021). In 2023, Qiu et al. [86] introduce a soft gripping system that is driven by tendons and specifically designed to handle blackberries, a delicate fruit that is prone to damage after being harvested.

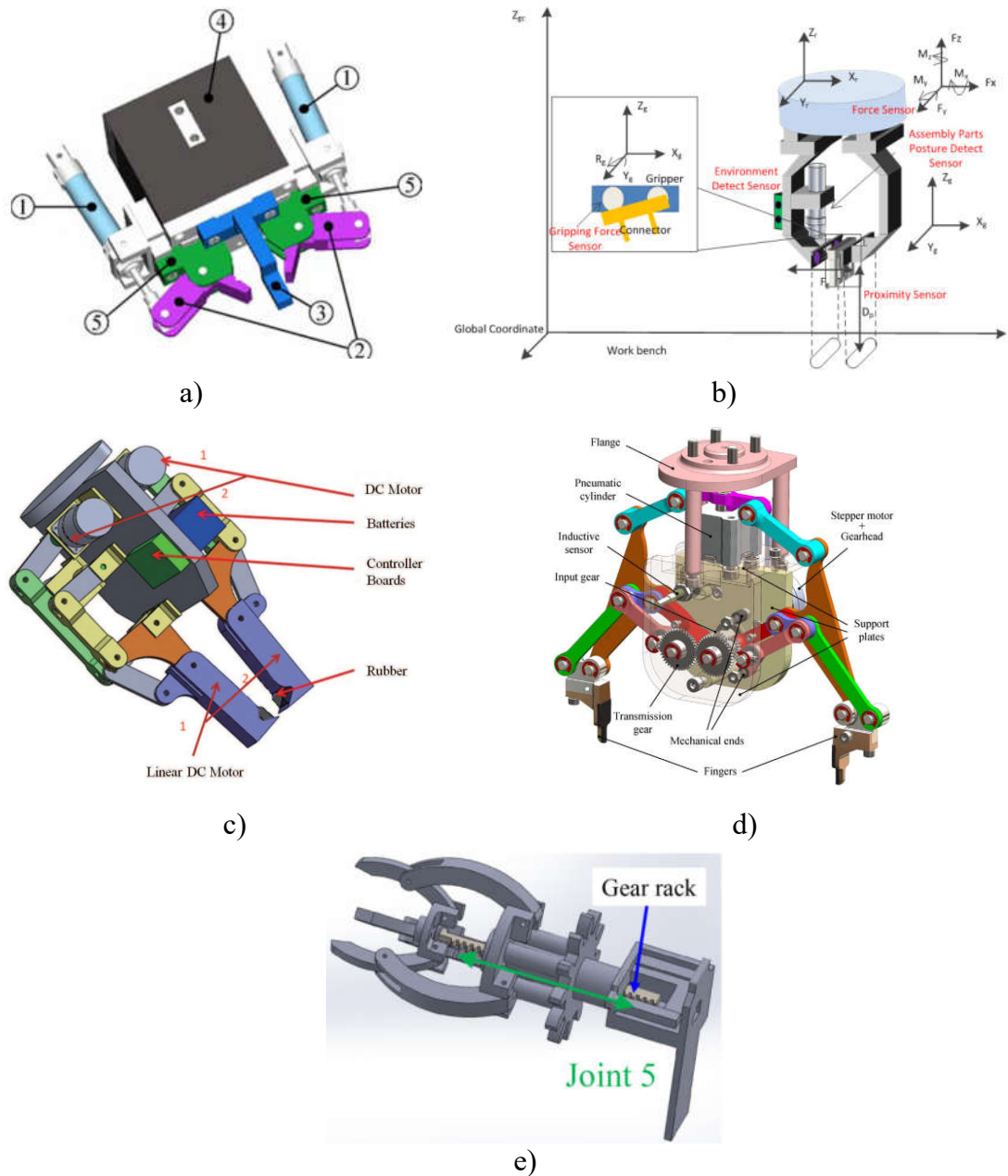


Figure 2. 19: Gripper applications for assembly systems: a) Multipurpose SPI3 gripper [76]; b) i-Hand [79]; c) 4-DOF gripper [80]; d) a variable-aperture gripper [83]; e) Three-jaw gripper [85].

Along with the development of traditional robotic grippers or soft grippers, compliant grippers are also interested in research by many scientists.

In 2013, Lee et al. conducted a comprehensive study on compliant insertion tasks in micro-assembly, presenting analytical, simulation, and experimental findings. The

study emphasized the importance of a compliant gripper (see Figure 2. 20) to address positional errors and prevent grip breakage during assembly. They derived an analytical model to analyze the motion and force profiles involved in compliant insertion. To implement this, thermal bimorph micro grippers with compliant tips were specifically designed and fabricated using a silicon DRIE process, and they were mounted on a precision motion stage. The researchers successfully performed a series of micro peg manipulation tasks, including pick up, rotation, and insertion. Additionally, they integrated a comb structure into the gripper to measure the deflection and calculate the insertion force, which is crucial for automated micro-assembly. However, it is important to acknowledge certain limitations of this design. Specifically, when operating at high temperatures, the epoxy layer may melt due to the generated actuator voltage, potentially damaging the gripper. Conversely, limiting the voltage to protect the clamps would result in reduced opening and closing of the jaws, thus failing to meet the design requirements [87].

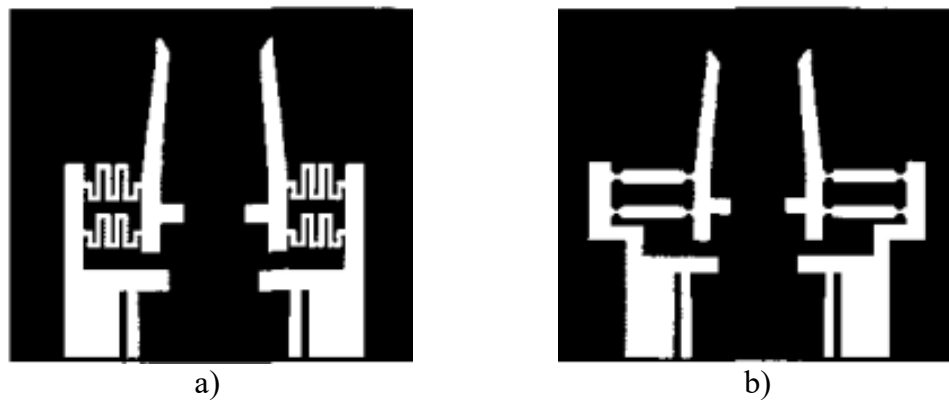


Figure 2. 20: Gripper tips with compliance structures [87]: a) Spring structures, and b) Flexure structures.

At the same time, Jain et al. introduced a novel multi-micromanipulation system design that utilizes ionic polymer metal composite (IPMC) micro grippers for robotic micro-assembly. The IPMC serves as a lightweight actuator for the development of the micro grippers, offering advantages such as large displacement, low mass force generation, and the ability to compensate for misalignment during micromanipulation. These capabilities are effectively employed in the handling of miniature parts, specifically pegs. The researchers conducted an analysis of the IPMC

micro gripper and manipulator to create a multi-micro manipulation system capable of shifting pegs between different hole positions within a large workspace. A prototype was developed to demonstrate the effectiveness of IPMC-based micro grippers in performing peg-in-hole assembly tasks within a multi-micro manipulation system (see Figure 2. 21). However, it should be noted that the jaws of this design exhibit low stiffness, resulting in significant deformation when gripping the peg. Consequently, the accuracy of gripping and positioning the peg center and hole center is compromised, achieving an approximate accuracy of only 68.42% [88], [89].

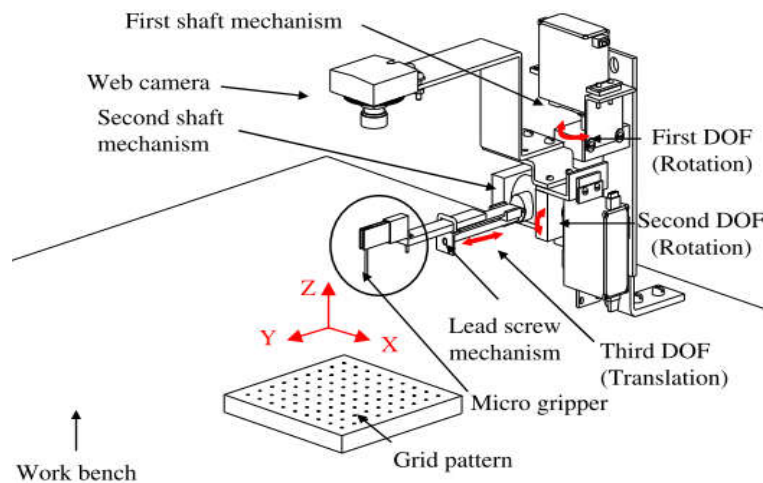


Figure 2. 21: Robotic Peg-in-hole Assembly [88], [89]

In 2014, Lu et al. introduced a monolithic 2-DOF flexure-based micro-gripper specifically designed for the grasp and rotation tasks involved in optical fiber assembly (refer to Figure 2. 22). The micro-gripper adopts an asymmetric structure where the left part is responsible for grasping, while the right part handles rotation. To enhance its performance in amplification ratio, the design of the right part incorporates a novel displacement amplification mechanism called the differential amplification mechanism. The dimensions of the flexure joints, links, and stress concentration of the micro-gripper are determined using the Pseudo Rigid Body Model methodology. Finite element analysis is conducted to validate the performance and optimize the parameters of the micro-gripper, resulting in a final version that exhibits high performance. However, despite the positive outcomes, the study does have some drawbacks such as: (i) the two clamps operate independently using separate piezoelectric sets which can lead to risks due to asynchronous movement of

the clamp; (ii) the model's complex structure introduces significant analytical errors (equivalent to 15%); (iii) the analysis method employed relies on a resource-intensive trial-and-error approach [44]. A year later, Jain et al. proposed a novel design of a multi-mobile micro manipulation system (MMS) that employs compliant bimorphs piezoelectric micro grippers for handling and grasping. The depicted model can be seen in Figure 2. 23. These grippers offer self-adjustment capabilities for peg misalignment during pick and place as well as peg-in-hole assembly. The bimorphs piezoelectric actuator enables bi-directional actuation, facilitating extended handling periods and generating high forces for grasping. The analysis conducted on the mobile MMS and piezoelectric micro gripper provides precise object positioning during robotic micro-assembly. Through the development of a prototype, it was demonstrated that compliant piezoelectric micro grippers are capable of handling diverse objects and performing multiple robotic micro-assembly tasks simultaneously within a large workspace. Similar to the previous study, the gripper exhibits significant jaw deformation (approximately 1.5 mm) when subjected to an applied voltage. Moreover, when the actuator voltage is reduced, the jaw deformation does not return to its original position, resulting in a hysteresis error of 0.2 mm. To mitigate this error by a factor of 10, a PD controller is employed. These observations underscore the operational challenges of this gripper, necessitating constant supervision from the operator [90].

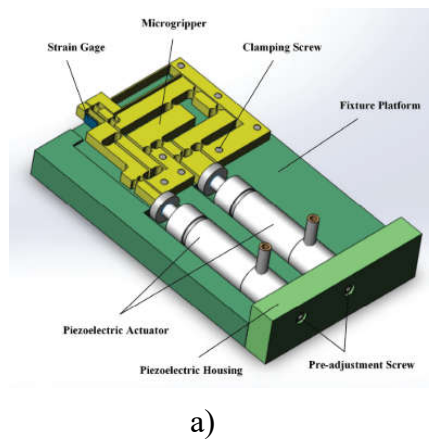


Figure 2. 22: Microgripper for optical fiber assembly [44]

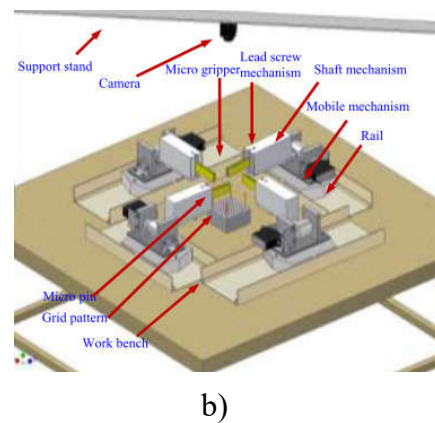


Figure 2. 23: Micro assembly by compliant piezoelectric micro grippers [90].

In 2017, Jiang et al [90] introduced a novel approach for automatically assembling large aircraft components such as canards and vertical tails, which involve large shafts. Their study presents a method that combines a 5 degrees of freedom spatial mechanism, compliance technology, and a servo feeding system to achieve precise shaft-hole assembly in aircraft manufacturing. They have developed experimental equipment with 5 degrees of freedom passive compliance and conducted tests to evaluate its performance. The test results demonstrate that the simulated nose blade can be automatically coupled, with a fit clearance of less than 0.05 mm between the nose blade shaft and bearing hole. However, it is evident that the system is designed with high complexity, and its assembly accuracy is suitable for objects with sizes in the range of hundreds of millimeters [91]. One year later, Nie et al. presented a novel robotic hand design specifically designed for assembly tasks. Their concept involved the combination of two grippers: an inner gripper for precise alignment and an outer gripper for stable holding. Unlike conventional robotic hands, which rely on complex compliant mechanisms, control strategies, and force sensing to perform assembly tasks, the proposed design offered a cost-effective solution for handling small objects like screws or washers. By leveraging the geometric constraints of the positioning fingers and the force of gravity, this design facilitated the alignment, picking up, and arrangement of various objects. Notably, it effectively addressed position errors associated with cylindrical objects or objects with cylindrical holes. The researchers conducted real-world tasks and quantitative analysis experiments to validate the aligning, picking, and arrangement capabilities of their design [92].

In the early 2020s, there were many studies on CG such as: Zhu et al. [93] discussed the development, modeling, production, and testing of a monolithic CG intended for micro-manipulation tasks. Zhang and Yan [94] presented a novel gripper that employs piezoelectric actuation to achieve precise micro-manipulation across a wide gripping range. The gripper is composed of an amplification mechanism, a guiding mechanism to make a constant force grasping. These elements enable the gripper to deliver substantial displacement output and consistent force output, allowing for high-precision manipulation of small objects. Qian et al [95] presented the design of a compliant piezo-driven gripper with micron-scale manipulation

capability and significant tip displacement, and so on. For a more comprehensive overview, references [7], [41] are considered useful resources. However, based on the survey results, there are no studies applicable to assembled systems.

All in all, the survey results show that despite numerous studies on compliance mechanisms, robotic grippers and compliant grippers have been published by researchers working outside of Vietnam throughout its history. However, an application-oriented CG for picking, positioning, and releasing objects with cylindrical profiles such as a vibrating motor "shaft and core" assembly system has never been demonstrated in actualization.

2.6.2. Research works in the field by domestic scientists

Though compliant mechanisms, robotic grippers, and compliant grippers have been researched and applied in many different fields. Research and development in these fields are facing significant challenges. Especially for Vietnam, the lack of laboratory equipment is one of the biggest challenges. However, it is still interesting to many domestic researchers. Below are some typical research projects.

2.6.2.1. Research on compliant mechanisms by domestic scientists

According to the survey results, there are currently very few research groups on CM in Vietnam. Specifically, until now there are only groups such as Pham's research group, Tran's research group, Dao's research group, Dang's research group, and Pham's research group.

This field has only just begun to be implemented by Vietnamese researchers since the 2010s. Specifically, Pham et al developed a compliant mechanism-based constant-force bistable micromechanism that can regulate force and provide overload protection in 2013 [96]. Dao and Huang [97] proposed a multi-objective optimization (MOO) design for a flexure-based mechanism with two degrees of freedom in 2016. In this study, the authors used a hybrid approach of the Grey-Taguchi coupled response surface method (RSM) and entropy measurement. In 2018, Tran et al. [98] proposed a threshold accelerometer that uses a compliant tristable mechanism to detect two distinct inertial signals when acceleration thresholds are exceeded along

one axis, illustrated in Figure 2. 24a.

In 2020, a comprehensive analysis of a flexure mechanism with damping factors was conducted by Nguyen et al. [99], which focused on its dynamic properties, especially its ability to generate small linear motion, introduced as Figure 2. 24b. In 2021, another author with the same name Nguyen et al. [100] proposed the best possible design for a flexible linear-guide used in a high-precision feed drive, shown as Figure 2. 24c. At the same time, Chau et al. [101] introduced a systematic computational method that is specifically designed to handle multiple-constrained optimization problems in CM with complex structures, indicated as Figure 2. 24(d). The proposed approach integrates statistics, numerical methods, computational intelligence, and optimization to achieve accurate and efficient results. This method offers practical benefits and can be widely applied in the field.

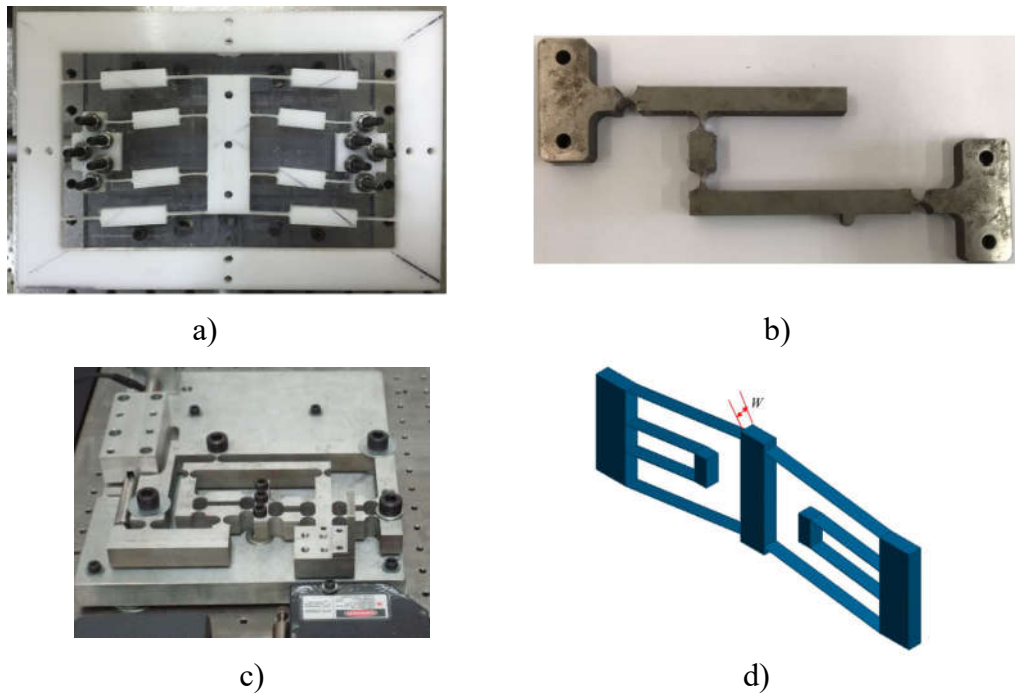


Figure 2. 24: A few studies on CM were done by Vietnamese scientists: a) A tristable mechanism [98]; b) A damping compliant mechanism [99]; c) A compliant linear mechanism [100]; d) Bistable compliant mechanism [101].

2.6.2.2. Research on robotic grippers and compliant grippers by domestic scientists

The robotic gripper industry in Vietnam is still quite new and there is not much

specific historical information about its development. However, in recent years, this industry has developed significantly thanks to the increase in research and application of technology in the production and fabrication of robotic grippers. Below are some typical studies conducted by researchers in domestic.

In 2016, Anh et al. [102] developed a 3-degree-of-freedom robot manipulator system capable of physically playing chess with a human. The system consists of three essential elements: A visual Studio-developed computer vision software that detects chess moves, a chess program that identifies the optimal response, and a robotic arm that physically executes the move on a physical chessboard. The research used a robotic arm for transferring heavy workpieces during the hot extrusion forging process [103]. In 2017, Think et al. [104] proposed a self-feeding system called FeedBot, designed for individuals who are unable to use their arms for self-feeding, particularly Parkinson's patients. Hung and Loc [105] suggested a control approach for a mobile welding robot that combines a kinematic controller and an integral sliding mode controller to accurately follow a desired welding trajectory

In 2020, a robotic system for self-directed pineapple harvesting was created for harvesting by Anh et al. [106]. Pham et al. [107] designed a robotic harvesting system for lettuce in hydroponic farms that employs computer vision technology. Dang et al. [108] designed and developed a soft robotic gripper with four pneumatic actuators made of hyperelastic material in 2021. The gripper has a two-degree-of-freedom mechanism for convenient up-and-down and left-and-right movement. It can handle objects up to 8 cm in geometric limit and up to 300 grams in gripping mass. Le et al. [109] introduced two distinct patterned profiles for pneumatic soft fingers, which were tested for their ability to grasp objects using both three and four-fingered grippers.

In 2022, a robot hand with two symmetrical groups of hybrid fingers that feature soft pads on their grasping interfaces was developed by Nguyen et al. [110]. The hand demonstrated the ability to grasp three distinct categories of objects: tea packs, toothbrushes, and mixing sticks. Another researcher with the same surname, Nguyen et al. [111] suggested a method that combines an algorithm and physical modeling to expedite the calculation process and develop an upper limb rehabilitation robot.

Figure 2. 25 describes some typical research results in recent times [106], [108]– [110].

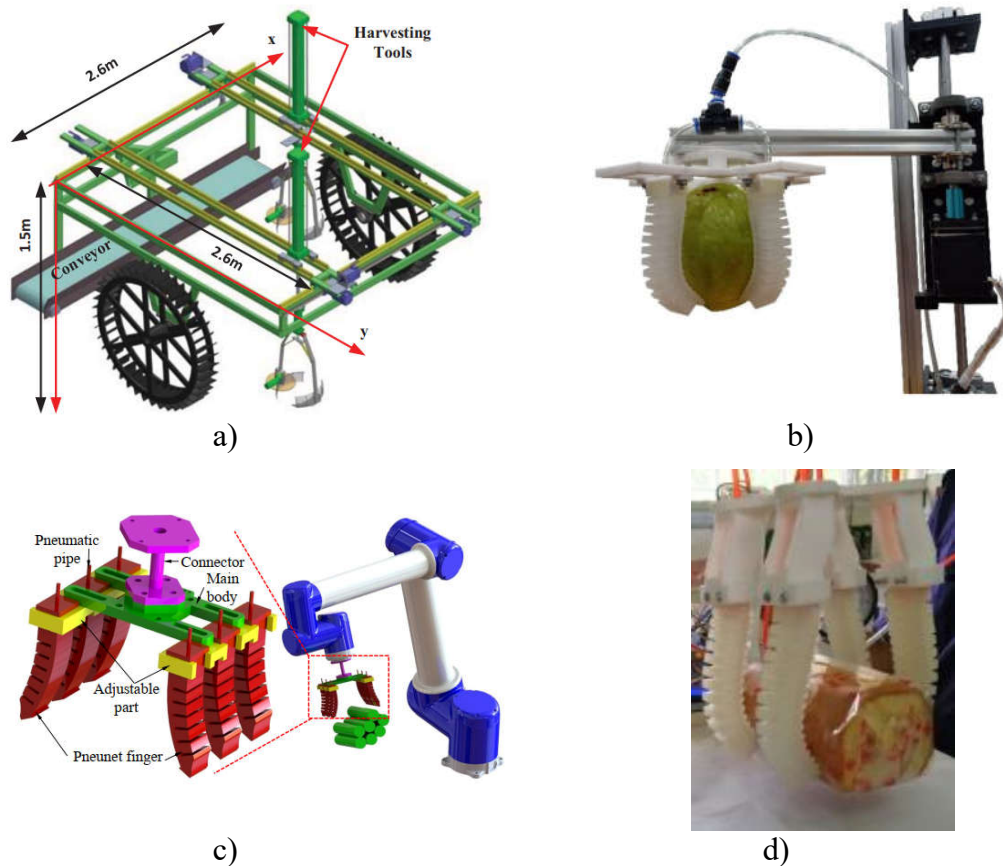


Figure 2. 25: Robotic gripper: a) Pineapple harvesting robot [106]; b) Food packaging system [108]; c) A Soft Pneumatic Finger [109]; c) A soft pneumatic hand for manipulating one group of objects [110].

Besides the research on the robotic gripper, CG has also been interesting in recent times, as shown in Figure 2. 26(a-f). In 2017, Dao et al. [112] proposed a novel method for the optimum design of a compliant microgripper (refer to Figure 2. 26a). To simultaneously improve displacement and frequency, the hybridization of the Taguchi method (TM) and the Differential evolution (DE) algorithm is implemented. Also this year, Lam et al [113] introduced a new micro gripper design that utilizes V-shaped electrothermal actuators for generating gripping force, as shown in Figure 2. 26b. Additionally, they incorporated a compliant mechanism into the design to enhance the displacements of the actuators.

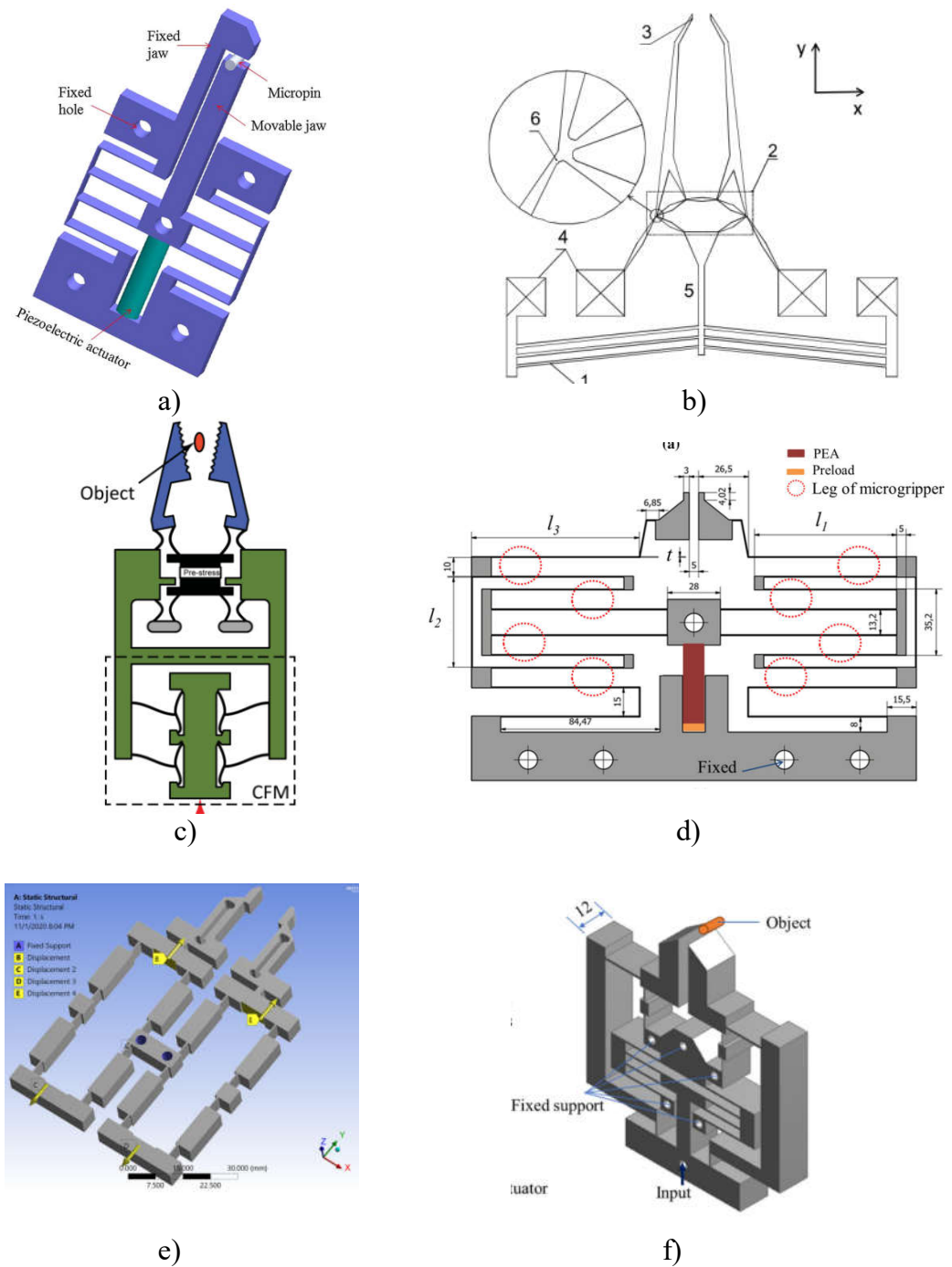


Figure 2. 26: Compliant grippers: a) Asymmetric CG [112]; b) Electrothermal CG [113]; c) Constant-force CG [114]; d) A sand crab-inspired CG [115]; e) Compliant CG [116]; f) A CG for advanced manufacturing application [117].

This innovative micro gripper can be effectively employed in micro devices such as micro-robots and micro assembling systems. One year later, Nguyen et al. [114] introduced a revolutionary design approach for a gripper that can manipulate objects

of different sizes while maintaining a constant gripping force by including a constant force mechanism, introduced in Figure 2. 26c. Then, Nguyen et al. [115] devised an innovative and effective hybrid algorithm for addressing the MOO design of a compliant microgripper that takes inspiration from the sand bubbler crab, as indicated in Figure 2. 26d. To perform a surrogate-assisted MOO, the researchers utilized a hybrid approach involving FEA, RSM, Kiging meta-model, and a multi-objective genetic algorithm. In 2021, Nguyen et al. [116] utilized a new bi-algorithm to design a compliant gripper, incorporating a multi-objective optimization design, illustrated in Figure 2. 26e. The recommended approach yielded more precise outcomes. In 2022, using an intelligent computing model, Nguyen et al. [117] introduced a novel design for a gripper that utilizes a symmetric structure and compliant mechanism to handle objects with a stable force, represented in Figure 2. 26f.

From the above survey results, it can be seen that the research on soft structures, robotic grippers, and compliant grippers in the country is still difficult, and the number of research works is still small. In particular, there have been no studies found on application studies for assembled systems. However, this is also a challenge and opportunity for young researchers in the future.

All in all, similar to survey results from studies conducted by international researchers, although there are also many publications on the compliant mechanism, robotic grippers, and compliant grippers, there has not been any research on developing grippers with the same function and application as the gripper proposed in this dissertation.

2.7. Summary

In this chapter, the following contents have been researched and synthesized.

The first is the concepts of compliant mechanism as well as the history, the classification of compliant mechanism is introduced in an overview. Furthermore, commonly used compliant FHs are also introduced.

Second, the concept of the actuator is presented, and some actuators that can be used for the compliant mechanism are listed. Next, the concepts of displacement amplifier and displacement sensor based on the CM are presented. Further, the reason

for integrating the displacement sensor into the gripper is presented and some related research results are also introduced to clarify the issue.

Finally, an overview survey of domestic and international research on the compliant mechanism, robotic grippers, and compliant grippers was carried out. The survey results show that there are still many opportunities for research on CM and applications in Vietnam.

Chapter 3 THEORETICAL FOUNDATIONS

In this chapter, some basic theories used to analyze, model, and optimize for compliant mechanisms are introduced. Regarding analytical methods, it includes methods such as the Taguchi method, Pseudo rigid body model, Lagrange method, Finite element method, Graphic design method, Vector method, and Statistical method. In terms of modeling, ANFIS is introduced as an effective tool used in the thesis. Relations to optimization, Metaheuristic algorithms, or intelligent optimization approaches are presented. In addition, statistical analysis techniques are also introduced to calculate the exact weight value and limit the search space for the optimization problem.

Compliant mechanisms are flexible structures that use the elastic deformation of materials to achieve mechanical functionality without the use of traditional joints, hinges, or bearings. To design compliance mechanisms, a variety of approaches can be used. Below is an overview of the main theoretical bases used for this thesis.

3.1. Design of experiments

Design of Experiments (DoE) is a statistical methodology used to plan, conduct, analyze, and interpret experiments. It is a systematic approach that allows to efficiently gather information, identify important factors, and understand the relationships between variables. The primary objective of DoE is to optimize the experimental process by minimizing the number of experiments required while maximizing the amount of useful information obtained. Commonly used methods for DoE such as Response surface methodology (RSM), Latin square design, Taguchi method, Full factorial design, and so on [118]. However, the Taguchi method (TM) [119] is often chosen to be used because of outstanding advantages such as [118], [120]:

- **Robustness:** The Taguchi method focuses on robust design, aiming to minimize the effects of noise factors.
- **Efficiency:** Taguchi designs, such as orthogonal arrays, allow for a reduced

number of experimental runs compared to full factorial or fractional factorial designs. This makes the Taguchi method more efficient in terms of time, cost, and resource requirements. It is particularly useful when there are limitations on the number of experiments that can be conducted.

- **Simplicity:** Taguchi designs are relatively easy to construct and implement. The orthogonal arrays provide a systematic and structured approach to determine the factor level combinations to be tested. This simplicity makes it accessible to designers who may not have extensive statistical knowledge or resources.

The TM is widely used for robust parameter designs [118], [120], [121]. To create a robust design, the TM suggests a three-stage process to achieve the desired product quality: (i) system design; (ii) parameter design; and (iii) tolerance design, as shown in Figure 3. 1.

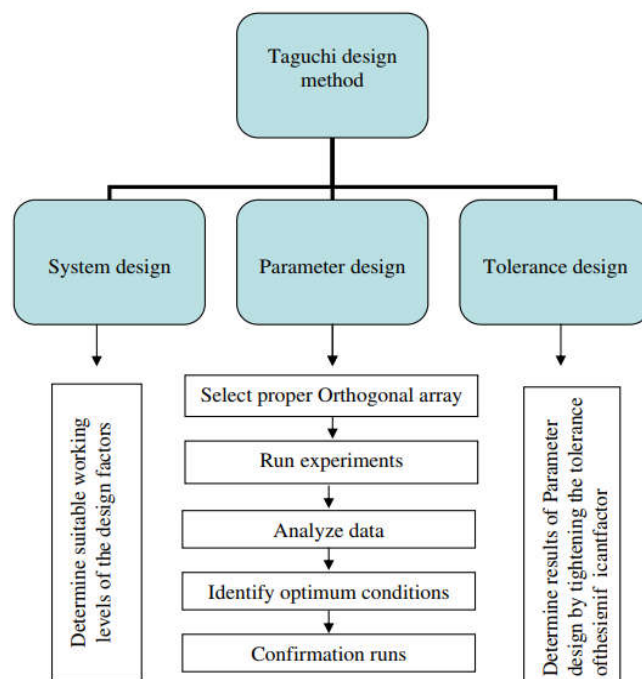


Figure 3. 1: Taguchi's experimental procedure [122].

- The system design is the process of choosing the technology and design which will reduce production costs and result in high-quality products. The parameter design refers to the selection process of the control factors and the determination of the optimal levels for each factor.

- The purpose of the parameter design is to find the most suitable factor levels so as to make a robust system that is less sensitive to variations in uncontrollable noise factors. There are two types of factors that affect a product's functional characteristics: control factors and noise factors. The control factors can easily be controlled, whereas the noise factors are either too difficult or impossible or expensive to control.
- The tolerance design process occurs after the parameter design and is used to reduce unwanted variations and improve quality. A better tolerance increases the product's cost or process because higher quality materials, components or machinery are needed.

Of the three design considerations, the TM primarily focuses on the parameter design because the use of this method can improve the quality and decrease costs while not requiring better materials, parts or production. The aim of the parameter design is to achieve minimum variations so the end product is consistently close to the desired target. The TM deals with the statistical and sensitivity analysis required in determining the optimum parameter settings and thereby achieving a robust quality response. The response to the parameter settings is considered as a measure that is not only the mean of the quality performance but also its variance. The mean and variance are then integrated into a single performance measure, known as the signal-to-noise (S/N) ratio. The Taguchi robust parameter design categories depend on the desired performance response, which is described as follows:

Smaller-the-better: S/N is defined as:

$$\eta = -10 \log \left(\frac{1}{q} \sum_{i=1}^q y_i^2 \right), \quad (3.1)$$

Larger-the-better: S/N is as:

$$\eta = -10 \log \left(\frac{1}{q} \sum_{i=1}^q \frac{1}{y_i^2} \right), \quad (3.2)$$

Nominal-the-best: S/N is characterized as:

$$\eta = -10 \log \left(\frac{1}{q} \sum_{i=1}^q (y_i - m)^2 \right), \quad (3.3)$$

where y represents the quality response; i is the number of an experiment; q is the number of experiment ‘ i ’ replications, and m denotes the desired response value.

With many outstanding advantages as above, this thesis chooses the Taguchi method as an effective tool to build experiments and applications in accurately calculating corresponding weight values for each design goal. In addition, TM is also applied in search space limitation techniques for optimization problems.

3.2. Modeling methods and approaches for compliant mechanisms

3.2.1. Analytical methods

In the study of CM, analysis of dynamic, and static analysis are two types of analysis used to study the behavior of mechanical systems. According to the statistical results of Ling et al. [123], the static and dynamic analysis of CM is mainly performed by the methods described in Figure 3. 2. Information on these analytical methods can be found in references [123].

In this thesis, the Pseudo-rigid-body model (PRBM), Lagrange method, Finite element method (FEM), and analytic method are proposed for modeling the static and kinetic analysis of the presented compliant grippers.

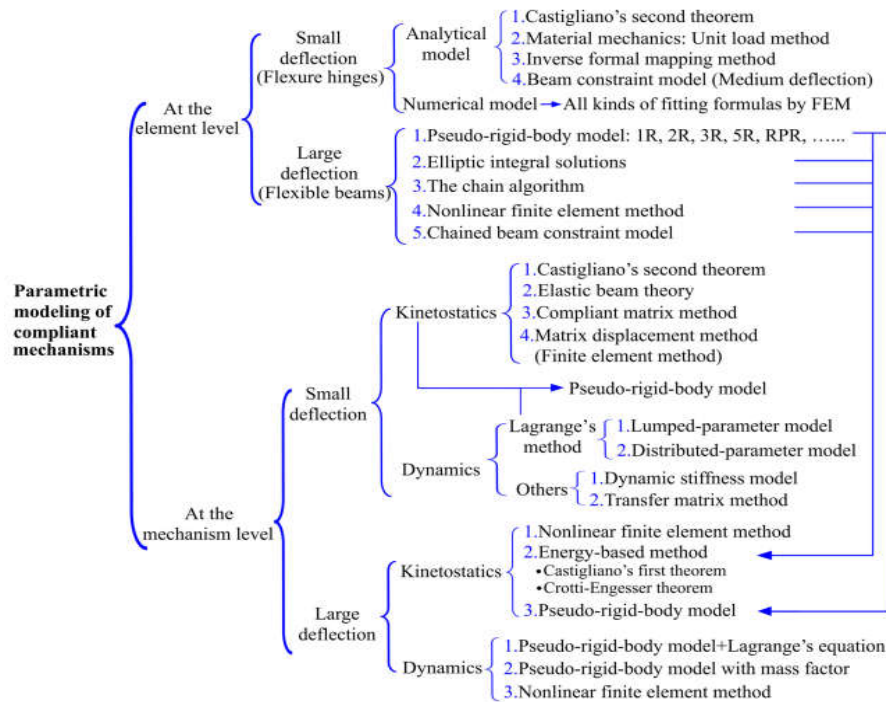


Figure 3. 2: Categorization of the kinetostatic and dynamic modeling strategies for CM [123].

3.2.1.1. *Pseudo-rigid-body model*

The pseudo-rigid-body model (PRBM) [16] is a theory used in the field of mechanical engineering to approximate the behavior of compliant mechanisms. The PRBM provides a simplified representation of a compliant mechanism by treating it as a series of rigid links connected by flexible elements, often referred to as flexures or springs. These flexures can deform under applied loads, allowing the mechanism to exhibit compliant behavior.

The basic principle behind the PRBM is that the flexures can be approximated as one-dimensional elements that only deform in the direction of applied forces. These flexures are typically assumed to behave linearly within their operating range. By modeling the flexures as equivalent linear springs, the compliance of the mechanism can be captured.

The key assumption of the PRBM is that the flexures do not deform out of plane, meaning they only bend or stretch along a single axis. This assumption simplifies the analysis and allows the mechanism to be modeled using standard rigid-body kinematics and dynamics principles. The compliance of the flexures is represented by equivalent stiffness values associated with each flexure.

Based on previous studies, it can be determined that the accuracy of this approximation can reach 99.5% [66], [124]. Recently, the PRBM has proven to be a valuable tool for the initial design and analysis of compliant mechanisms, providing insights into their performance before more detailed analysis or prototyping is undertaken [125]–[127]. Details of the PRBM method can be found in reference [16], however, summarized as follows:

According to Howell [16], a flexible beam with a length of l , as shown in Figure 3. 3, can be analyzed with an error of about 0.05% using the corresponding PRBM as shown in Figure 3. 4. The PRBM is composed of a massless rigid-body link with length γl and a torsion spring with constant K at the pin joint. It is known that:

$$K = \gamma K_{\theta} \frac{EI}{l} \quad (3. 4)$$

where γ is the characteristic radius factor, K is the stiffness coefficient, E is Young's modulus of the material, and I is the area moment of inertia of the beam. There is an

approximately linear relationship between the beam end angle, θ_0 , in Figure 3. 3 and the pseudo-rigid-body angle, Θ , in Figure 3. 4 as:

$$\theta_0 = c_\Theta \times \Theta, \quad (3. 5)$$

where the constant c_Θ is termed the parametric angle coefficient.

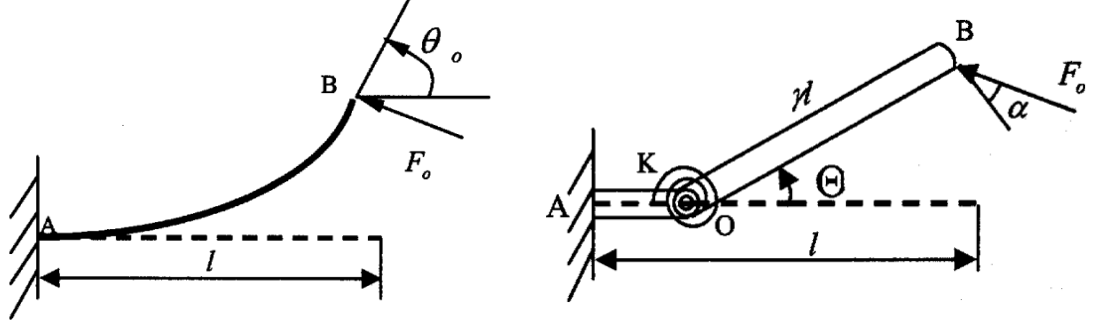


Figure 3. 3: A cantilever beam [66]. **Figure 3. 4:** PRBM of a cantilever beam [66].

In this dissertation, PRBM is used to analyze the behavior of a compliant gripper.

Details of the PRBM can be found in reference [128].

3.2.1.2. Lagrange-based dynamic modeling approaches

Assuming the object to be studied has a total mass of M , the kinetic energy T is defined as:

$$T = \frac{1}{2} M \dot{y}^2, \quad (3. 6)$$

where y denotes input displacement

The potential energy V involved in “ n ” torsional springs of FHs is computed by:

$$V = n \times \frac{1}{2} K_{ds} \theta_z^2, \quad (3. 7)$$

where K_{ds} presents the dynamic stiffness of each torsional spring, θ_z is the rotational angle along the z -axis.

The dynamic equation is determined by Lagrange’s equation [66]:

$$\frac{d}{d_t} \left(\frac{\partial T}{\partial \dot{y}} \right) - \frac{\partial T}{\partial y} + \frac{\partial V}{\partial y} = Q, \quad (3. 8)$$

where Q is the generalized force acting to produce a change in coordinate y .

Eq. (3. 8) is equivalent as below:

$$M \ddot{y} + K_{ds} y = P, \quad (3. 9)$$

This is a typical second-order differential equation of the undamped vibration system. The natural frequency of the system can be obtained as:

$$f = \frac{1}{2\pi} \sqrt{\frac{K_{ds}}{M}}, \quad (3.10)$$

It should be noted that although the effect of dumping, especially the viscoelastic behavior, has not been included in the dynamic equation of the compliance mechanism due to its complexity. In addition, the displacement sensor/grippers work with micro-displacements. Therefore, the effect of the damping phenomenon is not large. Therefore, this study ignores the influence of damping due to the hysteresis of the material structure and structure.

These equations help engineers and researchers can gain insights into the motion, forces, and energy dynamics of compliant mechanisms. This information is essential for design optimization, control strategies, and overall performance evaluation of compliant mechanisms in diverse applications, such as robotics, aerospace, and biomedical engineering. In addition, the use of this equation is simple, it is suitable for modeling complex structures. This is the reason why the Lagrange equation was chosen to be used in this thesis. Details of Lagrange's equation can be found in reference [66].

3.2.1.3. Finite Element Method

The Finite Element Method (FEM) is a computer approach used to provide approximative answers. It is used to solve complex engineering and mathematical problems by dividing them into smaller, simpler elements. FEM is widely employed in various fields such as structural analysis, heat transfer, fluid dynamics, electromagnetics, and many others [129]. In this thesis, a nonlinear finite element analysis (FEA) in ANSYS software was utilized to analyze the object's static and dynamic behavior. Through this analysis, the position of the strain gauge is determined. In addition, the results obtained through dynamic and static analysis are also used to evaluate the accuracy and effectiveness of the proposed methods.

The implementation process with 03 steps includes preprocessing, solution, and post-processing as diagrammed as shown in Figure 3. 5.

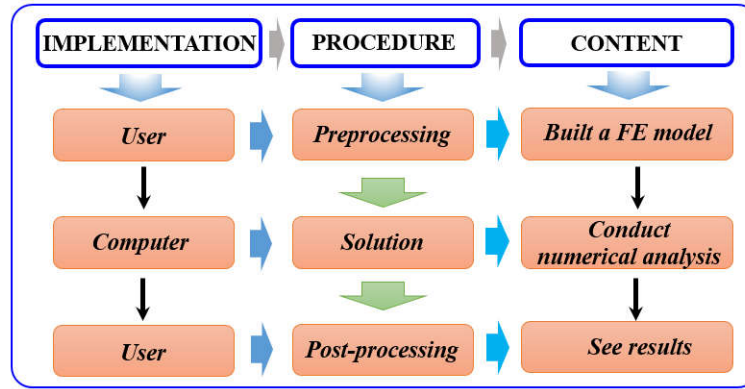


Figure 3. 5: Typical FEA procedure by commercial software.

During the analysis, some of the following relationships were used:

- Force-displacement relationship

$$\{F\} = [K]\{U\} \quad (3. 11)$$

$\{F\}$, $[K]$, and $\{U\}$ are loads, stiffness matrix, and displacement, consecutively.

- Stress-strain relationship

$$\sigma = E\varepsilon \quad (3. 12)$$

where σ , E , ε represent stress, Young's modulus of the material, and deformation, sequentially.

- Natural frequency:

$$[[K] - \omega^2 [M]]\{U\} = 0 \quad (3. 13)$$

where $[K]$, $[M]$, $\{U\}$ and ω^2 are stiffness matrix. Mass matrix, displacement matrix, and natural frequencies, sequentially.

3.2.1.4. *Graphic method, Vector method, and Mathematical analysis*

Besides using methods such as FEM, PRBM, and Lagrange's equation for dynamic and static analysis of CM. This study also uses methods such as the Graphic method, Vector method, and Mathematical analysis to describe the motion and behavior properties of the mechanism. Details of these methods can be found in reference [130].

3.2.2. **Data-driven modeling methods**

Dynamic and static analysis of CM is essential for their design, optimization, and

control. Besides the traditional approach, Data-driven methods, which use data to learn, model, and analyze systems, have become increasingly popular for dynamic and static analysis of CM. Currently, there are some commonly used data-driven techniques such as Artificial neural networks, Proper orthogonal decomposition, Gaussian mixture regression, extreme learning machine, K-nearest neighbors regression, and so on [131], [132].

Data-driven methods can provide valuable insights into the behavior of CM and help designers and engineers optimize their performance for specific applications. However, it is essential to emphasize that data-driven models are only as good as the quality and quantity of data used to train them. Therefore, careful experimentation and data collection are essential for the success of data-driven approaches for compliant mechanism analysis. In this thesis, an adaptive network-based fuzzy inference system (ANFIS), a modeling technique based on data-driven, is selected as a tool to support the optimization process because of the following advantages [133]: (i) Fast and accurate learning; (ii) Easy implementation; (iii) Capable of solving the complex nonlinear problem since it uses both artificial neural network and fuzzy logic. Below are the basics of ANFIS:

Adaptive network-based fuzzy inference system:

ANFIS was originally presented by Jang in 1993 [134]. ANFIS consists of a set of rules that describe the relationship between the input and output variables. These rules are expressed in the form of fuzzy IF-THEN statements. The ANFIS is a five-layer structure, as shown in Figure 3. 6.

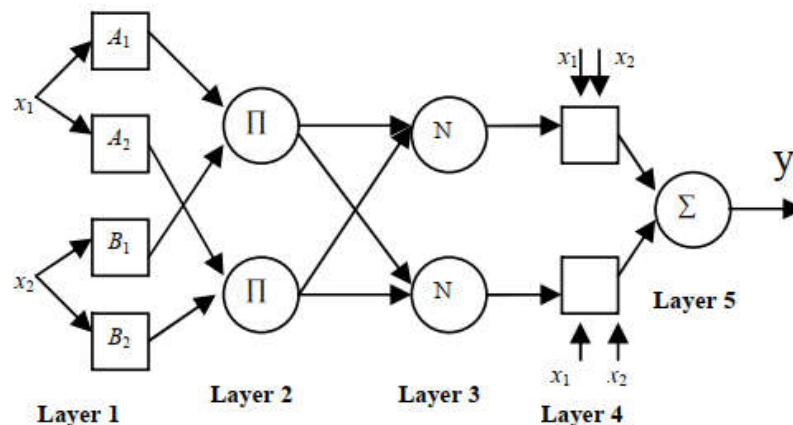


Figure 3. 6: Structure of ANFIS [135].

- (1) Layer 1 was believed to be the fuzzification layer, which fuzzified the inputs to determine the membership degrees for each input based on the fuzzy membership function provided. This layer's outputs can be identified as:

$$M_1^i = \mu_{A_i}(x) \quad (3.14)$$

where x indicates input to node i , and A_i presents the linguistic label associated with this node function. M_1^i illustrates the membership function of A_i .

- (2) Layer 2 consisted of the rule, a rule node, which collected inputs from the relevant fuzzification nodes and determined the firing strength of the rule. Each node in this layer is a circle node with the label Π . The output of each node represents the firing strength of a rule. It is equivalent to:

$$w_i = \mu_{A_i}(x) \times \mu_{A_i}(y) \dots i=1, 2, 3, \dots, N \quad (3.15)$$

- (3) Layer 3 is characterized as a normalized layer that assesses the ratio between the firing strength of a particular rule and the collective firing strengths of all rules. The layer comprises circular nodes represented as N symbols, with each node denoting a specific ratio. Specifically, the i^{th} node represents the ratio between the firing strength of the i^{th} rule and the total firing strengths of all rules, where \bar{w} represents the normalized firing strength of rules.

$$\bar{w} = \frac{w_i}{w_1 + w_2 + w_3, \dots, + w_n}, \quad i=1, 2, 3, \dots, N \quad (3.16)$$

- (4) The defuzzification layer, which takes in the initial inputs and produces the consequent parameters of the rule, is referred to as Layer 4. Each node in this layer, denoted by " i ", is a square node as:

$$M_1^i = \bar{w}_i f_i(px + qy, \dots, r), \quad i=1, 2, 3, \dots, N \quad (3.17)$$

where \bar{w}_i is the output of layer 3 and p, q, r are the parameter set.

- (5) Layer 5 consisted of a single node that computed the output as the total of all incoming signals, as seen below:

$$M_5^i = \sum_i \bar{w}_i f_i \frac{\sum w_i f_i}{w_i} \quad (3.18)$$

ANFIS training typically involves a hybrid procedure that combines the least squares method with a gradient descent algorithm. This procedure includes a forward and backward pass in each epoch. During the forward pass, input data is presented to the ANFIS, and the neuron outputs are calculated layer by layer. The least squares algorithm is used to compute the consequent parameters. Standard membership functions, including Gaussian, sigmoidal, triangular, trapezoidal, and bell types, are commonly used in ANFIS. However, choosing the most suitable membership functions can be difficult.

This dissertation employed the trapezoidal as a complete case study. The trapezoidal membership function is characterized as follows.

$$\mu_A(x, a, l, r, b) = \begin{cases} \frac{(x-a)}{(l-a)} & a \leq x \leq l \\ 1 & l < x < r \\ \frac{(x-b)}{(r-b)} & r \leq x \leq b \end{cases} \quad (3.19)$$

where μ_A represents the membership functions of the fuzzy set; a , b , l , and r denote parameters; and x is the variable.

More information on other data-driven techniques can be found in the reference [136].

3.2.3. Statistical methods

Statistical methods are a set of techniques and tools used for analyzing and interpreting data. Statistical methods enable researchers to draw meaningful inferences from data, test hypotheses, and make predictions. There are many statistical methods used to analyze data and make inferences based on sample data. Some commonly used statistical techniques may be listed as follows: Hypothesis testing [137], Regression analysis [138], analysis of variance (ANOVA) [139], T-tests [139], Chi-square tests [140], and so on. Method selection relies on the nature of the data and the nature of the problem being addressed. In this study, ANOVA can be used to examine the sensitivity of design parameters and demonstrate the significant contributions of each design factor to the quality output response. Using these findings, the design range for each parameter can be further fine-tuned. This

approach facilitates a more efficient and quicker convergence speed for the optimal process.

ANOVA's formula is defined by calculating a ratio F :

$$F = \frac{MST}{MSE} \quad (3.20)$$

where MST is the mean sum of squares attributable to treatment, whereas MSE is the mean sum of squares owing to error.

3.3. Optimization methods

Optimization of CM involves finding the best design parameters that can maximize performance while minimizing material usage and manufacturing complexity. Nikbakt et al. [141] have classified optimization problems into seven basic groups in terms of types of objective functions and design variables. Figure 3.7 provides a reference for these groups. Based on the characteristics of the optimization problem appearing in the above algorithms, the optimization problem is classified into 3 main groups Blind search algorithms, Heuristic search algorithms, and Meta-heuristic algorithms. For a visual representation of this classification, Figure 3.8 can be consulted.

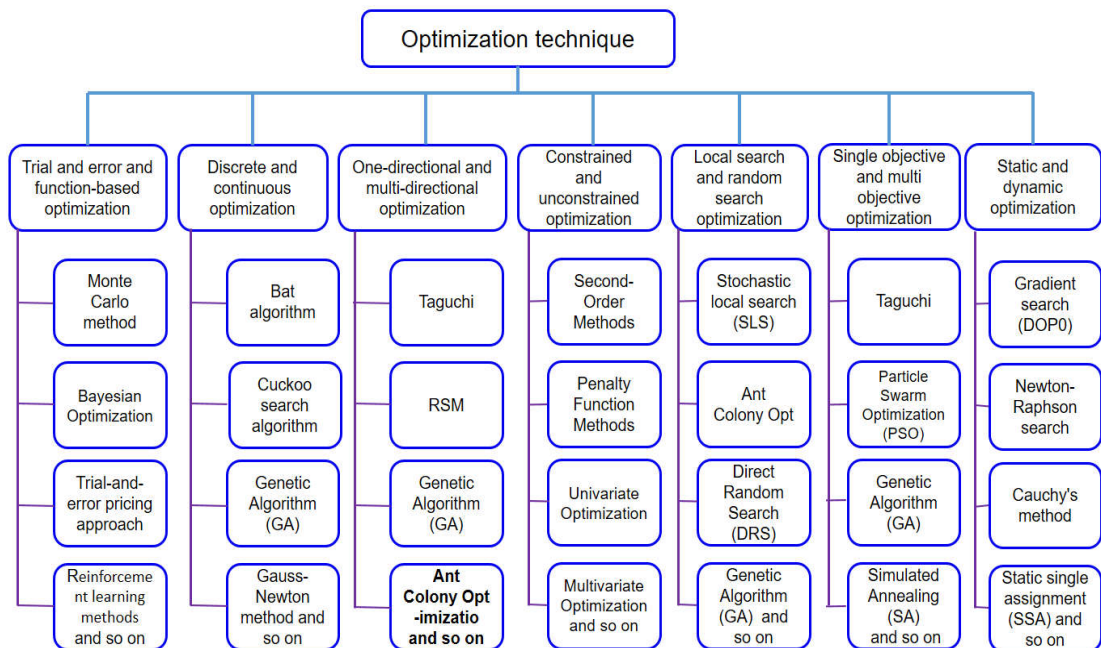


Figure 3.7: Classification of optimization techniques [141].

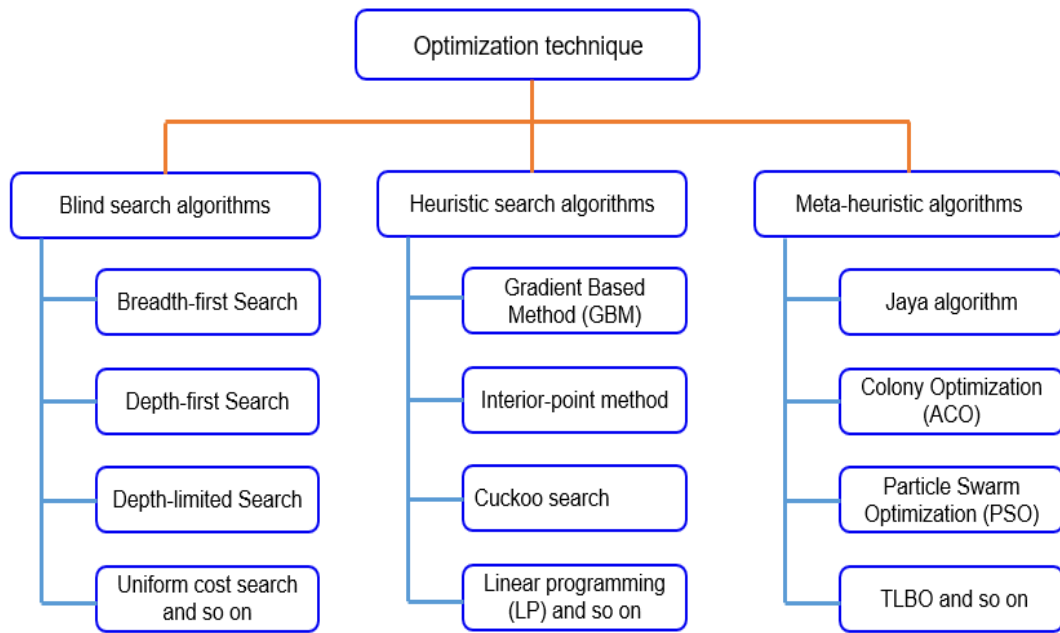


Figure 3. 8: Three main categories of optimization techniques.

These algorithms are all used in artificial intelligence and optimization problems. Each type of algorithm has its pros and cons (refer to Table 3. 1).

Table 3. 1: Blind search algorithms, heuristic search algorithms, and meta-heuristic algorithms.

Algorithm	Advantages	Disadvantages
Blind search	<ul style="list-style-type: none"> • Simple and easy to implement • Can be used for a wide range of problems • Guaranteed to find a solution if one exists within the search space 	<ul style="list-style-type: none"> • Highly inefficient for large search spaces • Cannot be used for problems with complex search spaces • Can become trapped in local optima and fail to find global optima
Heuristic search	<ul style="list-style-type: none"> • More efficient than blind search algorithms • Can be used for problems with complex search spaces 	<ul style="list-style-type: none"> • Can still get trapped in local optima and fail to find global optima

Algorithm	Advantages	Disadvantages
	<ul style="list-style-type: none"> • Can be customized to suit specific problem domains 	<ul style="list-style-type: none"> • Can be difficult to design and require significant domain knowledge • May not guarantee an optimal solution
Meta-heuristic	<ul style="list-style-type: none"> • Highly efficient and effective at finding good solutions • Can be used for problems with complex search spaces • Can handle multiple objectives and constraints 	<ul style="list-style-type: none"> • Can be difficult to implement and tune • May not guarantee an optimal solution • Can be computationally expensive for large search spaces

Based on the above analysis and the research objectives of this thesis, the author chooses metaheuristic algorithms as one of the effective tools to perform the optimization problem. In addition, to increase the efficiency of the design process, optimization calculation, and date-based optimization techniques are also used. The details of these two methods are introduced as follows:

3.3.1. Metaheuristic algorithms

Metaheuristic algorithms are a type of optimization algorithm that aims to obtain satisfactory solutions to intricate problems, which cannot be resolved by exact techniques. These algorithms are widely utilized in various fields, such as engineering, computer science, and other disciplines, to tackle problems with numerous variables or seek the best possible solution within an extensive search area [142]. Unlike traditional optimization algorithms, which rely on explicit mathematical models or rules to find a solution, metaheuristic algorithms use a more general, heuristic approach. They work by exploring the solution space and gradually improving the quality of the solutions over time, often by iteratively refining the solutions or by exploring new regions of the solution space. Some typical algorithms that are commonly used can be mentioned as GA [143], PSO [144], SA [145], Tabu

search [146], TLBO algorithm [147], Jaya [148], and so on.

All in all, metaheuristic algorithms can be very effective at finding good solutions to complex problems, particularly when traditional optimization methods are not feasible or practical.

3.3.2. Data-driven optimization

Data-driven optimization is a method of optimizing a process or system using data analysis techniques. The process involves collecting data from the system or process, analyzing the data to identify areas for improvement, and then implementing changes to optimize the system. This method is commonly used in industries such as engineering, finance, healthcare, and transportation. Data-based optimization involves several steps, including (i) Data collection, (ii) Data analysis, (iii) Optimization, (iv) Evaluation, and (iv) Continuous improvement [71], [149], [150]. Here are some methods for data-based optimization: TM [151], GRA [152], TLBO [153], ANFIS approach [137], Fuzzy logic in combination with TM [154], and so on. With many advantages such as easy implementation, fast convergence speed, can model of highly complex problems, etc.

In short, data-based optimization methods are powerful tools for solving complex problems in various fields. These methods are widely used because they can extract knowledge from data, model the relationships between variables, and optimize the performance of a system or process. However, these methods require careful consideration of data quality, model complexity, interpretability, and parameter tuning.

In this dissertation, TLBO, ANFIS, and Jaya techniques are used as effective tools. A brief overview of TLBO and Jaya is presented in Chapter 4 and Chapter 5, sequentially.

3.4. Weighting factors in multi-objective optimization problems

In multi-objective optimization problems (MOOPs), weight factor (WF) is used to balance the importance of different objectives [152], [155]. To use weighting factors in MOOPs, the first step is to identify the objectives of the problem. These objectives may be conflicting, and there may be no single solution that optimizes all of them simultaneously. The next step is to determine the relative importance of each

objective using weighting factors. This is typically done by assigning a weight to each objective that reflects its importance relative to the other objectives.

The weighting factors can be specified either by the decision maker or determined using a formal method. There are different methods for assigning weighting factors, e.g., direct assignment, minimal information method, eigenvector method, empty method, means of bivariate statistics, randomly determined [156]–[159], and so on. In this study, a weight calculation method is based on the proposed statistical method.

3.5. Summary

In this chapter, some basic theories used to analyze, model, and optimize the compliance mechanism have been introduced. In terms of analytical methods, there are methods such as the Taguchi method, Pseudo rigid body model, Lagrange method, finite element method, graphical method, vector method, and mathematical analysis. In terms of modeling, ANFIS is introduced as an effective tool. Regarding optimization, Metaheuristic algorithms and intelligent optimization methods were presented. In addition, statistical analysis techniques have also been introduced to accurately calculate the weight value and limit the search space for the optimization problem.

Chapter 4 DESIGN, ANALYSIS, AND OPTIMIZATION OF A DISPLACEMENT SENSOR FOR AN ASYMMETRICAL COMPLIANT GRIPPER

Chapter 4 presents a design and analysis of a displacement sensor that is embedded in an asymmetrical compliant gripper. The proposed sensor can directly measure the stroke of jaws. The force versus displacement of the sensor is analytically formulated. The dynamic equation is established using a PRBM and Lagrange's method. In enhancing the performances of the proposed sensor-integrated gripper, an optimization process is conducted by hybridization of TLBO and TM.

4.1. Research targets of displacement sensor for compliant gripper

In order to solve the direct measurement of the jaw's stroke of grippers, this chapter is aimed to consider two main issues as follows:

- The first target is to develop a displacement sensor being integrated into the gripper. This improves the economy and reduces bulkiness compared to grips that use commercial sensors. (Technical requirements of the proposed gripper will be presented in section 4.2.2.).
- The second target is to propose a new approach, which can be effectively applied to the process of analysis, design, and optimization of compliant grippers. In this approach, an exact weighted factor value calculation technique is also proposed.

To achieve these two goals, a design, calculation, and optimization process is outlined that includes three specific steps as follows: (i) Proposing design, describing operating principles and technical requirements of research objects. (ii) Displacement sensor behavior analysis. (iii) Implement the optimization process and evaluate the results.

4.2. Structural design of proposed displacement sensor

Based on the experience of the designer as well as related studies, the mechanical design of the displacement sensor is proposed as shown in Figure 4. 1 with initial design parameters as shown in Table 4. 1[152], and the technical requirements as well as the operating principle are developed by Ho et al. [160].

4.2.1. Mechanical design and working principle of a proposed displacement sensor

4.2.1.1. Description of structure of displacement sensor

A displacement sensor is developed in Figure 4. 1 a. The platform of the sensor is embedded with strain gauges to directly identify the working travel. In a realistic scenario, the platform of the sensor is intended to be used in conjunction with an asymmetrical compliant gripper, as portrayed in Figure 4. 1b. The gripper comprises a micro-pin, a stationary jaw, a movable jaw, and a PEA. However, since the platform's behavior is akin to that of the microgripper, the focus of the study was on analyzing the quality characteristics of the platform instead of the gripper. The suggested platform is mainly composed of a mobile platform, four sets of FHs, rigid bodies, and twelve strain gauges that are integrated.

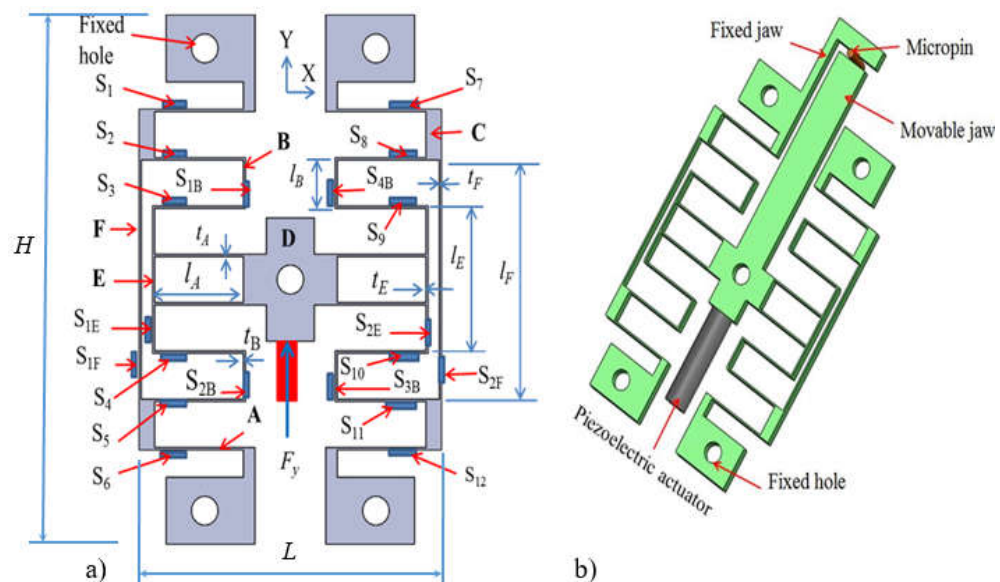


Figure 4. 1: Design structure: a) Displacement sensor and b) Asymmetrical compliant gripper.

Table 4. 1: Initial design parameters.

Parameters		Value	Unit
L	Length of the positioning platform	68.16	mm
H	Hight of the positioning platform	109.5	mm
W	Width of the positioning platform	8.0	mm
t_A	Thickness of flexure hinge A	0.75	mm
l_A	Length of flexure hinge A	25	mm
t_B	Thickness of flexure hinge B	0.7	mm
l_B	Length of flexure hinge B	12	mm
t_E	Thickness of flexure hinge E	0.85	mm
l_E	Length of flexure hinge E	30.5	mm
t_F	Thickness of flexure hinge F	1.0	mm
l_F	Length of flexure hinge F	70.5	mm

In order to achieve a stable grasping structure and a broad range of displacement, the gripper is designed with a symmetrical structure. The FHs include A, B, E, and F types. The elastic bodies are glued by strain gauges on the FH surfaces. A flexure hinge group is linked with an F group through C rigid link. A force gauge or piezoelectric actuator applies a force, denoted F_y , on the D mobile platform. Material AL7075 with parameters as shown in Table 4. 2 was selected as a suitable material for compliant mechanism applications [161], [162].

Table 4. 2: Mechanical characteristics of AL7075.

Yield strength (MPa)	Young's modulus (MPa)	Density (kg/m ³)	Poisson's ratio
503	72000	2770	0.33

The A flexure hinge group, comprising eight elastic bodies of identical dimensions (length of l_A , width of w , and thickness of t_A), is horizontally positioned with the primary aim of aiding the D mobile platform's translational movement in the

y-axis direction. The B flexure hinges have the length (l_B), width (w), and thickness (t_B) dimensions. Such design can allow a displacement range for the D platform. Using rigid bodies in the B group would have the opposite effect, reducing the platform's displacement. Therefore, FHs were employed to construct the B group.

FHs have strain gauges attached to their surfaces in various groups using a suitable adhesive. The positions of the strain gauges were determined through FEA simulation using Ansys software. Through FEA simulation, positions with maximum stress (von Mises stress) and maximum strain are determined. These are the most sensitive positions for the sensor. This implies that strain gauges should be attached at these positions. The strain gauges can be glued to the top surface or bottom surface of a flexure hinge or both. However, the results obtained are the same in value. It means that the strain in the tension state and the strain in the compression state are equal but the strain in the tension state has a positive value and vice versa, the strain in the compression tension state has a negative value (refer to reference [163], [164]). Based on this argument, the A group is bonded with twelve strain gauges numbered S_1 through S_{12} , while the B group is fitted with four strain gauges numbered S_{1B} through S_{4B} . The E and F groups have two strain gauges each, labeled as S_{1E} , S_{2E} and S_{1F} , S_{2F} , respectively (refer to Figure 4. 1a). The platform is secured in place using screws on the fixed holes.

For flexible use in a variety of required situations, the frequency of the platform can be increased. The frequency increase has the following advantages:

- Higher accuracy: this is because the higher frequency allows for more accurate measurement of small displacements because the impact of noise and other sources of error is reduced.
- Resolution: higher frequency sensors can detect smaller changes in position than lower frequency sensors.
- Response time: increasing the frequency of a displacement sensor can improve its response time, allowing it to more accurately track rapid changes in position.
- Bandwidth: increasing the frequency of a displacement sensor can improve its

bandwidth, allowing it to measure over a wider frequency range.

There are two basic ways that can be applied: changing the value of design parameters or using reinforcing materials. However, changing the value of the design parameter can cause a decrease in the deformability of the flexure hinges. Therefore, in this thesis, silicone rubber (SR) with mechanical characteristics as in Table 4. 3 is selected as the reinforcement material when necessary. Moreover, the addition of a silicone rubber pad can help absorb some of the vibrations during operation.

Table 4. 3: Mechanical characteristics of Silicone rubber.

Young's modulus (MPa)	Density (kg/m ³)	Poisson's ratio
1.35	910	0.49

The SR used in this study had a length of 45 mm, a width of 8 mm, and a thickness of 2 mm, and was utilized to fill the cavities. Figure 4. 2 shows the SR bending deformation. By reinforcing stiffness and increasing frequency, the SR contributes to the platform's enhanced speed since a higher frequency corresponds to a faster platform.

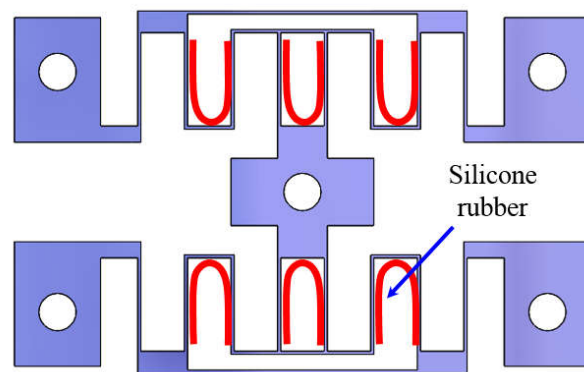


Figure 4. 2: Silicon rubber is reinforced along the contour of the cavity.

4.2.1.2. The working principle of a displacement sensor

To facilitate the design of a displacement sensor, a half-Wheatstone bridge circuit is employed (refer to Figure 4. 3) [59], [160].

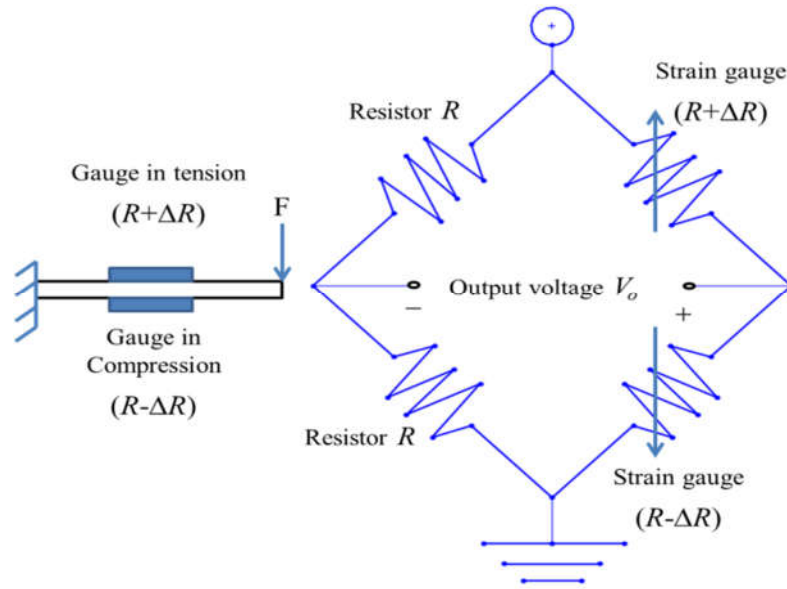


Figure 4. 3: A proposed half-Wheatstone bridge circuit

The proposed displacement sensor is calculated by using the elastic theory of FHs and the half-Wheatstone bridge circuit. In Figure 4. 3, as the platform is in tension, the R resistance causes an increase ΔR . Nevertheless, as the platform is in compression, the resistance R is in a reduction ΔR .

The strain sensor's gauge factor can calculate by the following equation:

$$G = \frac{\Delta R}{R \times \varepsilon}, \quad (4. 1)$$

where the gauge factor is G , ΔR is the variation of gauge resistance, R is a nominal value and ε is strain.

The following equation describes the relationship between strain (ε) and resulting stress (σ):

$$\sigma = E \times \varepsilon, \quad (4. 2)$$

Equation (4. 3) provides a close approximation of the circuit's output voltage:

$$V_o = \frac{1}{2} G \varepsilon \times V_{ex} = \frac{\Delta R}{2R} \times V_{ex}, \quad (4. 3)$$

where V_o is the circuit output and V_{ex} is the excitation voltage.

The circuit's output voltage may be roughly calculated by substituting Eqs. (4. 1) and (4. 2) into (4. 3):

$$V_o = \frac{G\sigma}{2E} \times V_{ex}, \quad (4.4)$$

According to Eq.(4.4), the output voltage is proportional to the tension placed on the FHs.

To evaluate the responsiveness of the displacement sensor gauge, Group A is selected for the examination. The linear stiffness of every single A-group FH is computed as follows:

$$K_A = \frac{Ewt_A^3}{l_A^3}, \quad (4.5)$$

where the stiffness of FH is noted as K .

The force F_y and displacement δ of an FH is computed as:

$$F_y = K_A \times \delta, \quad (4.6)$$

The force F_y and the stress of the FH are calculated by.

$$\sigma = \frac{6F_y l_A}{wt_A^2}, \quad (4.7)$$

The substituting of Eqs. (4.5), (4.6), and (4.7) into (4.4) leads to:

$$V_o = \frac{3V_{ex} G t_A}{l_A^2} \times \delta, \quad (4.8)$$

Eq. (4.8) is equivalent as below:

$$V_o = S \times \delta, \quad (4.9)$$

where S represents the sensitivity of the strain gauge, and S is calculated by:

$$S = \frac{3V_{ex} G t_A}{l_A^2}, \quad (4.10)$$

Combining Eqs. (4.2) and (4.7), the strain and the geometric parameters of the FH are defined by.

$$\varepsilon = \frac{6F_y l_A}{Ewt_A^2}, \quad (4.11)$$

Through calibrations, it is possible to determine the sensitivity S of the strain gauge. This value can be measured by considering the output displacement of the platform of the displacement sensor and the output voltage. Equation (4.11) demonstrates the significant effect of the FH's geometric parameters on the strain.

Besides, a few suitable strain gauges should be identified through FEA simulation.

4.2.2. Technical requirements of a proposed displacement sensor

In practice, the manufacturing of DC motors requires an actual diameter of the motor shaft is about 600-800 μm [12], [13], [152], [165]. To solve the shaft-motor assembly, the proposed displacement sensors must meet the following specifications:

- (i). A large displacement measurement range: greater than 1000 μm .
- (ii). A high frequency: greater than 60 Hz.
- (iii). A minimal gripping effort.

In particular, the large travel displacement helps to be flexible in use. The high frequency of vibration helps the structure have better rigidity when operating and the minimum clamping effort helps save energy.

4.3. Behavior analysis of the displacement sensor

After the sensor structure is proposed and the operating principle is described, the mechanical behavior of the proposed displacement sensor is analyzed and evaluated. These behaviors include strain and stress relationships, stiffness, and frequency response. During the analysis, the devices listed in APPENDIX 1.

4.3.1. Strain versus stress

In this part, appropriate locations are identified to embed strain gauges into the platform. Strain and stress are connected through Hooke's law, and stress and fatigue are represented by Eq.(4. 12). Fatigue is a significant concern for compliant joints under fully reversed stress. This connection is concisely explained in [166].

$$N = (\sigma / a)^{1/b}, \quad (4. 12)$$

$$a = (1 / S_e) \times (f \times S_{ut})^2, \quad (4. 13)$$

$$b = -\frac{1}{3} \log \left(\frac{f \times S_{ut}}{S_e} \right), \quad (4. 14)$$

where N is the failure cycle, S_{ut} is ultimate strength, S_e is endurance strength limit and f is constant.

In this thesis, due to the symmetrical construction of the gripper, only haft of the

structure (groups A, B, E, and F of FHs on the left side positions) are assessed. To start the analysis, the prototypes are fabricated with the initial design parameter (refer to Table 4. 1). The addition of SR to the flexure micro-positioning platform aimed to strengthen its stiffness, resulting in an enhanced frequency and faster speed. It is noted that the viscoelastic behavior of SR can impact the strain value.

The calibration equipment comprised a force gauge for generating force F_y , a sensor gauge at 2.5 V, a computer, and a DAQ. To minimize the impact of vibrations, the prototype was mounted on an anti-vibration table. The strain of each position was measured separately. Figure 4. 4 shows the block diagram of the strain measuring system, and Figure 4. 5 depicts the platform is worked with SR and without SR. The experiments were measured 5 times. Force was increased gradually with values of 2.2 N, 4.6 N, and 7.8 N. The data from DAQ is transferred to LABVIEW software to describe the strain.

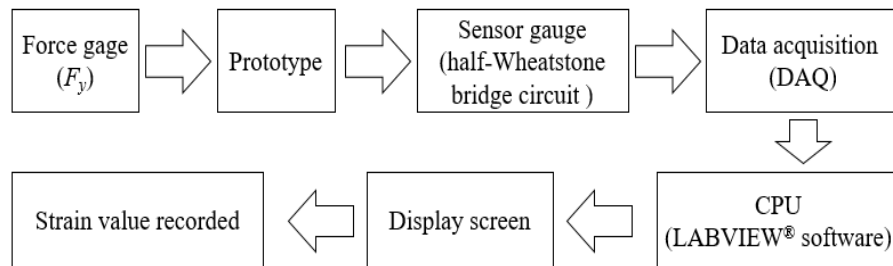


Figure 4. 4: Block diagram of the strain measurement system

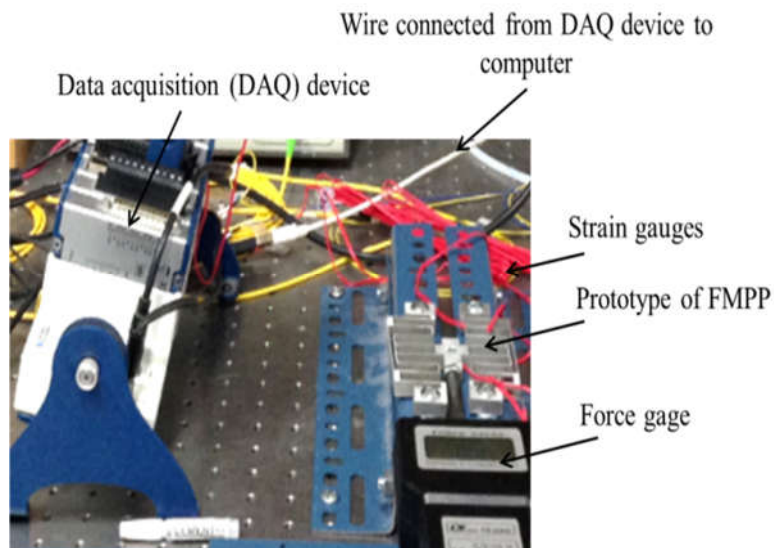


Figure 4. 5: Measured strain for displacement sensor platform.

After conducting the experiments, ANSYS software was utilized for an FEA to verify the results. The model has meshed automatically, and the FH underwent refinement to achieve the required level of analysis accuracy, as depicted in Figure 4. 6. SOLID 92 type of 10-node tetrahedral element was used for meshing, with the boundary conditions illustrated in the same figure. Group B had the highest stress value, and the order of next groups consists of A, E, and F, as shown in Figure 4. 7 and Figure 4. 8. Additionally, the maximum displacement appeared at platform D, in Figure 4. 9.

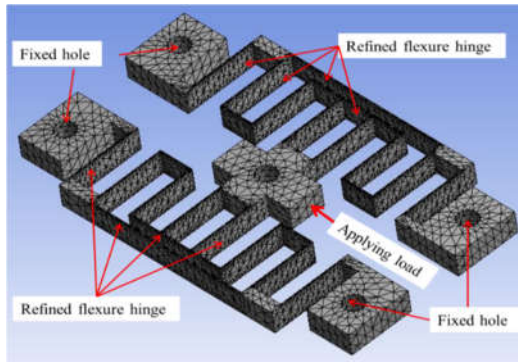


Figure 4. 6: Meshed model of the displacement sensor platform.

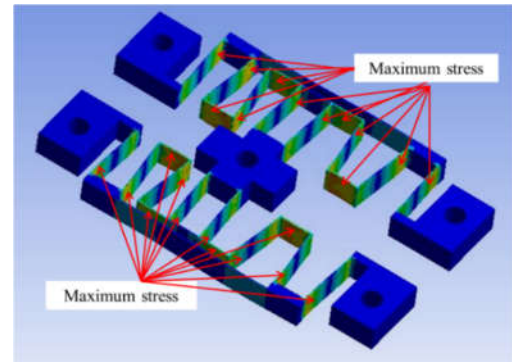


Figure 4. 7: Stress distribution of displacement sensor platform.

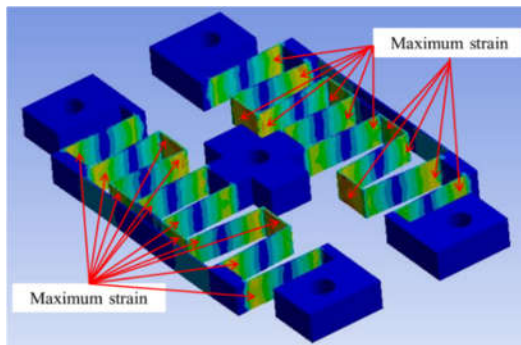


Figure 4. 8: Strain distribution of displacement sensor platform.

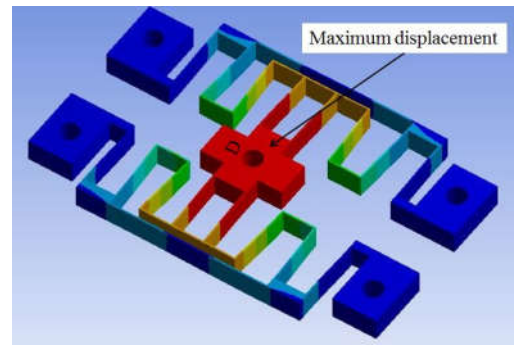


Figure 4. 9: Displacement distribution of displacement sensor platform.

The experimentations were performed on the flexible hinges A, B, E, and F. And then, the stresses were evaluated. In relation to position (7), Figure 4. 10 illustrates that the physical strain with SR-embedded case was 16.63% lower than that from FEA that did not involve the SR. The experiment was closed to the FEA with a deviation of 1.31%. Regarding position (8), Figure 4. 11 found the physical strain

with SR- embedded case was 31.62% less than the FEA value that excluded the SR. The experiment demonstrated good conformity with the FEA results with a deviation of 5.43%. In Figure 4. 12, the physical strain for a position (9) with the SR-embedded was 16.90% lower than the FEA values without the SR. The experimental findings showed a deviation of only 5.60% from the FEA, indicating good consistency between the two. As depicted in Figure 4. 13, the physical strain for a position (10) with the SR-embedded was 21.26% lower than the FEA result without the SR. The experimental results showed a deviation of only 1.67% from the FEA. As shown in Figure 4. 14, the physical strain for a position (11) with the SR-embedded was 6.63% lower than the FEA without the SR. The experimental findings demonstrated a good agreement with the FEA with a deviation of 2.64%. Similarly, in Figure 4. 15, the physical strain for a position (12) with the SR-embedded was 20.80% lower than the FEA without the SR. The experimental results showed a deviation of 3.50% from the FEA. In summary, for group A, position (11) had the maximum strain.

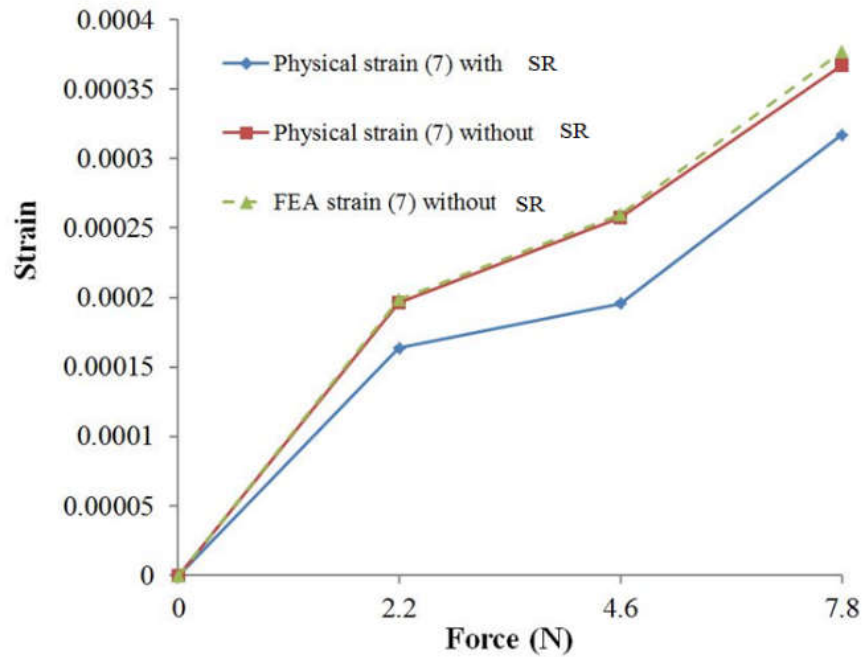


Figure 4. 10: Relationship between strain and position (7) for group A in situations where SR is filled and where it is absent.

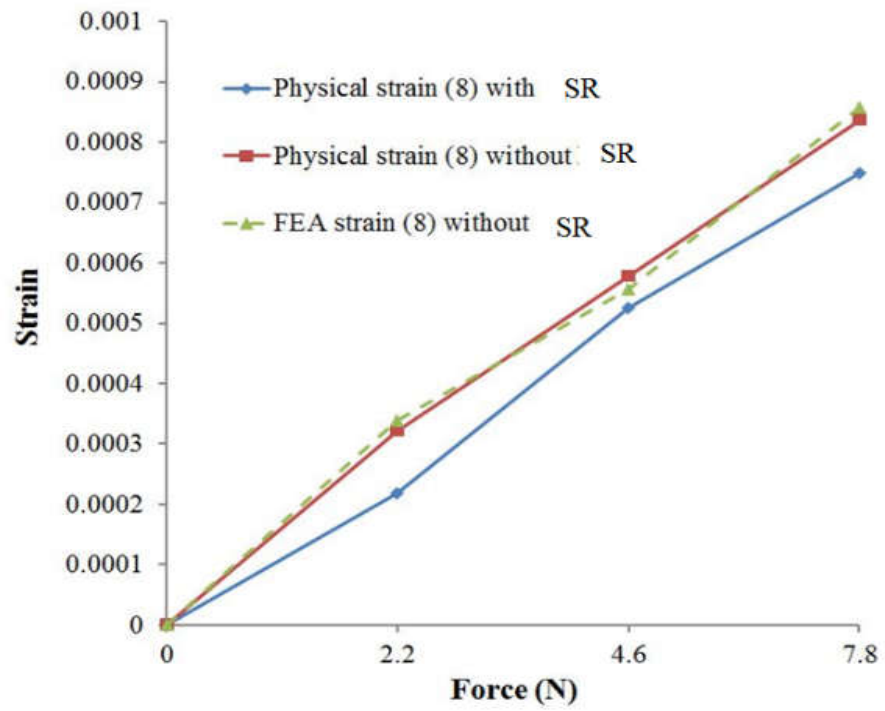


Figure 4. 11: Relationship between strain and position (8) for group A in situations where SR is filled and where it is absent.

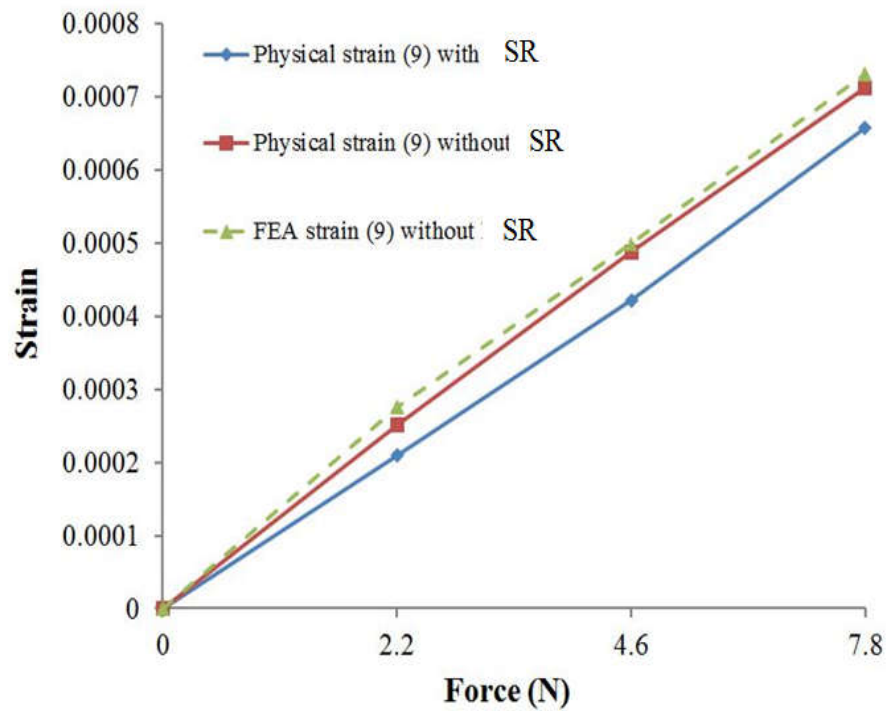


Figure 4. 12: Relationship between strain and position (9) for group A in situations where SR is filled and where it is absent.

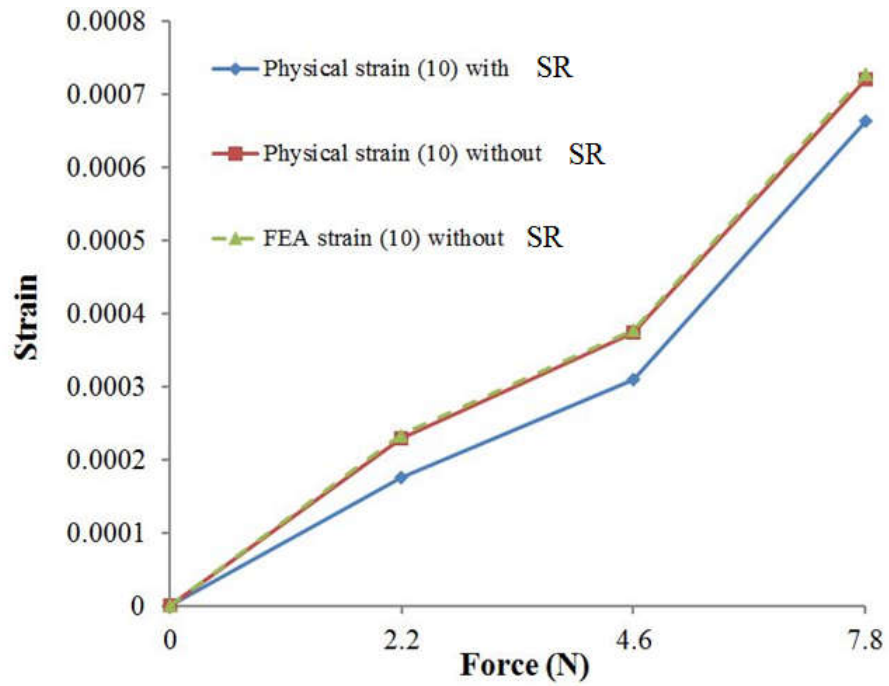


Figure 4. 13: Relationship between strain and position (10) for group A in situations where SR is filled and where it is absent.

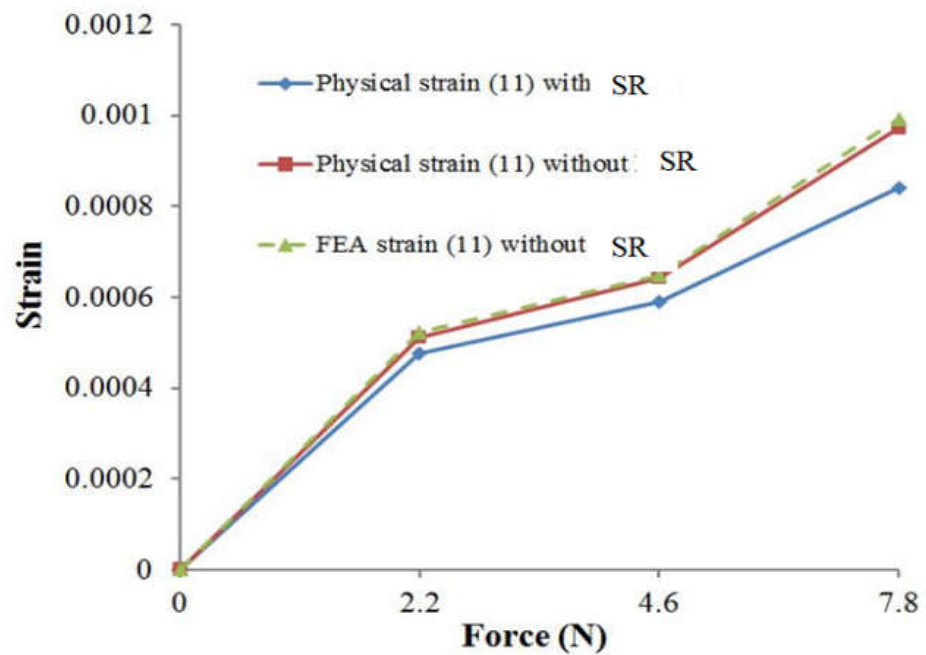


Figure 4. 14: Relationship between strain and position (11) for group A in situations where SR is filled and where it is absent.

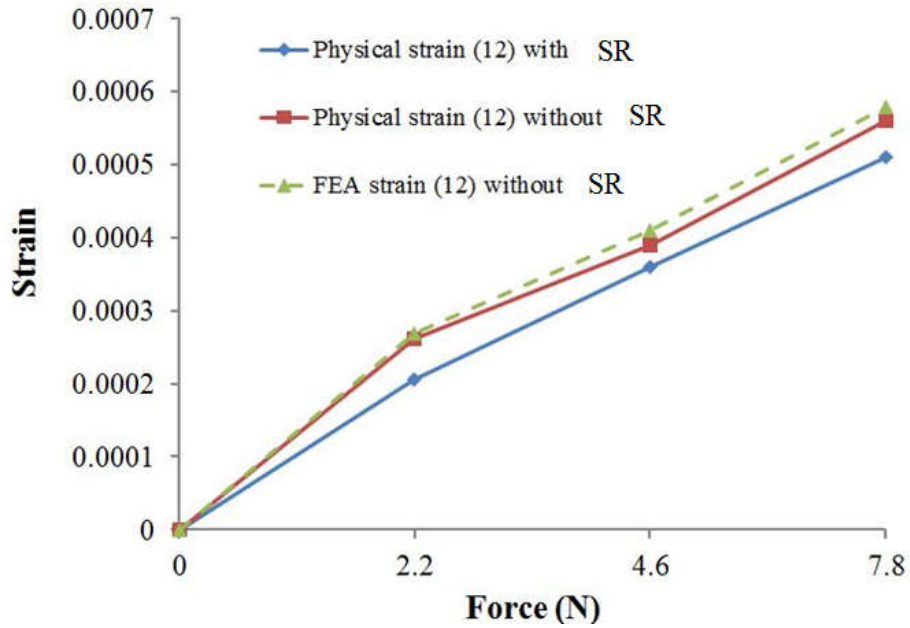


Figure 4. 15: Relationship between strain and position (12) for group A in situations where SR is filled and where it is absent.

As depicted in Figure 4. 16, the use of embedded SR resulted in a 16.62% decrease in physical strain values for a position (S_{1B}) compared to FEA without SR. The experimental results closely aligned with the FEA, exhibiting only a 1.43% error.

Considering position (S_{2B}), the physical strain with the SR-embedded case was lower 31.96%, than that without SR, as in Figure 4. 17. Despite a higher error rate of 5.43%, the experimental results are closed to the FEA results. It should be noted that position (S_{2B}) exhibited the highest strain magnitude.

In Figure 4. 18, the physical strain for a position (S_{1E}) was 16.60% lower than that from the SR-embedded case. The experimental results had a 1.41% error compared with FEA. Similarly, Figure 4. 19 shows for a position (S_{2B}), the physical strain with the SR-embedded case was 30.89% lower than that without SR. The experimental results had an error of 5.34% with FEA. Notably, the maximum strain occurred at position (S_{2E}).

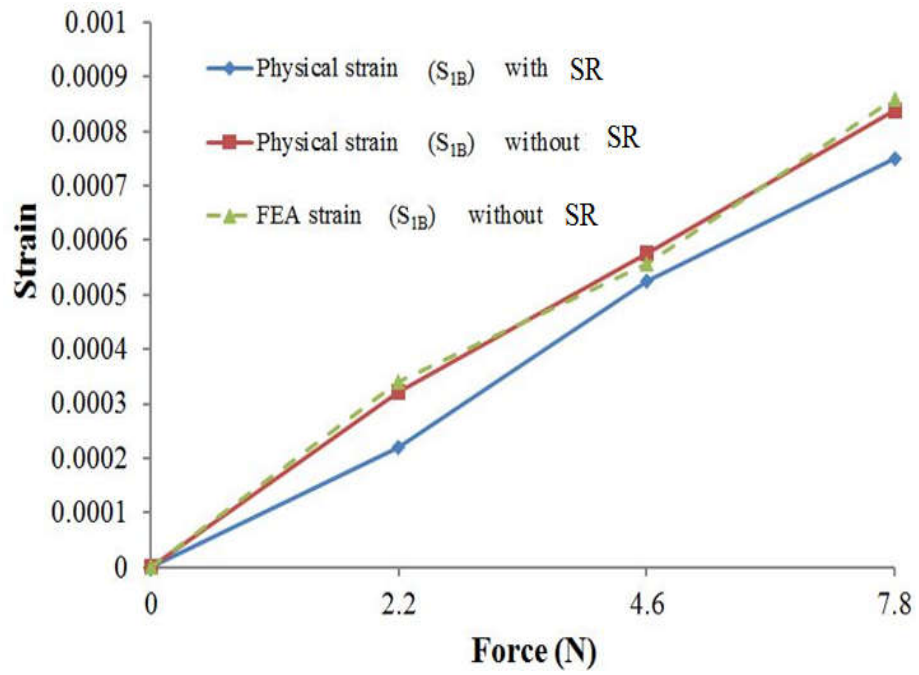


Figure 4. 16: Relationship between strain and position (S_{1B}) for group B in situations where SR is filled and where it is absent.

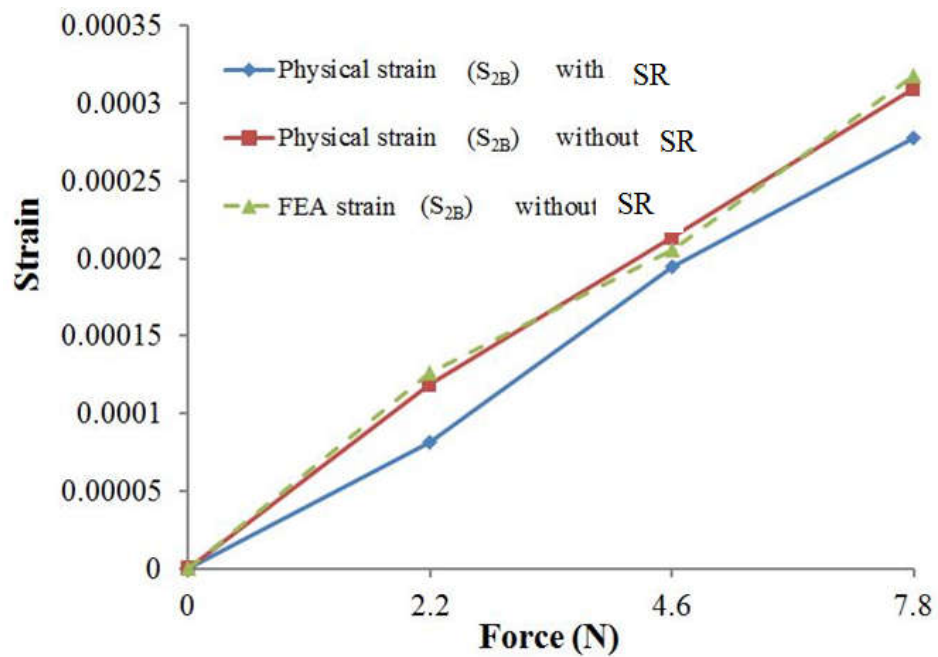


Figure 4. 17: Relationship between strain and position (S_{2B}) for group B in situations where SR is filled and where it is absent.

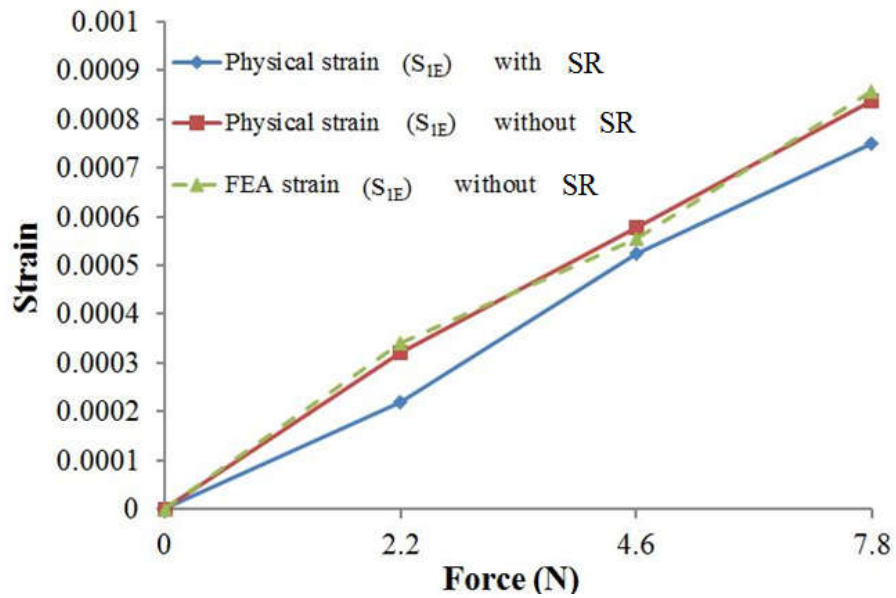


Figure 4. 18: Relationship between strain and position (S_{1E}) for group E in situations where SR is filled and where it is absent.

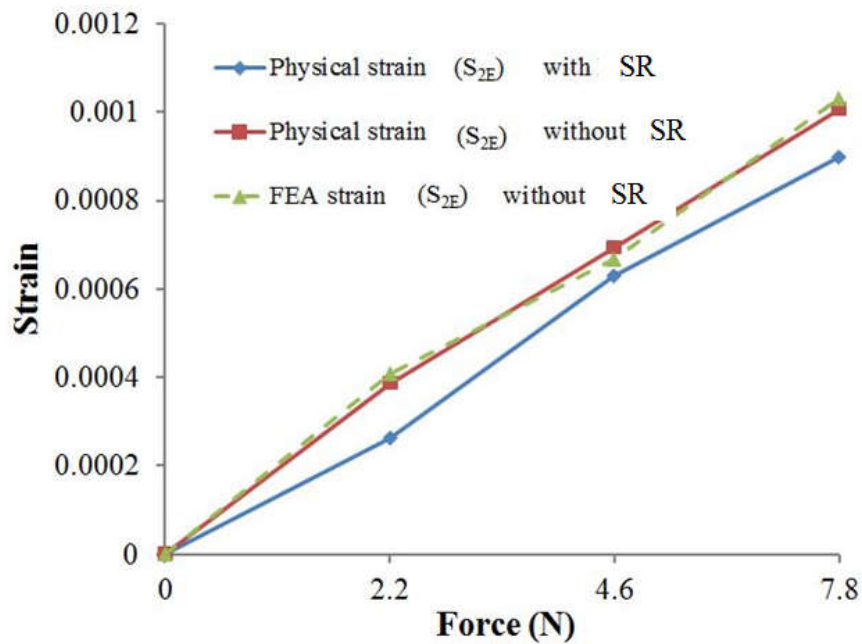


Figure 4. 19: Relationship between strain and position (S_{2E}) for group E in situations where SR is filled and where it is absent.

As illustrated in Figure 4. 20, the physical strain values for a position (S_{1F}) were approximately 15.63% lower when the SR was embedded compared to the FEA without SR. The experiments and FEA have an error of 1.52%. Moreover, for a

position (S_{2F}), the physical strain was 30.81% lower than the SR-embedded case without SR, as shown in Figure 4. 21. An error of 5.16% between the experiment and FEA. Notably, the maximum strain occurred at position (S_{2F}).

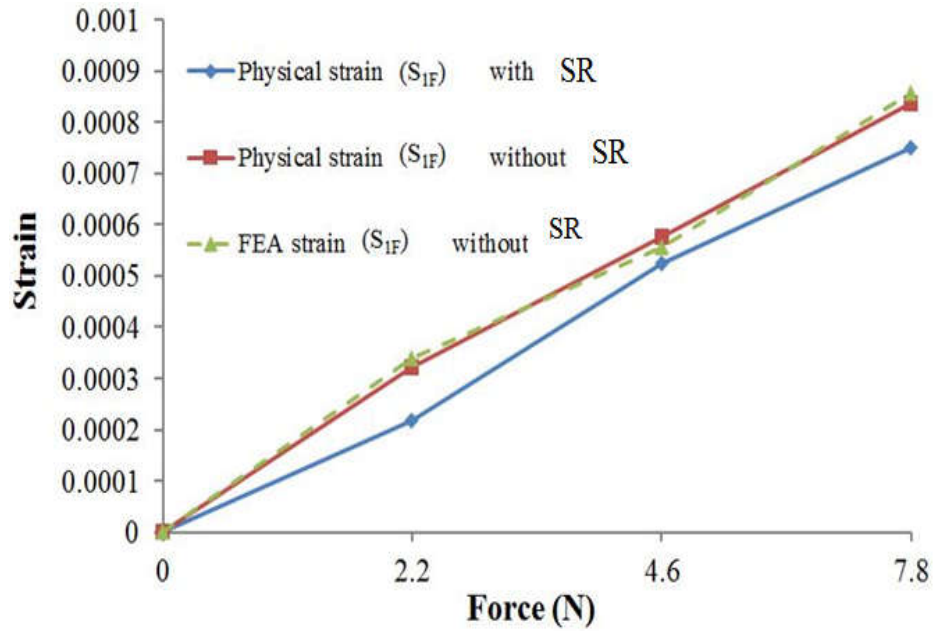


Figure 4. 20: Relationship between strain and position (S_{1F}) for group F in situations where SR is filled and where it is absent.

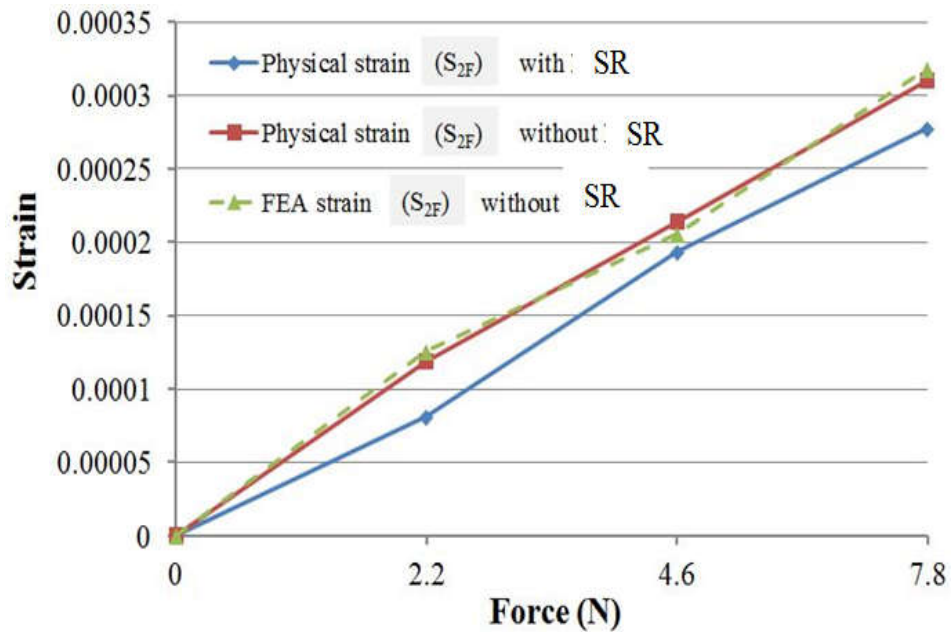


Figure 4. 21: Relationship between strain and position (S_{2F}) for group F in situations where SR is filled and where it is absent.

In order to determine the stress at various positions, Hook's law was utilized, which required calculating the strain beforehand. As stated in Table 4. 4, the highest stress was at position (S_{2B}), followed by (S_{2E}) and (11), with group F having the lowest stress. (S_{2B}) exhibited the maximum strain compared to the other positions, necessitating its careful consideration due to its impact on the platform's fatigue life according to Eq.(4. 12). In order to examine the interrelationship between strain, stress, and voltage, PEAs were conducted with voltage values in from 0 to 0.6 V, and the experiments were performed in Figure 4. 5. The strain was used to compute the corresponding stresses. The maximum strain was at position (S_{2B}), followed by (S_{2E}) and (11), while group F had the lowest strain, as indicated in Figure 4. 22. Moreover, Figure 4. 23 revealed that the maximum stress was at position (S_{2B}), followed by (S_{2E}) and (11), with group F having the lowest stress. In addition, Figure 4. 22 and Figure 4. 23 also show that the relationship between voltage and strain/stress is nonlinear. This is because the piezoelectric effect also exhibits mechanical hysteresis, which means that the strain produced by an applied voltage depends on the previous loading history of the material [167].

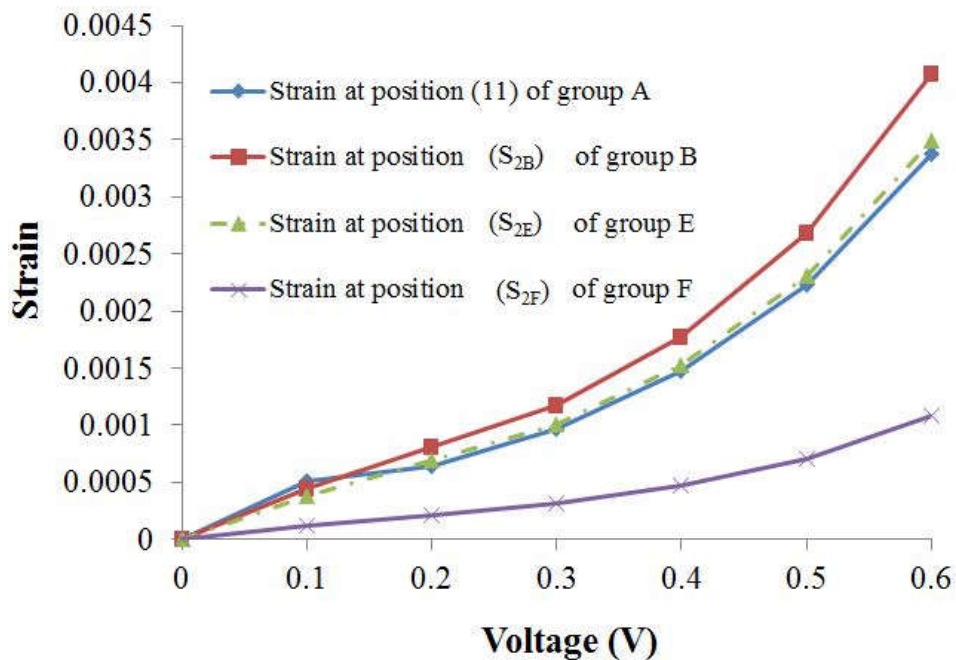


Figure 4. 22: Strain distributions for positions (11): At flexure hinges A, S_{2B} of B, S_{2E} of E, and S_{2F} of F.

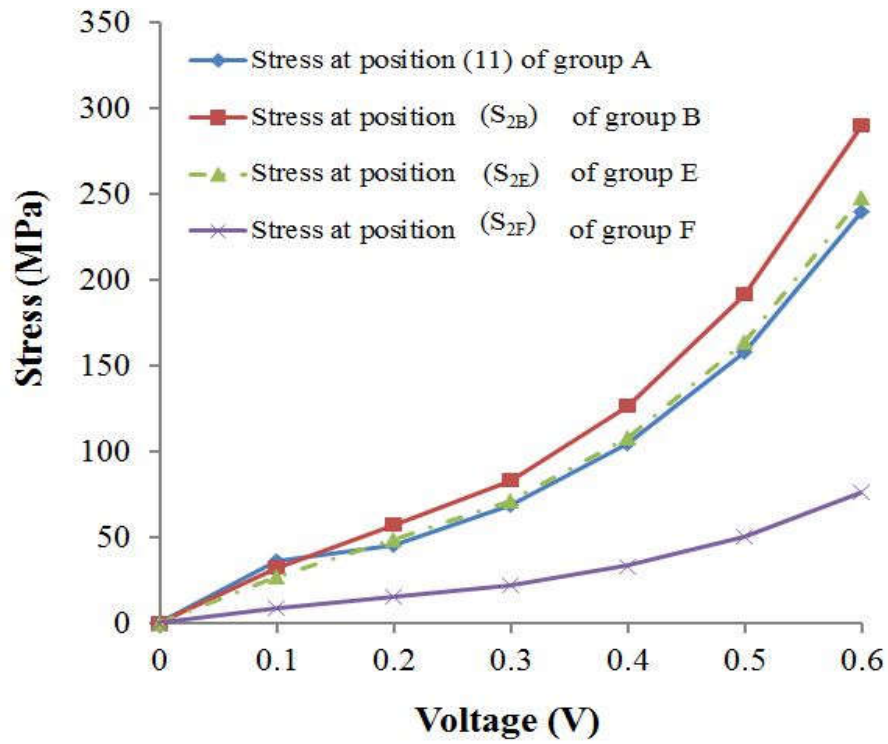


Figure 4. 23: Stress distributions for positions (11): At flexure hinges A, S_{2B} of B, S_{2E} of E, and S_{2F} of F.

Table 4. 4: stress values at various positions.

Measuring position	Corresponding stress (MPa)
Position (7)	26.78
Position (8)	60.94
Position (9)	51.93
Position (10)	51.62
Position (11)	70.48
Position (12)	41.05
Position (S _{1B})	37.49
Position (S _{2B})	85.31
Position (S _{1E})	32.14
Position (S _{2E})	73.13
Position (S _{1F})	9.91
Position (S _{2F})	25.57

4.3.2. Stiffness analysis

The SR served another purpose as well, which was to fortify the rigidity of the platform being created. This was achieved by leveraging the elasticity of the body to induce alterations in the platform's dynamic response.

Multiple experiments and simulations were conducted to study this particular trait of the SR. The block diagram of the stiffness measurement system was described as Figure 4. 24, and the experiments were performed with and without the filled SR as Figure 4. 25. Forces were acted with 0.25 N, 0.5 N, 0.85 N, and 1.3 N. The prototype was immobilized, and a laser displacement sensor was utilized to detect its displacement. The digital signal showed the displacement value. The experiment was conducted four times.

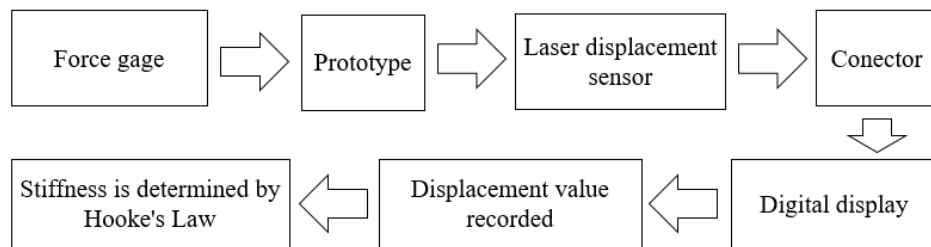


Figure 4. 24: Block diagram of the stiffness measurement system.

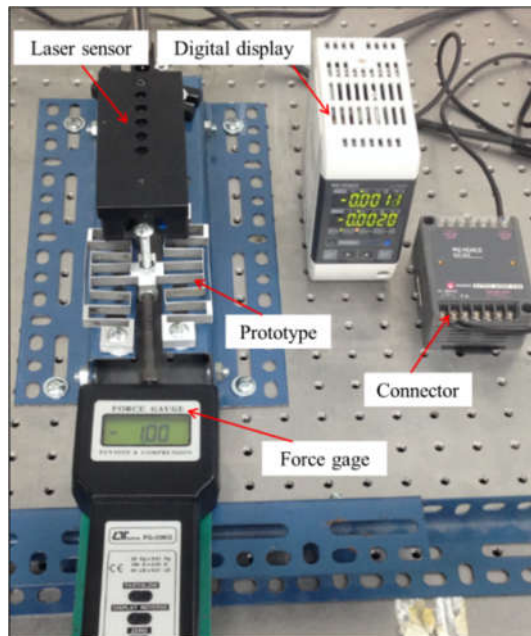


Figure 4. 25: Experiment fort measuring the displacement of displacement sensor.

Table 4. 5 displays that the average stiffness was approximately 0.002 N/ μm in the absence of the SR and 0.003 N/ μm with the SR-case. It means that the stiffness of the displacement sensor was enhanced by incorporating the viscoelastic SR. These findings are significant for the design of flexure-based micro-positioning platforms, as they suggest that additional SR can strengthen the stiffness. The experimental and simulation results were similar.

Table 4. 5: Displacement with various forces.

Displacement (μm)	Force (N)			
	0.25	0.50	0.85	1.30
Experiment: no SR	125.0	164.0	288.0	352.0
Experiment: with SR	86.0	91.0	153.0	200.0
FEA: no SR	128.0	172.0	294.0	356.0
FEA: with SR	94.0	110.0	158.0	210.0

In an effort to demonstrate an increase in stiffness, numerous experiments and simulations were performed, particularly with a load exerted on the x -axis. To execute these experiments, the displacement sensor was firmly affixed to the table, and the forces of 0.25 N, 0.5 N, 0.85 N, and 1.3 N were applied to the x -axis. Figure 4. 26 illustrates the experimental displacement specifically along the x -axis. Table 4. 6 displays that without the SR, the average stiffness for applied loads in the x -direction was approximately 0.008 N/ μm , whereas, with the SR-embedded case, the average stiffness was 0.012 N/ μm . This indicates that the stiffness was increased.

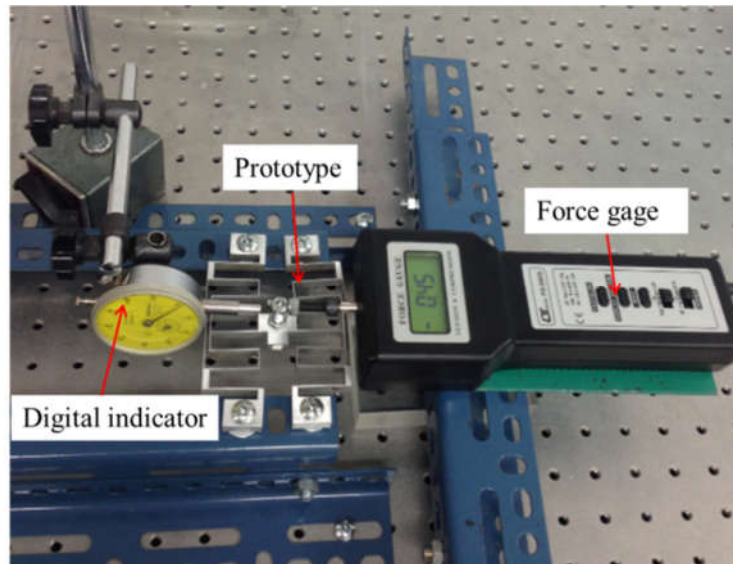


Figure 4. 26: Measurement of stiffness in x-direction of displacement sensor.

Table 4. 6: Displacement along the x-direction.

Displacement (μm)	Force (N)			
	0.25	0.50	0.85	1.30
Experiment: no SR	30.0	50.0	70.0	140.0
Experiment: with SR	20.0	30.0	40.0	110.0
FEA: no SR	34.0	48.0	64.0	143.0
FEA: with SR	23.0	33.0	45.0	114.0

4.3.3. Frequency response

To assess the dynamic characteristics of the platform in case of no pre-stress within the 100 Hz to 500 kHz range, the first natural frequency was tested. An accelerometer was used to measure the frequency response after applying excitation using a modal hammer, which was placed opposite the location of the accelerometer. A force sensor was installed at the end of the hammer to measure the applied force, and data acquisition and analysis were carried out using a modal analyzer and CUTPRO software on a computer.

The experiment was conducted five times, following the procedure outlined in Figure 4. 27 và Figure 4. 28, for both the cases with and without the embedded SR. The

results showed that the SR increased the stiffness of the platform, with a frequency of 110.3 Hz for the case with the SR and 109.8 Hz for the case without the SR, recorded in Table 4. 7. In summary, the response would also be faster with the SR.

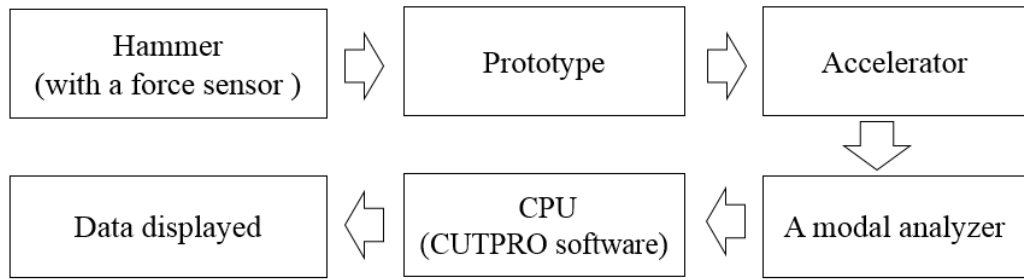


Figure 4. 27: Block diagram of measuring frequency by hammer

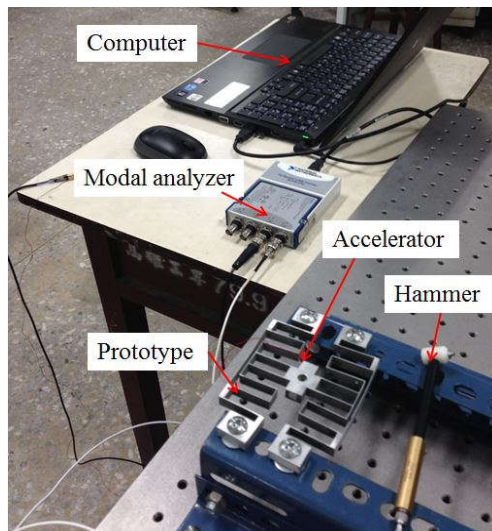


Figure 4. 28: Experiments for measuring frequency by hammer.

Regarding pre-stress, the PEA was driven by a high-speed bipolar amplifier, and the retro-reflective tape was attached to the center of the moving object. Measurement of displacement was carried out using a laser vibrometer sensor with nanoscale precision, while a frequency response analyzer was employed in the experiment. The experiments were measured five times. The experiment procedure on PEA with and without embedded SR is depicted in Figure 4. 29 and Figure 4. 30. The data was collected in Table 4. 7 and visualized in Figure 4. 31 and Figure 4. 32. Specifically, the PEA tested with the filled SR exhibited a frequency of 223 Hz, which was considerably higher than the frequency of 149 Hz observed in the PEA without the SR. The stiffness was by SR.

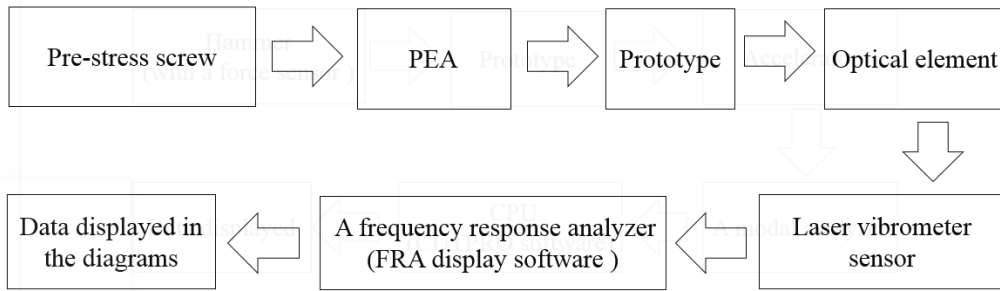


Figure 4. 29: Block diagram of measuring frequency by PEA

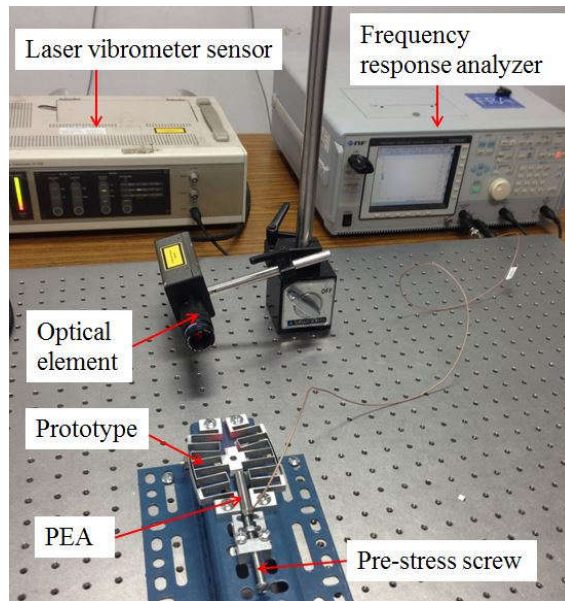


Figure 4. 30: Experiments for measuring frequency with exerted PEA.

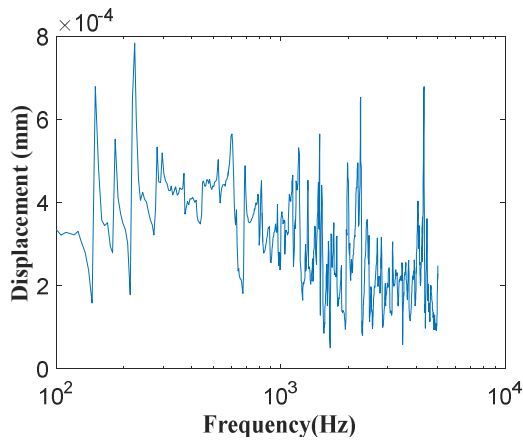


Figure 4. 31: Frequency versus displacement for exerted PEA without SR.

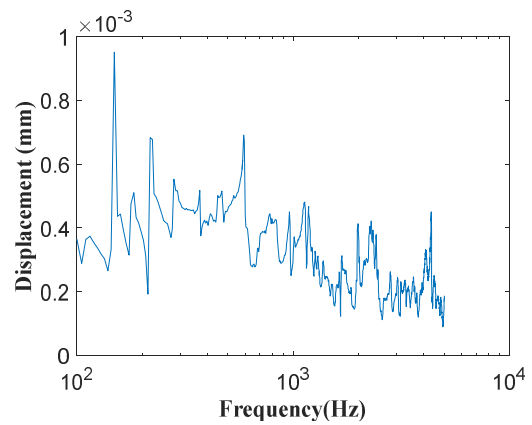


Figure 4. 32: Frequency versus displacement for exerted PEA with filled SR.

Table 4. 7: First natural frequency.

No PEA and no SR (Hz)	No PEA with embedded SR (Hz)	With PEA but no SR (Hz)	With PEA with embedded SR (Hz)
109.8	110.3	149	223

In summary, embedding the SR within the open cavities led to a noticeable increase in frequency. This indicates that the presence of the SR had a strong impact on the stiffness of the positioning platform. In practical terms, a compliant positioning platform that becomes stiffer will experience a corresponding increase in frequency. Consequently, the proposed platform was able to operate more efficiently at a higher frequency, resulting in improved speed and performance.

4.4. Design optimization of a proposed displacement sensor

4.4.1. Description of optimization problem of a proposed displacement sensor

In order to attain both a broad range of displacement and rapid response time, the hands of the compliant micro-gripper were combined with a micro-positioning stage, depicted in Figure 4. 33 a and b. Comprising a micro pin for grasping, a stationary jaw/hand, a mobile jaw, and a PEA, the microgripper shared analogous performance traits with the platform. Thus, this study focused on examining the quality attributes of the platform rather than scrutinizing the gripper. The material of the gripper is AL7075 which has properties as shown in Table 4. 2 (refer to [168]).

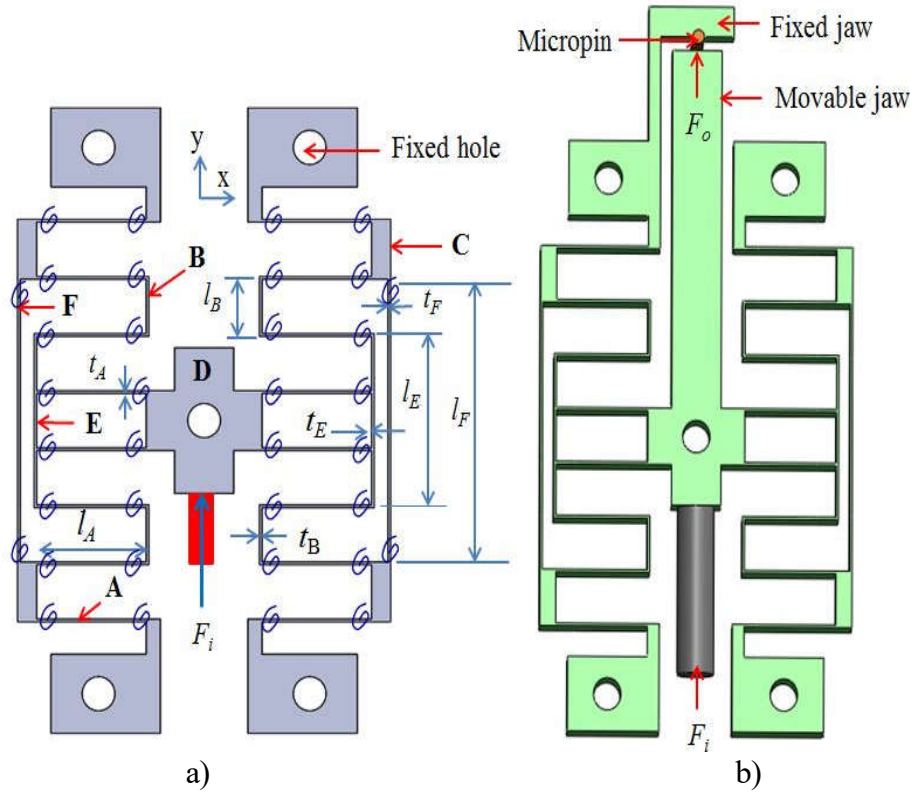


Figure 4.33: PRBM scheme: a) Displacement sensor and b) Model of asymmetrical compliant gripper.

The compliant microgripper's specifications dictate that the object it grips must be held by a force of 5 N. It desires an output force of 5 N. It means the gripper needs a stable gripping force. To enhance the multiple responses of the gripper, it is crucial to optimize the length and thickness of the FHs. The dynamic equation of structure is built by the pseudo-rigid-body model [61]. As depicted in Figure 4.33a, the mass of flexure hinges A, B, C, D, E, and F was computed using the following method.

$$M_A = N_A \times \rho \times (l_A \times w_A \times t_A), \quad (4.15)$$

$$M_B = N_B \times \rho \times (l_B \times w_B \times t_B), \quad (4.16)$$

$$M_C = \rho \times N_C \times (10.5 \times 3.5 \times 8), \quad (4.17)$$

$$M_D = \rho \times (22.5 \times 20.66 \times 8) - \rho \times 4 \times (7.5 \times 5.18 \times 8) - \rho (\pi \times 3^2 \times 8), \quad (4.18)$$

$$M_E = \rho \times N_E \times (l_E \times w_E \times t_E), \quad (4.19)$$

$$M_F = \rho \times N_F \times (l_F \times w_F \times t_F), \quad (4.20)$$

in which

$M_A, M_B, M_C, M_D, M_E,$ and M_F : masses of parts A, B, C, D, E, and F, respectively.

ρ : density of the material.

N_A : number of FHs (16 elements).

N_B : number of hinges B (4 elements).

N_C : number of rigid links (2 elements).

N_D : number of platforms D (1 element).

N_E : number of hinges E (2 elements).

N_F : number of hinges F (2 elements).

The overall mass M of the gripper is computed as.

$$M = M_A + M_B + M_C + M_D + M_E + M_F, \quad (4.21)$$

From the dynamic equation of the Lagrange principle, the natural frequency can be determined. Assumed that the platform is moved with velocity \dot{y} where B links are assumed as an ideal rigid link. The platform's kinetic energy T was estimated as follows.

$$T = \frac{1}{2} M \dot{y}^2, \quad (4.22)$$

According to the PRBM, the potential energy V of 36 torsional springs of FHs was found by the following formula:

$$V = 36 \times \frac{1}{2} K_{ds} \theta_z^2, \quad (4.23)$$

The dynamic stiffness K_{ds} of each spring was computed, including A, B, E, and F flexure hinges

$$K_{ds} = 2\gamma k_\Theta \times \left(32 \times \frac{EI_A}{l_A} + 4 \times \frac{EI_F}{l_F} \right), \quad (4.24)$$

where $\gamma = 0.85$, $k_\Theta = 2.669$. E is Young's modulus of a material. I_A is a moment of inertia of area, $I = wt^3/12$. $\theta_z = y/2l_A$ is the rotational angle around the z-axis.

Hence, Eq. (4.23) yields as.

$$V = 36 \times \frac{1}{2} K_{ds} \left(\frac{y}{2l_A} \right)^2, \quad (4.25)$$

An assumed free motion, the dynamic equation was formulated by Lagrange as:

$$\frac{d}{dt} \left(\frac{\partial T}{\partial \dot{y}} \right) - \frac{\partial T}{\partial y} + \frac{\partial V}{\partial y} = 0, \quad (4.26)$$

Eq. (4.26) became as.

$$M \ddot{y} + \frac{9K_{ds}}{l_A^2} y = 0, \quad (4.27)$$

Eq. (4.27) was yielded as.

$$M \ddot{y} + Ky = 0, \quad (4.28)$$

where \ddot{y} is acceleration.

The stiffness of the structure was determined by.

$$K = \frac{9K_{ds}}{l_A^2}, \quad (4.29)$$

The displacement of the structure was computed by considering the displacement of flexures A, B, E, and F as.

$$f_1(\mathbf{X}) = 12\sigma \left(\frac{l_A^2}{3Et_A} + \frac{l_B^2}{3Et_B} + \frac{l_E^2}{3Et_E} + \frac{l_F^2}{3Et_F} \right), \quad (4.30)$$

The natural frequency of the gripper structure was computed by.

$$f_2(\mathbf{X}) = \frac{1}{2\pi} \sqrt{\frac{9K_{ds}}{Ml_A^2}}, \quad (4.31)$$

The stress at flexure A was calculated by.

$$\sigma = \frac{6F_i l_A}{w_A t_A^2}, \quad (4.32)$$

Where $f_1(\mathbf{X})$ is the displacement and $f_2(\mathbf{X})$ is the frequency. σ is the stress, F_i is the input force, \mathbf{X} is the design variable, and E is Young's modulus.

Considering the grabbing force to the micro pin, the response force of the moveable jaw was computed as follows.

$$F_o = K \times f_1(\mathbf{X}), \quad (4.33)$$

where F_o is the gripping force of the gripper.

4.4.1.1. Definition of design variables

In this investigation, the lengths and thicknesses of flexure hinges (A and B) are the first group of design variables. Besides, the thicknesses of flexure hinges (E and F) are the second group of design variables. They are considered as a vector

$$\mathbf{X} = [l_A, l_B, t_A, t_B, t_E, t_F]^T.$$

Following are the minimum and maximum values assigned to the design variables:

$$\left\{ \begin{array}{l} 15 \text{ mm} \leq l_A \leq 35 \text{ mm} \\ 7 \text{ mm} \leq l_B \leq 17 \text{ mm} \\ 0.5 \text{ mm} \leq t_A \leq 1.0 \text{ mm} \\ 0.5 \text{ mm} \leq t_B \leq 0.9 \text{ mm} \\ 0.5 \text{ mm} \leq t_E \leq 1.2 \text{ mm} \\ 0.5 \text{ mm} \leq t_F \leq 1.5 \text{ mm} \end{array} \right. \quad (4.34)$$

4.4.1.2. Definition of objective functions

In this study, three main cost functions are included. (i) $f_1(\mathbf{X})$ is the displacement of gripper, (ii) $f_2(\mathbf{X})$ is a first natural frequency, (iii) $f_3(\mathbf{X})$ is the gripping effort. The optimization problem was described by.

$$\text{Max } f_1(\mathbf{X}) = 2\sigma \left(\frac{l_A^2}{3Et_A} + \frac{l_B^2}{3Et_B} + \frac{l_E^2}{3Et_E} + \frac{l_F^2}{3Et_F} \right), \quad (4.35)$$

$$\text{Max } f_2(\mathbf{X}) = \frac{1}{2\pi} \sqrt{\frac{10K_{ds}}{Ml_A^2}}, \quad (4.36)$$

$$\text{Min } f_3(\mathbf{X}) = \left| \frac{F_o}{F_i} - 1 \right|, \quad (4.37)$$

As mentioned earlier, the individual objective functions will be converted into a single scalar function by normalization as follows:

$$f(\mathbf{X}) = -w_1 \times \frac{f_1(\mathbf{X})}{f_1^a} - w_2 \times \frac{f_2(\mathbf{X})}{f_2^a} + w_3 \times \frac{f_3(\mathbf{X})}{f_3^a} \quad (4.38)$$

where $w_1, w_2,$ and w_3 represent WF of $f_1(\mathbf{X}), f_2(\mathbf{X}),$ and $f_3(\mathbf{X}),$ respectively. “-” in Eq. (4.38) shows a maximum and “+” indicates a minimum. $f_1^a, f_2^a,$ and f_3^a are the mean value of each cost function.

In summary, size optimization includes two types. The first type is optimization design that solely relies on the statistical performance of response and does not take uncertain behaviors into account. The second type is reliability-based optimization design which considers uncertainty factors, e.g., tolerances, machining methods,

material, etc. The present work focuses on the deterministic type. However, the insights gained from studying the second type can be useful for future projects.

4.4.1.3. Definition of constraints

The compliant gripper is only efficiently worked in the elastic limit of AL-7075. Therefore, it has constraints involved in safety conditions as follows.

$$g(x) = \sigma \leq \frac{\sigma_y}{S}, \quad (4.39)$$

where σ_y is the yield strength of Al-7075 and safety factor S of 1.5 is selected to ensure a safety condition.

4.4.1.4. The proposed method for optimizing the displacement sensor

This process includes two steps as follows:

- **Step 1:** TM is used to organize experiments, and evaluate the influence of design parameters on the output responses. Thereby, the search space of the optimization problem is limited to reduce the time and cost of computation. In addition, through this statistical analysis technique, the weight value for each design objective is also accurately determined.
- **Step 2:** The TLBO optimization algorithm is applied with the search space and weight value determined in step 1.

a) Technique to calculate the weighting factor

A multi-objective optimization method of three objectives maximum $f_1(\mathbf{X})$, maximum $f_2(\mathbf{X})$, and minimum $f_3(\mathbf{X})$ are considered. The overall objective equation is described as Eq.(4.38). Three goals are contradictory. The Pareto principle has been implemented [169]. Regarding this optimization issue, the WF of each cost function is computed. Normally, the WF is defined by experiences in the field. Unlike this, the WFs are precisely calculated in this thesis.

The calculation procedure of WFs is as follows. Because $f_1(\mathbf{X})$, $f_2(\mathbf{X})$, and $f_3(\mathbf{X})$ have different dimension units. To prevent the effect of adopting various units and decrease variability, the S/N ratio of each response is normalized as Z_i ($0 \leq Z_i \leq 1$).

$$z_i = \frac{\eta_i - \min \eta_i}{\max \eta_i - \min \eta_i}, \quad (4.40)$$

For each level of each parameter, the max-min range of the normalized S/N ratio was defined as.

$$r_{ij} = \max \{z_{i,j,1}, z_{i,j,2}, \dots, z_{i,j,k}\} - \min \{z_{i,j,1}, z_{i,j,2}, \dots, z_{i,j,k}\}, \quad (4.41)$$

Where $j = 1, 2, \dots, p$, p is the number of design parameters, $k = 1, 2, \dots, l$, l is the number of experimental levels of each response. $z_{i,j,k}$ is the normalized mean value of S/N for the i^{th} response of the parameter j^{th} at the k^{th} experiment.

The WF was computed using the following formula:

$$w_i = \frac{\sum_{j=1}^p r_{ij}}{\sum_{i=1}^m \sum_{j=1}^p r_{ij}}, \quad (4.42)$$

where w_i is the weight factor of i^{th} response and $w_i \geq 0$.

The sum of the WFs for all responses is equal to one.

$$\sum_{i=1}^m w_i = 1. \quad (4.43)$$

b) Teaching-learning-based optimization algorithm

The TLBO algorithm was proposed by Rao, which is a activity of the teaching-learning process [153]. This optimizer considers two primary modes of learning: (i) through a teacher (known as the teacher phase), and (ii) through interaction with other learners (called the learner phase). In the optimization process, a group of learners is treated as a population, the diverse topics presented to the learners are considered as the optimization problem's design variables, and a learner's performance is compared to the fitness value of the optimization problem.

TLBO is suggested to optimize an objective function with three conflicting objectives (maximum $f_1(\mathbf{X})$, maximum $f_2(\mathbf{X})$, and minimum $f_3(\mathbf{X})$). The implementation procedure is broken down into five fundamental steps:

❖ *Step 1: Identify the optimization problem*

The combined/summed objective function of the problem is illustrated by.

$$f(\mathbf{x}) = -w_1 f_1(\mathbf{x}) - w_2 f_2(\mathbf{x}) + w_3 f_3(\mathbf{x}) \quad (4.44)$$

S.t. $\mathbf{X} \in x_i = 1, 2, \dots, nd$

where nd is the population size, \mathbf{X} represents the vector of design variables. x_i indicates a design variable. It has the upper limit of $U_{L,i}$, the lower limit of $U_{L,i}$. w_1 , w_2 , and w_3 note the weight factor.

❖ **Step 2: Initialize a population**

In this step, a population is produced at random through a large number of students enrolled in many courses. The aggregate of the population is depicted as follows:

$$pop = \begin{bmatrix} x_1^1 & \cdots & x_2^1 & x_{nd-1}^1 & x_{1-nd}^1 \\ x_1^2 & \cdots & x_2^2 & x_{nd-1}^2 & x_{nd}^2 \\ \vdots & \cdots & \vdots & \vdots & \vdots \\ x_1^{np-1} & \cdots & x_2^{np-1} & x_{nd-1}^{np-1} & x_{nd}^{np-1} \\ x_1^{np} & \cdots & x_2^{np} & x_{nd-1}^{np} & x_{nd}^{np} \end{bmatrix} \begin{matrix} \rightarrow f(\mathbf{X}^1) \\ \rightarrow f(\mathbf{X}^2) \\ \rightarrow \cdots \\ \rightarrow f(\mathbf{X}^{np-1}) \\ \rightarrow f(\mathbf{X}^{np}) \end{matrix}, \quad (4.45)$$

in which: each row is a candidate (learner) in the population (class). $f(\mathbf{X}^{1,2,\dots,np})$ is the value of the objective function. pop represents the population.

❖ **Step 3: Teacher phase**

The most optimal way to explain the targeted fitness function is by using the teacher $\mathbf{X}_{teacher} = \mathbf{X}_{\min f(\mathbf{X})}$, where the value of the function is at its minimum. In TLBO, the teacher strives to enhance the individuals' comprehension in the class to the best of their capacity, thereby enabling the learners to attain knowledge similar to that of the teacher ($\mathbf{X}_{mean} \rightarrow \mathbf{X}_{teacher}$). The following modifications can be made to the instructor phase's mathematical equation:

$$\mathbf{X}^{new,i} = \mathbf{X}^i + r(\mathbf{X}_{teacher} - T_F \mathbf{X}_{mean}), \quad (4.46)$$

where $\mathbf{X}^{new,i}$ represent the updated value of \mathbf{X}^i and \mathbf{X}^i represents the current value of i , r denotes a random value that can vary between $[0, 1]$, and T_F is the teaching factor, which is randomly selected as either 1 or 2 for each iteration. The following equation identifies \mathbf{X}_{mean} as a valid solution:

$$\mathbf{X}_{mean} = \left[m \left(\text{pop} \left(\sum_{j=1}^{np} x_1^j \right) \right) m \left(\text{pop} \left(\sum_{j=1}^{np} x_2^j \right) \right) \cdots \left(\text{pop} \left(\sum_{j=1}^{np} x_{nd-1}^j \right) \right) \times \left(\text{pop} \left(\sum_{j=1}^{np} x_{nd}^j \right) \right) \right] \quad (4.47)$$

where $m(\cdot)$ is the average value of the data set.

This phase is characterized by the emergence of superior pupils, who replace the population's deficient members.

❖ **Step 4: Learner phase**

This is the second most crucial step in the TLBO algorithm. In this phase, students can increase their knowledge by randomly interacting with classmates. A student can acquire new information from another learner if the latter has superior expertise. Following is an explanation of the learning process at this stage:

$$\begin{cases} \mathbf{X}^{new,i} = \mathbf{X}^i + r(\mathbf{X}^i - \mathbf{X}^j) & \text{if } f(\mathbf{X}^i) < f(\mathbf{X}^j) \\ \mathbf{X}^{new,i} = \mathbf{X}^i + r(\mathbf{X}^j - \mathbf{X}^i) & \text{if } f(\mathbf{X}^i) > f(\mathbf{X}^j) \end{cases} \quad (4.48)$$

where i, j are the i^{th} and j^{th} solutions respectively, \mathbf{X}^j is a different solution from \mathbf{X}^i . \mathbf{X}^{new} will be selected when assumed that the fitness function is the best. It means \mathbf{X}^i will become \mathbf{X}^{new} , otherwise, \mathbf{X}^i will be accepted.

❖ **Step 5: Algorithm termination**

The method stops instantly once the initial number of loops has been executed. The final group of students reflects the optimal outcome of the design factors.

c) Hybrid teaching learning-based optimization algorithm

On the basis of combining the benefits of TM and TLBO, so-called HTLBO. Following was a description of each strategy (Figure 4. 34).

The HTLBO algorithm has outstanding features such as: (i) Can handle the multi-objective problem; (ii) having No control parameters; and (iii) having Fast convergence speed and low computation time.

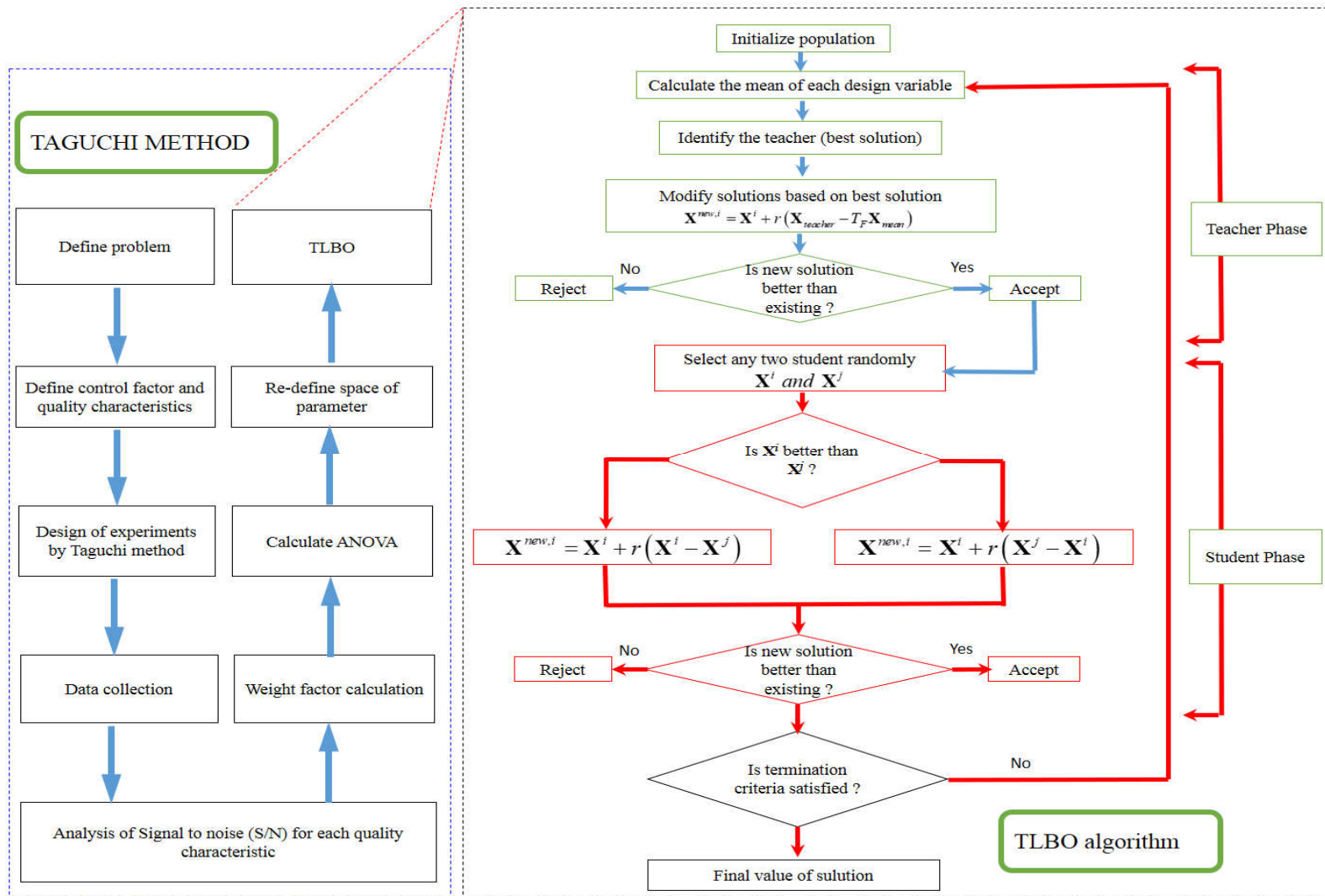


Figure 4. 34: Flowchart of proposed HTLBO

4.4.2. Optimal Results and Discussion

4.4.2.1. Determining Weight Factor

The designer, based on their expertise, and the assistance of experts, divided each element into three tiers, as depicted in Table 4. 8. To establish the number of experiments, the TM employed the $L_{27}(3^{13})$ orthogonal array. Table 4. 9 shows the data collected for the reaction force (F_o) at the jaw and the stress (σ).

Table 4. 10 contains the non-normalized values for the quality responses. The S/N ratio for gripping effort (η_3) was determined using Eq. (3. 2), while the S/N ratios for displacement (η_1) and the first natural frequency (η_2) were computed using Eq.(3. 1). The final column of the table shows the average values for each response.

Table 4. 8: Parameters and their upper and lower limits.

Factor	Symbol	Unit	Levels		
			1	2	3
l_A	A	mm	15	25	35
l_B	B	mm	7	12	17
t_A	C	mm	0.5	0.75	1.0
t_B	D	mm	0.5	0.7	0.9
t_E	E	mm	0.5	0.85	1.2
t_F	F	mm	0.5	1.0	1.5

Table 4. 9: Numerical experiments using Taguchi technique.

No.	A	B	C	D	E	F	F_o (N)	σ (MPa)
1	15	7	0.5	0.5	0.5	0.5	4.9965	32.903
2	15	7	0.5	0.5	0.85	1.0	5.0027	30.036
3	15	7	0.5	0.5	1.2	1.5	5.0010	29.57
4	15	12	0.75	0.7	0.5	0.5	4.9901	19.073
5	15	12	0.75	0.7	0.85	1.0	4.9973	15.282
6	15	12	0.75	0.7	1.2	1.5	5.0016	15.141
7	15	17	1.0	0.9	0.50	0.5	4.9991	12.655
8	15	17	1.0	0.9	0.85	1.0	4.9989	10.254
9	15	17	1.0	0.9	1.2	1.5	4.9983	9.838

No.	<i>A</i>	<i>B</i>	<i>C</i>	<i>D</i>	<i>E</i>	<i>F</i>	F_o (N)	σ (MPa)
10	25	7	0.75	0.9	0.5	1.0	5.0055	30.103
11	25	7	0.75	0.9	0.85	1.5	5.0024	21.847
12	25	7	0.75	0.9	1.2	0.5	5.0077	20.25
13	25	12	1.0	0.5	0.5	1.0	5.0121	46.784
14	25	12	1.0	0.5	0.85	1.5	5.0041	33.803
15	25	12	1.0	0.5	1.2	0.5	5.0003	24.594
16	25	17	0.5	0.7	0.5	1.0	4.9978	48.709
17	25	17	0.5	0.7	0.85	1.5	4.9900	45.559
18	25	17	0.5	0.7	1.2	0.5	4.9994	44.03
19	35	7	1.0	0.7	0.5	1.5	5.0021	40.786
20	35	7	1.0	0.7	0.85	0.5	4.9987	34.469
21	35	7	1.0	0.7	1.2	1.0	5.0047	30.551
22	35	12	0.5	0.9	0.5	1.5	5.0535	69.862
23	35	12	0.5	0.9	0.85	0.5	5.1168	63.457
24	35	12	0.5	0.9	1.2	1.0	5.0706	61.126
25	35	17	0.75	0.5	0.5	1.5	4.9980	65.868
26	35	17	0.75	0.5	0.85	0.5	4.9996	52.934
27	35	17	0.75	0.5	1.2	1.0	4.9981	44.346

Table 4. 10: Results and S/N ratios.

No.	f_1 (μm) Non-normalized	f_2 (HZ) Non-normalized	f_3 (%) = $\left \frac{F_o}{F_i} - 1 \right $ Non-normalized	η_1 of f_1 (dB)	η_2 of f_2 (dB)	η_3 of f_3 (dB)
1	356.44	207.53	0.07	51.0397	46.3416	23.0980
2	305.65	218.36	0.054	49.7045	46.7835	25.3521
3	293.25	218.23	0.02	49.3448	46.7783	33.9794
4	192.26	176.14	0.198	45.6778	44.9172	14.0667
5	140.53	204.47	0.054	42.9554	46.2126	25.3521
6	123.16	232.65	0.032	41.8094	47.3341	29.8970
7	128.06	145.74	0.018	42.1483	43.2716	34.8945
8	92.638	164.50	0.022	39.3358	44.3233	33.1515
9	74.373	181.64	0.034	37.4283	45.1842	29.3704

No.	f_1 (μm) Non-normalized	f_2 (HZ) Non-normalized	f_3 (%) = $\left \frac{F_o}{F_i} - 1 \right $ Non-normalized	η_1 of f_1 (dB)	η_2 of f_2 (dB)	η_3 of f_3 (dB)
10	475.53	163.88	0.11	53.5436	44.2905	19.1721
11	402.14	172.31	0.048	52.0875	44.7262	26.3752
12	377.90	176.62	0.154	51.5475	44.9408	16.2496
13	579.28	127.58	0.242	55.2578	42.1157	12.3237
14	400.58	148.81	0.082	52.0538	43.4526	21.7237
15	376.12	151.29	0.006	51.5065	43.5962	44.4370
16	1486.6	62.675	0.044	63.4439	35.9419	27.1309
17	1273.9	78.396	0.2	62.1027	37.8859	13.9794
18	1212.2	73.967	0.012	61.6715	37.3808	38.4164
19	728.25	114.52	0.042	57.2456	41.1776	27.5350
20	615.88	122.33	0.026	55.7899	41.7507	31.7005
21	553.41	126.89	0.094	54.8609	42.0685	20.5374
22	3355.2	53.899	1.07	70.5144	34.6316	-0.5877
23	3040.8	56.412	2.336	69.6598	35.0274	-7.3695
24	2958.7	56.305	1.412	69.4220	35.0109	-2.9967
25	2178.6	61.685	0.04	66.7635	35.8036	27.9588
26	1866.8	65.283	0.008	65.4220	36.2960	41.9382
27	1604.1	69.06	0.038	64.1046	36.7845	28.4043
Average value	$f_1^a = 933.05 \mu\text{m}$	$f_2^a = 134.48 \text{ Hz}$	$f_3^a = 0.239\%$			

Table 4. 11 displays the S/N ratio of each factor at different levels of displacement. The results of this study are included as:

- Factor A: Largest S/N ratio is level 3, next is level 2, and lowest is level 1.
- Factor B: Largest S/N ratio is level 3, next is level 2, and lowest is level 1.
- Factor C: Largest S/N ratio is at level 1, next is level 2, and lowest is level 3.
- Factor D: Largest S/N ratio is level 1, next is level 3, and lowest is level 2.
- Factor E: Largest S/N ratio is level 1, next is level 2, and lowest is level 3.
- Factor F: Largest S/N ratio is level 1, next is level 2, and lowest is level 3.

All in all, A is the highest contribution, next are C, B, E, and D, and the smallest is F.

Table 4. 11: Mean S/N ratios for the displacement.

Level	A	B	C	D	E	F
1	44.38	52.80	60.77	56.13	56.18	54.94
2	55.91	55.43	53.77	53.95	54.35	54.74
3	63.75	55.82	49.51	53.97	53.52	54.37
Delta	19.37	3.03	11.25	2.18	2.66	0.57
Rank	1	3	2	5	4	6

Using the same line of reasoning as previously stated, Table 4. 12 and Table 4. 13 reveal the allocation of design parameter contributions to frequency and gripping effort. Specifically, in terms of frequency, factor A has the greatest impact, trailed by factors B, C, E, and D, with factor F having the least impact. Regarding gripping effort, factor B has the greatest influence, followed by factors C, D, A, and F, with factor E having the least influence.

Table 4. 12: Frequency - mean S/N ratios.

Level	A	B	C	D	E	F
1	45.680	44.320	39.530	41.990	40.940	41.500
2	41.590	41.370	42.370	41.630	41.830	41.500
3	37.620	39.210	42.990	41.270	42.120	41.890
Delta	8.060	5.110	3.460	0.729	1.180	0.390
Rank	1	2	3	5	4	6

Table 4. 13: Gripping effort - mean S/N ratios.

Level	A	B	C	D	E	F
1	0.05578	0.06867	0.57978	0.06222	0.20378	0.31422
2	0.09978	0.60356	0.07578	0.07800	0.31444	0.23000
3	0.56289	0.04622	0.06289	0.57822	0.20022	0.17422
Delta	0.50711	0.55733	0.51689	0.51600	0.11422	0.14000
Rank	4	1	2	3	6	5

Prior to executing the optimization procedure, refinement of the design parameters' search space was carried out utilizing the S/N ratios and ANOVA analysis. The ANOVA analysis was based on the S/N ratios of the three responses, and the software Minitab was utilized to obtain the ANOVA results.

The findings in Table 4. 14 are indicated below.

- Factor A: Strongest S/N ratio is level 3, the next is level 2, and the smallest is level 1. So, level 2 was the lower bound, and level 3 are the upper bound. This is a way to limit the un-significant variables.
- Factor B: Level 1 and Level 3 were set in the lower and upper bounds.
- Factor C: Levels 2 and 1 were the lower and upper bounds.
- Factor D: Levels 3 and 1 were the lower and upper bounds.
- Factor E: Levels 2 and 1 were the lower and upper bounds.
- Factors A, B, C, D, and E were statistically significant with p -values <0.05 .
- Factor F had a p -value >0.05 and it was therefore ignored in the optimization.
- In summary, the order contribution to displacement was A, C, B, E, and D, F with F-ratios of 2373.45, 807.09, 67.74, 46.35, 39.42, and 2.07, respectively.

Table 4. 14. ANOVA for displacement

Factor	DOF	Seq SS	Adj SS	Adj MS	F-ratio	p-value	Contribution
A	2	1708.97	1708.97	854.485	2373.45	0.000	70.99%
B	2	48.78	48.78	24.388	67.74	0.000	2.03%
C	2	581.13	581.13	290.567	807.09	0.000	24.14%
D	2	28.38	28.38	14.192	39.42	0.000	1.18%
E	2	33.37	33.37	16.687	46.35	0.000	1.39%
F	2	1.49	1.49	0.745	2.07	0.163	0.06%
Error	14	5.04	5.04	0.360			0.21%
Total	26	2407.17					100.00%

Note: Confidence level at least 95%

Case 1: The design parameter search spaces for the displacement were narrowed down using the following refinement process.

$$\begin{cases} 25 \text{ mm} \leq l_A(A) \leq 35 \text{ mm} \\ 12 \text{ mm} \leq l_B(B) \leq 17 \text{ mm} \\ 0.5 \text{ mm} \leq t_A(C) \leq 0.75 \text{ mm} . \\ 0.5 \text{ mm} \leq t_B(D) \leq 0.9 \text{ mm} \\ 0.5 \text{ mm} \leq t_E(E) \leq 0.85 \text{ mm} \end{cases} \quad (4.49)$$

Table 4. 15 has a few conclusions as follows.

- Factor A: Highest S/N ratio is level 1, the next is level 2, and the smallest is level 3. Therefore, level 2 is the lower bound, and level 1 is the upper bound.
- Similar limits were applied to the remaining factors, revealing that their contributions are ranked as follows: A, B, C, E, and D have significant effects on the frequency, with the F factor having the least effect. The F-ratios for these factors are 1120.19, 453.06, 234.37, 25.85, 9.11, and 3.37, respectively.
- The p -values for A, B, C, D, and E are less than 0.05, indicating their statistical significance, while the F factor's p -value is 0.064, making it insignificant.
- Consequently, F was ignored in the optimization. Factor A is the highest impact on the frequency, the next are B, C, E, and D, and F is the lowest.

Table 4. 15. ANOVA for frequency.

Factor	DOF	Seq SS	Adj SS	Adj MS	F-ratio	p-value	Contribution
A	2	292.804	292.804	146.402	1120.19	0.000	60.45%
B	2	118.426	118.426	59.213	453.06	0.000	24.45%
C	2	61.261	61.261	30.631	234.37	0.000	12.65%
D	2	2.380	2.380	1.190	9.11	0.003	0.49%
E	2	6.756	6.756	3.378	25.85	0.000	1.39%
F	2	0.880	0.880	0.440	3.37	0.064	0.18%
Error	14	1.830	1.830	0.131			0.38%
Total	26	484.338					100.00%

Note: Confidence level at least 95%

Case 2: The design parameter search spaces for the frequency were narrowed down using the following refinement process.

$$\left\{ \begin{array}{l} 15 \text{ mm} \leq l_A(A) \leq 25 \text{ mm} \\ 7 \text{ mm} \leq l_B(B) \leq 12 \text{ mm} \\ 0.75 \text{ mm} \leq t_A(C) \leq 1.0 \text{ mm} . \\ 0.5 \text{ mm} \leq t_B(D) \leq 0.7 \text{ mm} \\ 0.85 \text{ mm} \leq t_E(E) \leq 1.2 \text{ mm} \end{array} \right. \quad (4.50)$$

Similar way for gripping effort, Table 4. 16 shows that:

- Factor B: Largest S/N ratio is level 2, next is level 1, and lowest is level 3. Consequently, level 2 upper limit, and level 1 lower limit.
- Order of contributions to the gripping effort: B, D, C, A, E factors, and F is lowest with F-ratios of 7.33, 4.92, 4.44, 2.59, 1.04, and 0.90, respectively.
- Factors B, C, and D were statistically significant with $p\text{-value} < 0.05$.
- Factors A, E, and F were excluded in the optimization due to their $p\text{-value} > 0.05$.
- Factor C: Lower limit is level 2 and level 1 is upper limit.
- Factor D: Lower limit is level 2 and level 3 is upper limit.

Table 4. 16. ANOVA for gripping effort.

Factor	DOF	Seq SS	Adj SS	Adj MS	F -ratio	p -value	Contribution
A	2	384.0	384.0	192.01	2.59	0.111	9.17%
B	2	1088.0	1088.0	544.00	7.33	0.007	25.98%
C	2	659.0	659.0	329.52	4.44	0.032	15.74%
D	2	729.8	729.8	364.90	4.92	0.024	17.43%
E	2	154.3	154.3	77.16	1.04	0.379	3.68%
F	2	133.9	133.9	66.97	0.90	0.428	3.20%
Error	14	1038.7	1038.7	74.19			24.80%
Total	26	4187.8					100.00%

Note: Confidence level at least 95%

Case 3: The design parameter search spaces for gripping effort were narrowed down using the following refinement process.

$$\begin{cases} 7\text{mm} \leq l_b(B) \leq 12\text{mm} \\ 0.5\text{mm} \leq t_A(C) \leq 0.75\text{mm} \\ 0.7\text{mm} \leq t_b(D) \leq 0.9\text{mm} \end{cases} \quad (4.51)$$

The S/N ratio from Table 4. 10 was used to compute the normalized S/N ratio values through Eq. (4. 40) in Table 4. 17. Mean range was determined for each level for each factor by Eq.(4. 41), and the weight factor for each response was calculated using Eq.(4. 42), presented in Table 4. 18, Table 4. 19, and Table 4. 20. The WF values for displacement are 0.3083 (30.83%), frequency is 0.3891 (38.91%), and gripping effort is 0.3026 (30.26%).

Table 4. 17: The values of normalized S/N ratios (z_i).

S/N ratios			Normalized S/N ratios (z_i)		
η_1 (dB)	η_2 (dB)	η_3 (dB)	z_1 of η_1	z_2 of η_2	Z_3 of η_3
51.0397	46.3416	23.0980	0.4114	0.9219	0.5881
49.7045	46.7835	25.3521	0.3710	0.9567	0.6316
49.3448	46.7783	33.9794	0.3602	0.9562	0.7981
45.6778	44.9172	14.0667	0.2493	0.8097	0.4138
42.9554	46.2126	25.3521	0.1671	0.9117	0.6316
41.8094	47.3341	29.8970	0.1324	1.0000	0.7193
42.1483	43.2716	34.8945	0.1427	0.6802	0.8158
39.3358	44.3233	33.1515	0.0577	0.7630	0.7822
37.4283	45.1842	29.3704	0.0000	0.8307	0.7092
53.5436	44.2905	19.1721	0.4871	0.7604	0.5123
52.0875	44.7262	26.3752	0.4431	0.7947	0.6514
51.5475	44.9408	16.2496	0.4267	0.8116	0.4559
55.2578	42.1157	12.3237	0.5389	0.5892	0.3801
52.0538	43.4526	21.7237	0.4420	0.6944	0.5616
51.5065	43.5962	44.4370	0.4255	0.7057	1.0000
63.4439	35.9419	27.1309	0.7863	0.1032	0.6659

<i>S/N</i> ratios			Normalized <i>S/N</i> ratios (z_i)		
η_1 (dB)	η_2 (dB)	η_3 (dB)	z_1 of η_1	z_2 of η_2	z_3 of η_3
62.1027	37.8859	13.9794	0.7458	0.2562	0.4121
61.6715	37.3808	38.4164	0.7327	0.2164	0.8838
57.2456	41.1776	27.5350	0.5990	0.5153	0.6737
55.7899	41.7507	31.7005	0.5550	0.5604	0.7542
54.8609	42.0685	20.5374	0.5269	0.5855	0.5387
70.5144	34.6316	-0.5877	1.0000	0.0000	0.1309
69.6598	35.0274	-7.3695	0.9742	0.0312	0.0000
69.4220	35.0109	-2.9967	0.9670	0.0299	0.0844
66.7635	35.8036	27.9588	0.8866	0.0923	0.6819
65.4220	36.2960	41.9382	0.8461	0.1310	0.9518
64.1046	36.7845	28.4043	0.8063	0.1695	0.6905

Table 4. 18: The WF for the displacement.

Level	The average of the normalized signal-to-noise ratios for each level					
	A	B	C	D	E	F
Level 1	0.2102	0.4645	0.7054	0.5653	0.5668	0.5293
Level 2	0.5587	0.5440	0.4939	0.4994	0.5113	0.5231
Level 3	0.7957	0.5560	0.3653	0.4998	0.4864	0.5121
Range r_{ij}	0.5855	0.0915	0.3401	0.0660	0.0804	0.0172
$w_1 = 0.3083$						

Table 4. 19: The WF for the frequency.

Level	The average of the normalized signal-to-noise ratios for each level					
	A	B	C	D	E	F
Level 1	0.8700	0.7625	0.3857	0.5797	0.4969	0.5409
Level 2	0.5480	0.5302	0.6090	0.5509	0.5666	0.5410
Level 3	0.2350	0.3603	0.6583	0.5224	0.5895	0.5711
Range r_{ij}	0.6350	0.4022	0.2725	0.0573	0.0926	0.0302
$w_2 = 0.3891$						

Table 4. 20: The WF for the gripping effort.

Level	The average of the normalized signal-to-noise ratios for each level					
	A	B	C	D	E	F
Level 1	0.6766	0.6227	0.4661	0.6982	0.5403	0.6515
Level 2	0.6137	0.4357	0.6343	0.6326	0.5974	0.5464
Level 3	0.5007	0.7326	0.6906	0.4602	0.6533	0.5931
Range r_{ij}	0.1760	0.2968	0.2245	0.2380	0.1130	0.1051
$w_3 = 0.3026$						

4.4.2.2. Optimal results

Case 1

As previously stated, for case 1, varied parameters have different influences on the responses.

This indicates that the significance of each response is contingent on the WF. To substantiate this perspective, a variety of weight factors were randomly chosen and used to solve the optimization problem. These WFs achieved as: $w_1 = 0.45$, $w_2 = 0.25$, $w_3 = 0.30$; $w_1 = 0.50$, $w_2 = 0.22$, $w_3 = 0.28$; $w_1 = 0.40$, $w_2 = 0.40$, and $w_3 = 0.20$. To ensure the stability of the algorithm, the optimization was performed ten times [170]. The outcomes derived from the amalgamated objective function value were subsequently compared to the best results attained in this thesis [168], which were calculated using weight factors of $w_1 = 0.3083$, $w_2 = 0.3891$, $w_3 = 0.3026$.

The findings presented in Table 4. 21 indicate that the use of weight factors derived from calculations led to significantly different optimal values of the design variable (x_{val}) and the combined objective function value at the solution (f_{val}), as compared to those obtained using randomly selected weight factors.

Moreover, the use of calculated weights resulted in a much lower optimal value of the combined objective function than when randomly chosen weights were employed. Therefore, it can be concluded that standardized equations should be used to calculate weight factors in order to obtain more precise solutions.

Table 4. 21: Case 1: The optimal solutions at different weight factors.

Responses	Calculated WFs		Random WFs									
	$w_1 = 0.3083$	$w_2 = 0.3891$	$w_3 = 0.3026$	$w_1 = 0.45$	$w_2 = 0.25$	$w_3 = 0.30$	$w_1 = 0.50$	$w_2 = 0.22$	$w_3 = 0.28$	$w_1 = 0.40$	$w_2 = 0.40$	$w_3 = 0.20$
Displacement (μm)	1120.21	801.34	437.53	564.50								
Frequency (Hz)	148.14	145.78	141.11	150.03								
Gripping effort (N)	0.942	0.958	0.957	0.956								
x_{val}	[25; 17; 0.52; 0.62; 0.85; 1.5]	[25; 16.4; 0.5; 0.58; 0.5; 1.4]	[25; 16.9; 0.52; 0.62; 0.78; 1.34]	[25; 17; 0.53; 0.71; 0.63; 1.1]								
f_{val}	-1.4288	-1.3414	-1.2472	-1.041								

After proposing an optimal algorithm, its effectiveness was compared with other population-based optimization algorithms, namely GA [171], PSO [172], and AEDE [173]. The parameters for each optimizer include as.

- GA: population size= 25, maximum iteration= 5000, tolerance= 10^{-6} , and crossover coefficient= 0.80.
- PSO: population size= 25, tolerance= 10^{-6} , and maximum iteration= 5000.
- AEDE: population size= 25, mutant factor= 0.85, threshold= 10^{-4} , delta= 10^{-6} , and maximum iteration= 5000.

The function evaluation number (FEN) is computed by multiplying the population size with the generation number. FEN is a common criterion and was selected in this comparison. Table 4. 22 displays that the proposed HTLBO achieved superior results compared to AEDE, PSO, and GA.

Table 4. 22: Case 1: Comparison of the recommended approach with other optimizers.

Quality outcome	Different optimizers			
	HTLBO	AEDE	PSO	GA
Displacement (μm)	1120.21	790.04	793.25	1105.37
Frequency (Hz)	148.14	135.16	133.66	131.53
Gripping effort (N)	0.942	0.954	0.967	0.960
Number of function evaluation	20	1760	560	820
Evaluation rate	0.075	0.953	0.673	1.393

Case 2:

In Case 2, the WFs are listed in Table 4. 21. The outcomes presented in Table 4. 23 indicate that calculating the WFs is necessary to obtain more dependable solutions. According to Table 4. 24, the results showed that the proposed HTLBO has a superior evaluation rate compared to AEDE and PSO, GA.

Table 4. 23: Case 2: The optimal solutions at different weight factors.

Responses	Calculated WFs	Random WFs		
		$w_1 = 0.3083$	$w_1 = 0.45$	$w_1 = 0.50$
	$w_2 = 0.3891$	$w_2 = 0.25$	$w_2 = 0.22$	$w_2 = 0.40$
	$w_3 = 0.3026$	$w_3 = 0.30$	$w_3 = 0.28$	$w_3 = 0.20$
Displacement (μm)	1382.41	1330.60	1328.15	1300.60
Frequency (Hz)	160.05	137.87	126.23	101.42
Gripping effort (N)	0.963	0.974	0.975	0.978
X _{val}	[15; 12; 1.0; 0.5; 1.0; 0.75]	[15; 12; 0.75; 0.53; 1.0; 1. 5]	[15; 11.5; 0.75; 0.5; 1.2; 1.13]	[15; 12; 0.85; 0. 7; 1.2; 0.93]
f _{val}	-1.6129	-1.4679	-1.3598	-1.1986

Table 4. 24: Case 2: Comparison of the recommended approach with other optimizers.

Responses	Different optimizers			
	HTLBO	AEDE	PSO	GA
Displacement (μm)	1302.41	735.61	719.34	987.64
Frequency (Hz)	160.05	134.20	135.06	126.00
Gripping effort (N)	0.963	0.978	0.983	0.980
Number of function evaluation	20	1620	540	820
Evaluation rate	0.075	775.89	0.743	1.393

Case 3:

The third case employed a similar computational process. Table 4. 25 showed that optimal solutions can achieve an exact solution when calculating WFs. Moreover, the results in Table 4. 26 demonstrate that the proposed HTLBO outperformed AEDE, PSO, and GA.

Table 4. 25: Case 3: The optimal solutions at different weight factors.

Responses	Calculated WFs	Random WFs		
		$w_1 = 0.45$	$w_1 = 0.50$	$w_1 = 0.40$
	$w_1 = 0.3083$	$w_2 = 0.25$	$w_2 = 0.22$	$w_2 = 0.40$
	$w_2 = 0.3891$	$w_3 = 0.30$	$w_3 = 0.28$	$w_3 = 0.20$
	$w_3 = 0.3026$			
Displacement (μm)	1924.15	1376.88	1208.92	1130.24
Frequency (Hz)	170.45	165.02	158.46	150.17
Gripping effort (N)	0.935	0.942	0.947	0.951
xval	[15; 11.67; 0.62; 0.86; 0.7; 1.25]	[15; 12; 0.5; 0.9; 0.71; 1.5]	[15; 10; 0.53; 0.7; 0.86; 0.77]	[15; 10; 0.5; 0.7; 0.99; 0.5]
fval	-1.6190	-1.4517	-1.3443	-1.2036

Table 4. 26: Case 3: Comparison of the recommended approach with other optimizers.

Responses	Different optimizers			
	HTLBO	AEDE	PSO	GA
Displacement (μm)	1924.15	803.64	798.66	1201.33
Frequency (Hz)	170.45	156.38	143.15	135.19
Gripping effort (N)	0.935	0.95	0.95	0.94
Number of function evaluation	20	1700	580	820
Evaluation rate	0.075	0.841	0.823	1.393

Upon analysis of the results, case #3 was the most suitable solution for the gripper design. This decision was made based on three criteria, including displacement, frequency, and gripping forces, which were slightly better than those of cases #1 and case #2.

4.4.3. Verifications

The compliant gripper was developed using Case 3 as the matching design. The 3D model was built using Solidworks software, and the initial behaviors were determined by ANSYS 16 software and then verified experimentally [168].

A prototype of the gripper was manufactured by WEDM. The block diagram of the displacement measurement system is shown in Figure 4. 35, and the experiments are performed as shown in Figure 4. 36a. As shown in Figure 4. 36a, the prototype was fixed at holes, and a force gauge was used to apply the force F . The displacement was measured using a laser displacement sensor. A connector was utilized to transfer the signal to a digital display.

The setup for the first natural frequency was demonstrated in Figure 4. 29 and Figure 4. 36b. The PEA was energized with the aid of a high-speed bipolar amplifier, with the retro-reflective tape placed in the center of the movable object. PEA was preloaded and displacement was measured with a nanoscale high-resolution laser

vibrometer sensor. These signals are analyzed by a frequency response analyzer, the analysis results are displayed on the screen.

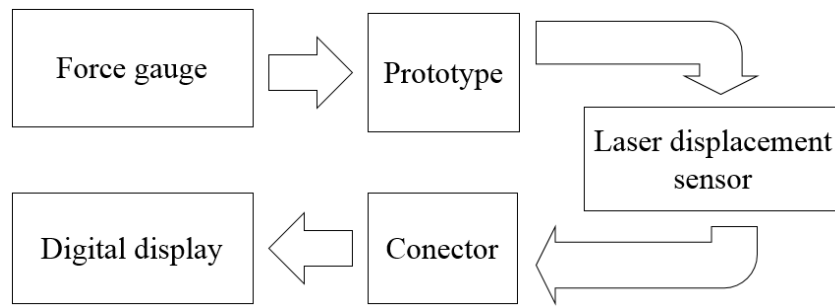


Figure 4. 35: Block diagram of displacement measurement system

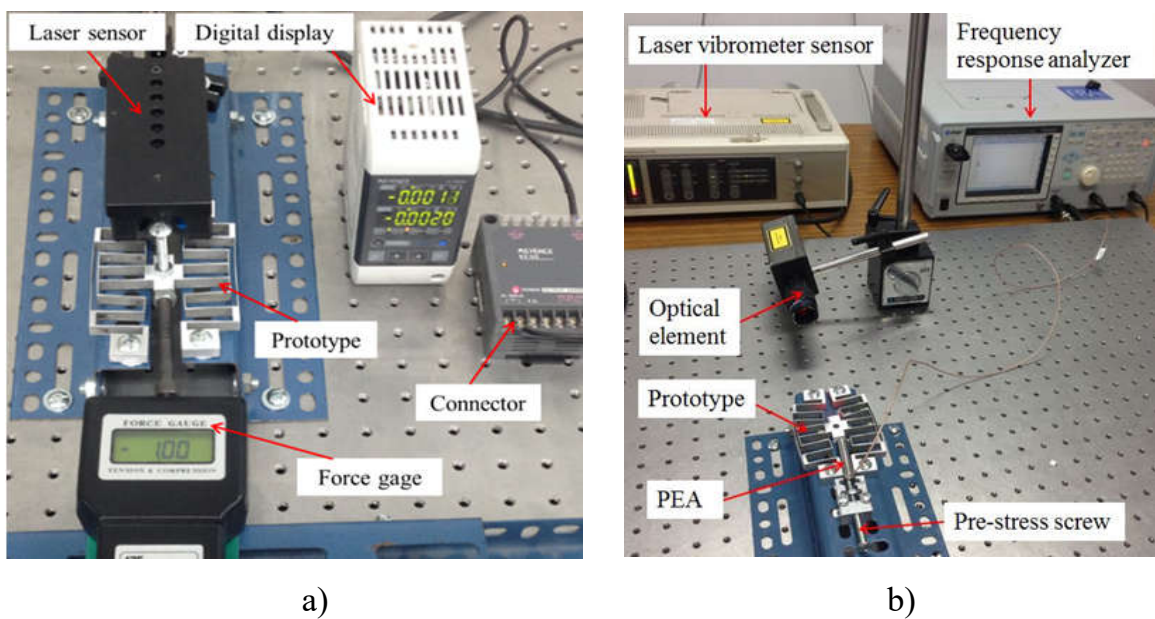


Figure 4. 36: Experimental tests: a) Displacement and b) Frequency.

Figure 4. 37 shows the strain test. A force of 5 N was from a force gauge. The sensor gauges were attached to the FHs to measure the actual strain with measured five times. The data collected were sent to the DAQ. LABVIEW[®] software was used to show the strain. The stress was computed as.

$$\sigma_a = \varepsilon_a \times E \quad (3. 21)$$

where σ_a is the actual stress and ε_a is the actual strain.

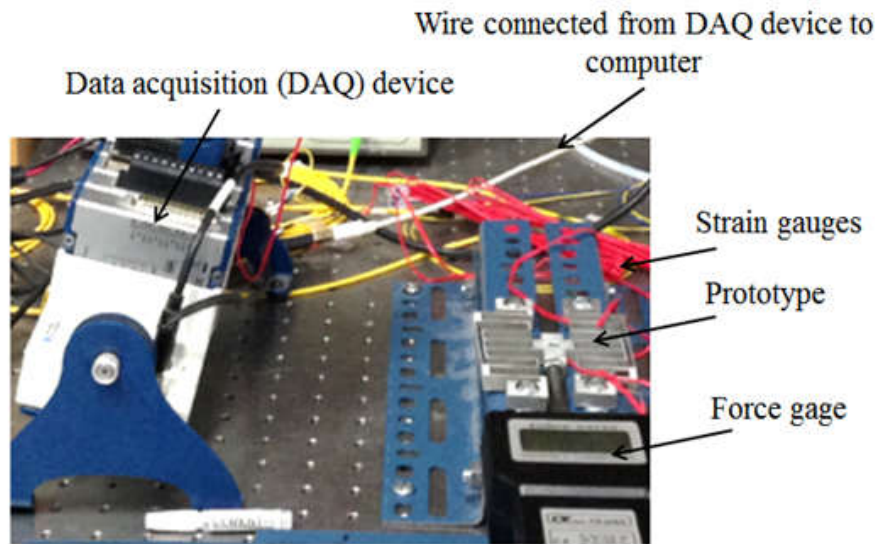


Figure 4. 37: Test of physical strain.

Table 4. 27 shows that the experimental results are close to the predicted results.

Table 4. 27: Experimental results.

Quality outcome	HTLBO	Experiment	FEA	Error (%) between HTLBO and experiment	Error (%) Between HTLBO and FEA
Displacement (μm)	1924.15	1831.40	1845.15	4.82	4.10
Frequency (Hz)	170.45	164.63	164.90	3.41	3.25
Stress (MPa)	46.71	44.54	44.06	4.64	5.67

Comparative results in Table 4. 27 show that: for displacement, the result obtained from the HTLBO (1924.15 μm) is larger than those obtained from the experiment (1831.40 μm) and FEA simulation results (1845.15 μm). The relative error between the obtained results of HTLBO and experimental, HTLBO and FEA simulation is 4.82%, and 4.1%, respectively. In terms of frequency, the result obtained from the proposed method is 170.45 Hz, it is larger than the result obtained from the experiment (164.63 Hz) and the simulation result of FEA (164.90 Hz) corresponding to a relative error of 3.41% and 3.25%, respectively. Conversely, in terms of stress,

the analytical result obtained from the proposed method is 46.71 MPa, which is larger than the result obtained from experimental (44.54 MPa) and simulation FEA (44.06 MPa). It means that the gripper allows large displacement but its stress is still below the allowable yield strength. The relative error between the obtained results of HTLBO and experimental, HTLBO and FEA simulation is 4.64%, and 5.67%, respectively. According to the experience of experts and the results of studies in the same field, the results obtained from this thesis (approximately 6%) are completely acceptable [39], [174], [175]. Although these errors are still within the acceptable range, there are factors such as errors in meshing, manufacturing, and materials that could potentially reduce these deviations. Consequently, the hybrid optimization algorithm suggested was sturdy and efficient in enhancing the compliant gripper.

4.5. Summary

In this chapter, a displacement sensor has been developed. It was integrated into an asymmetrical compliant gripper. The gripper was turned into a displacement sensor with a resolution of micrometers by placing strain gauges in the FHs. The relationship between force and displacement of the proposed sensor was analytically formulated. The dynamic equation was established using the PRBM and Lagrange's method. Specifically, the open cavities of the gripper were filled with silicone rubber to increase stiffness, resulting in a relative improvement in frequency. It is demonstrated that the requisite displacement can be achieved through the sensor element incorporated in the gripper. The gripper's stiffness could be increased with rubber, and the frequency can be improved. The HTLBO was used to optimize the displacement, frequency, and gripping effort. The WFs for each response were properly computed. The results of this chapter could be covered as follows:

- The developed CG had a displacement of 1924.15 μm and a frequency of 170.45 Hz corresponding to a maximum stress of 46.71 MPa. It was completely consistent with the initial hypothesis.
- The proposed algorithm was better than that of the other optimizers.
- The optimal solutions generated by the HTLBO were deemed superior to those generated by other algorithms.

- The predicted results were in excellent agreement with the simulation and empirical validations.

The research contents in Chapter 4 have been published by Ho and co-authors [59], [163], [168] in **Microsyst Technol Journal** (2016, SCI - Q2), **Microsyst Technol Journal** (2018, SCI – Q2), and **Vietnam Journal of Mechanics** (2020, ACI).

Chapter 5 COMPUTATIONAL MODELING AND OPTIMIZATION OF A SYMMETRICAL COMPLIANT GRIPPER FOR CYLINDRICAL SAMPLES

Chapter 5 presents the design of a compliant gripper that has a symmetrical structure. The gripper's kinematic models have been developed based on the mechanics of motion, which helps determine the relative velocity of joints and links. The design also includes a static model that focuses on stiffness, displacement, stress, force-displacement relationship, and amplification ratio. Additionally, a dynamic model has been established using PRBM and Lagrange's principle. To optimize the gripper, a new approach that combines ANFIS and Jaya algorithm has been developed. The WF for each response is calculated. The predicted results are evaluated through simulations and experiments.

5.1. Basic application of symmetrical compliant gripper for cylinder samples

In order to meet the practical requirement for a DC vibrating motor assembly system in Figure 1. 3 (Chapter 1), a symmetrical compliant gripper is developed for the DC motor assembly, as shown in Figure 5. 1a. To manipulate the shaft towards the core in an assembled system for a mobile phone vibration motor. As depicted in Figure 5. 1b, the core of the mobile phone vibration motor possesses a circular hole, while the shaft has a size ranging from 600 μm to 800 μm [12], [13], [152], [165]. The operation of the system was as follows:

The punch (1) was directed vertically by a stationary (2) and four rods (3). The CG (4) was positioned through fixed holes (5) on the top surface of a non-vibrating optical table (8). The PEA (6) was positioned in the center of the DA and was preloaded through the screw (7). The core (12) was arranged on the platform (11). The core and platform were moved simultaneously along the horizontal direction on ray 2 (10). Ray 2 was displaced on ray 1 (9). Initially, the shaft was positioned to be

in line with CG's hand.

Then, using the initial force from PZT, the left and right jaws of CG applied a clamping force F_2 to secure the shaft. The center of the shaft was then aligned with the center of the core using rays, which were adjusted using a servo motor. During the final stage, the punch would descend with a force of F_1 to assemble the shaft into the core. F_1 force was described as the pressing force exerted by the designated press machine and could be modified to meet the designer's specifications. The magnitude of F_1 was regulated by external motors and actuators. Outside the core will be a wound wire and a part of the vibration motor of the mobile phone is formed.

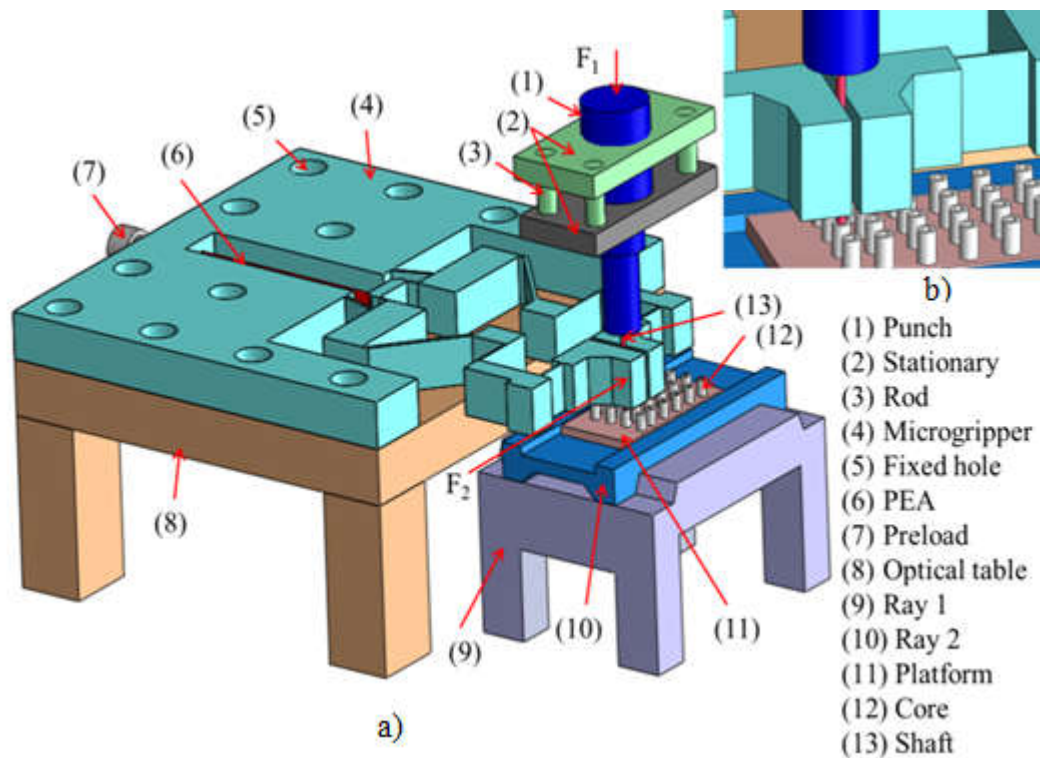


Figure 5. 1: Assemble system for the mini vibrating motors: a) Assembling system, b) Details of motor shaft and core.

5.2. Research targets of symmetrical compliant gripper

The manipulation of electronic components is very complex and involved grasping accuracy. Especially in the field of assembling small-sized, high-precision devices, such as those used in game machines or mobile device components [12].

According to the studies [12], [13], [165], to design a suitable gripper for the DC motor assembly, the present investigation performs on two main targets for the

symmetrical compliant gripper as follows:

- A CG with applicability in the proposed shaft-type part locating and the gripping system is proposed to be developed. An application in a vibrating motor assembly system is described and considered as a hypothesis for study. The shaft and core assembly of a vibrating motor which applies to mobile phones are considered an object of study (refer to Figure 1. 3). The sizes are measured as $\phi 0.6\text{mm}\times 10\text{mm}$ for the shaft and $\phi 2.5\text{mm}\times 3\text{mm}$ for the core based on the previous studies [12], [13], [165]. (Technical requirements of the proposed gripper will be presented in section 5.2.2.)
- Developed a new approach to the analysis, design, and optimization of compliant grippers. This approach should achieve the following points: ease of use, high reliability, and good economic efficiency.

5.3. Mechanical design of symmetrical compliant gripper

To accomplish the targets, first, the mechanical design and operating principle of the gripper will be described. Based on the proposed design and operating principle, the initial behavior of the gripper is also analyzed through kinematic, static, and dynamic analysis [12], [13], [165]. The results obtained from these analyzes are the basic knowledge for the designers in the field of precision engineering as well as compliant mechanism.

5.3.1. Description of structural design

In order to create a gripper suitable for the potential applications mentioned earlier for vibrating DC motor assembly [20], a CG with square type was developed (Figure 5. 2 a) in combination with displacement amplification mechanism (DA). The presented gripper was designed based on the square wave signal type in digital waves, providing a simple structure and stiffness (Figure 5. 2 b). The use of sine or cosine wave signals would make the topology of the gripper more complex. Material AL7075 with parameters as shown in Table 4. 2 was selected as a suitable material for this design [161], [162]. Elastic FHs were used for the motion of the gripper, and the left hand's displacement and gripping were designed to match those of the right

hand, which was dependent on the designer's experience. The PEA was used to generate a force. Additionally, a preload was used to ensure good initial interference between the actuator and the gripper. This study was performed by Ho et al. [165].

During the last phase of design, a structure called the 2L-type DA was combined with the gripper to increase its stroke. This allowed the gripper to pick up micro-objects of varying sizes ranging from a few micrometers to hundreds of micrometers due to its large stroke. The study proposed a symmetrical topology of two levers for amplification, which further improved the working travel of the gripper. The amplification ratio of one lever was $R_{1a} = l_o/l_i$, and the amplification ratio of two levers was approximately $R_{2a} = 4R_{1a}$, as illustrated in Figure 5. 3a and b.

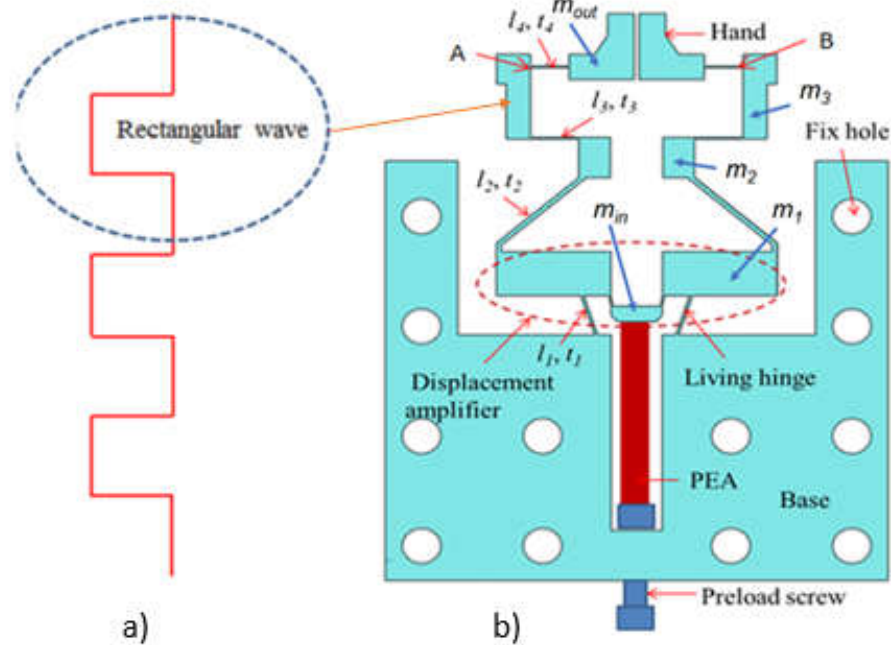


Figure 5. 2: CAD model: a) Rectangular shape and b) Symmetric compliant gripper.

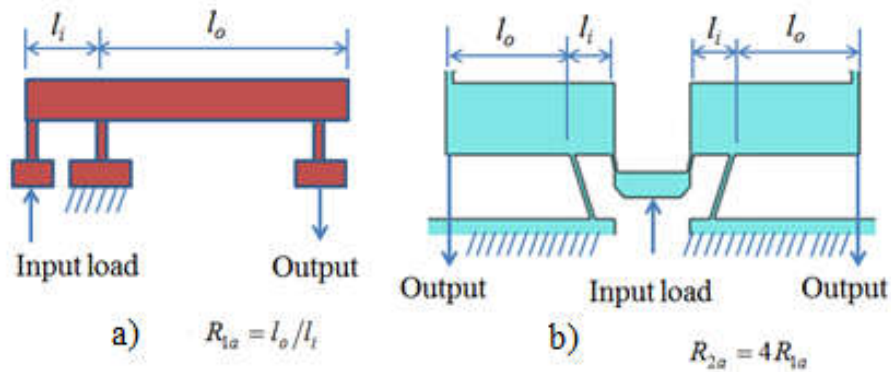


Figure 5. 3: Levers: a) Lever mechanism, b) Double lever mechanism.

This design aimed to make sure that the magnitude of F_2 was equal on both sides of the jaws. The magnitude of F_2 was calculated as the reaction force of the FH (l_4) at points A and B, as shown in Figure 5. 4.

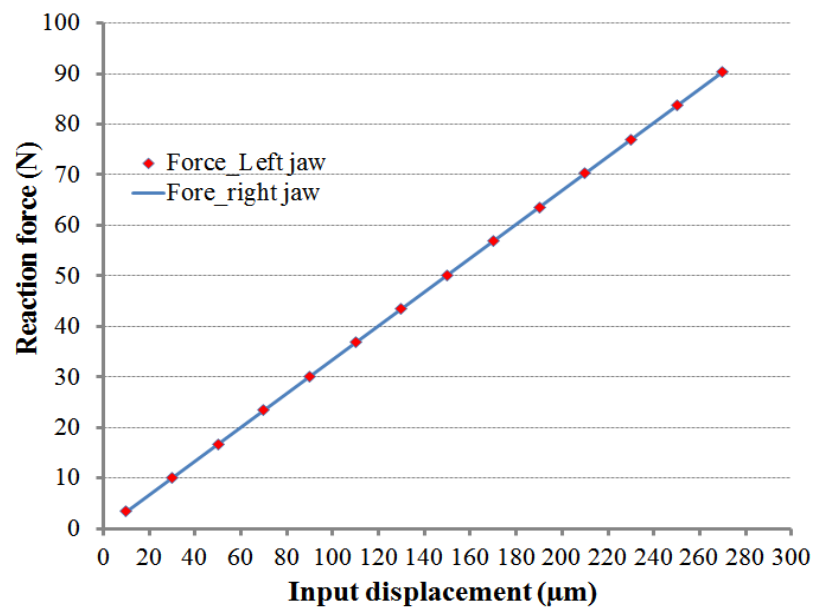


Figure 5. 4: The reaction force of the left and right jaws.

5.3.2. Technical requirements of proposed symmetrical compliant gripper

According to the practice requirements of DC motor assemble system [12], [165] and based on a study by Ho et al. [165], the proposed symmetrical CG must meet the following specifications:

- a) Hand grips are constructed with a square wave design. This model can ensure that both jaws move symmetrically.
- b) Having a large displacement measurement range ($>1000\mu\text{m}$), and a high frequency ($> 60\text{Hz}$).
- c) The equivalent stress of CG must be lower than the yield stress of the material.

5.3.3. Behavior analysis of the proposed compliant gripper

5.3.3.1. Kinematic analysis

To take advantage of the symmetric property, a kinematic series was used to construct one-half of the proposed gripper, as displayed in Figure 5. 5 (refer to [12]). By utilizing the schematic diagram, it became possible to examine the kinematic actions of the micro-gripper, including the correlation between joint positions and

velocities. At point A, a revolute joint was identified as a living hinge, while the main flexure beams were OB , CD , EF , and GH . Figure 5. 6a and b depict the microgripper's motion vector and rotational angle changes.

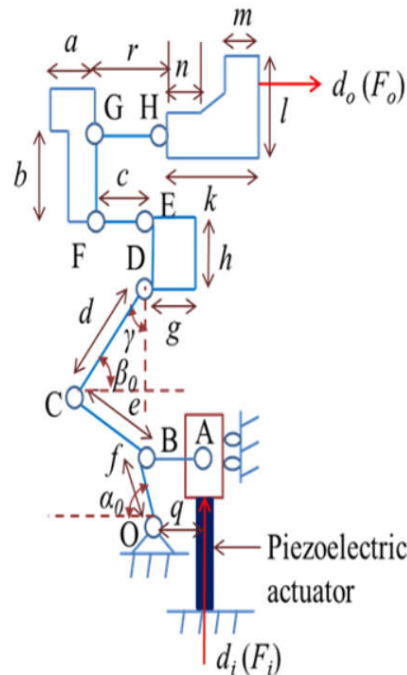


Figure 5. 5: Kinematic model of the symmetrically compliant gripper.

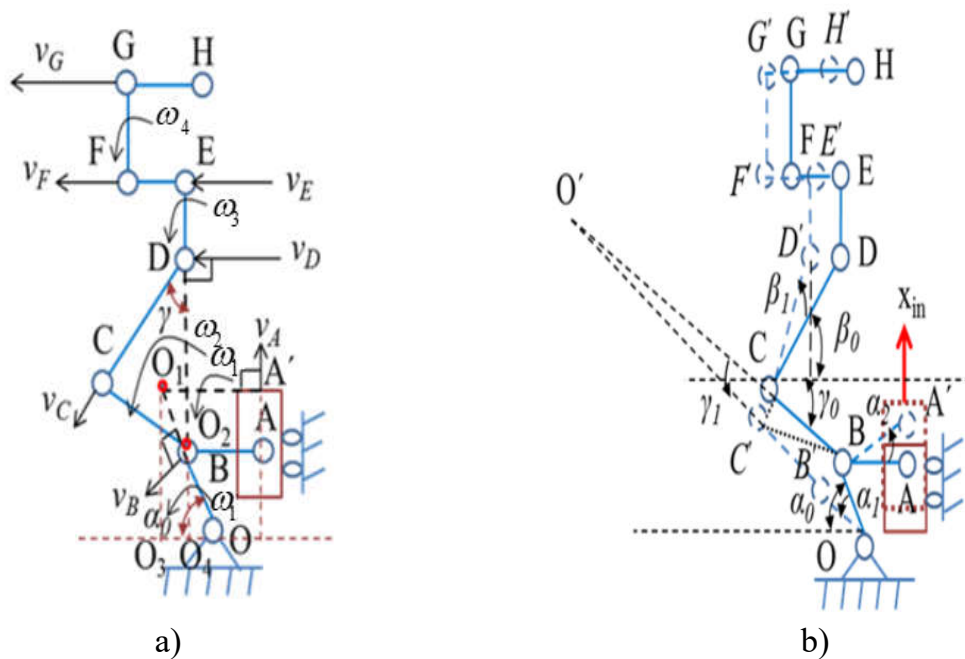


Figure 5. 6: Schematic diagram: a) Motion vector and b) Rotational angle changes of the symmetrical compliant gripper.

To compute the working stroke amplification ratio of the suggested gripper, the instantaneous velocity centers O , O_1 , and O_2 , F of the links OB , OBA , $BCDE$, and

FGH , subsequently, as demonstrated in Figure 5. 6a. The instantaneous velocities are $v_A, v_B, v_C, v_D, v_E, v_F, v_G,$ and v_H of the points $A, B, C, D, E, F, G,$ and $H,$ correspondingly, which can be calculated as follows:

$$q = OA \quad (5. 1)$$

$$O_1A' = OA + OO_3 \quad (5. 2)$$

$$OO_3 = O_1O_3 \times \cot \alpha_0 \quad (5. 3)$$

Using the geometrical and motion diagrams in Figure 5. 6a, equation (5. 4) is computed.

$$O_1O_3 = OB \times \sin \alpha_0 + (OB \times \cos \alpha_0) \times \tan \alpha_0 \quad (5. 4)$$

$$O_2C = CD \times \tan \gamma \quad (5. 5)$$

$$O_2D = \frac{CD}{\cos \gamma} \quad (5. 6)$$

$$O_2E = O_2D + DE \quad (5. 7)$$

$$v_A = O_1A' \times \omega_1 = v_i \quad (5. 8)$$

$$v_B = OB' \times \omega_1 \quad (5. 9)$$

$$v_C = O_2C \times \omega_2 \quad (5. 10)$$

$$v_D = O_2D \times \omega_2 = (O_2O_4 + O_2D) \times \omega_1 = (OB \sin \alpha_0 + O_2D) \times \omega_1 \quad (5. 11)$$

$$v_E = O_2E \times \omega_2 = ED \times \omega_3 \quad (5. 12)$$

$$v_F = v_E \quad (5. 13)$$

$$v_G = v_H = GF \times \omega_4 = (HE + DE) \times \omega_3 \quad (5. 14)$$

$$\omega_2 = \left(\frac{OB \sin \alpha_0 + O_2D}{O_2D} \right) \omega_1 \quad (5. 15)$$

$$\omega_3 = \left(\frac{O_2E}{ED} \right) \omega_2 \quad (5.16)$$

$$\omega_4 = \left(\frac{HE + DE}{GF} \right) \omega_3 \quad (5.17)$$

$$\omega_4 = \left(\frac{HE + DE}{GF} \right) \times \left(\frac{O_2D}{ED} \right) \times \left(\frac{OB \sin \alpha_0 + O_2D}{O_2D} \right) \times \omega_1 \quad (5.18)$$

$$\frac{\omega_4}{\omega_1} = \left(\frac{HE + DE}{GF} \right) \times \left(\frac{O_2D}{ED} \right) \times \left(\frac{OB \sin \alpha_0 + O_2D}{O_2D} \right) \quad (5.19)$$

where, ω_1 , ω_2 , ω_3 , and ω_4 is the angular velocity of the links O_1A' , O_2C , ED , and GF , respectively

Assuming that a force produced by the PEA causes the gripper to move a little displacement x_{in} . OB , BC , and CD are aligned with the horizontal direction of the corresponding initial angles α_0 , γ_0 , and β_0 , as illustrated in Figure 5. 6b. The anticlockwise direction is chosen as the positive direction. The angle increments α_1 , β_1 , and γ_1 for entire moving linkages are given, as in Figure 5. 6b. The rotational angles ψ_o , ψ_A – ψ_H of the FHs O , A – H are achieved.

Assuming that the rotational angle of each joint was extremely small, the following equations were used to compute their dimensions:

$$\psi_O = \alpha_1 = B\hat{O}B' = \frac{BB'}{OB} = \frac{0.2798}{f} \quad (5.20)$$

$$\psi_A = \alpha_2 = \tan \alpha_2 = \frac{x_{in}}{AB} = A\hat{B}A' = \frac{0.279}{2.5} \quad (5.21)$$

$$\psi_B = \alpha_1 + \alpha_2 \quad (5.22)$$

$$\psi_C = \alpha_1 + \gamma_1 \quad (5.23)$$

$$\psi_D = \beta_1 + \gamma_1 = (90 - \beta_0 - \sin \beta_0) + \gamma_1 \quad (5.24)$$

$$\beta_1 = 90 - \beta_0 - \sin \beta_0 = D\hat{C}D' = \frac{DD'}{CD} = \frac{0.70074}{d} \quad (5.25)$$

$$\gamma_1 = \frac{OB \sin \alpha_1 + BC \sin \gamma_0}{BC} - \gamma_0 = C\hat{O}'C = C\hat{B}'C' = \frac{CC'}{BC} = \frac{0.36762}{e}$$

$$\Psi_E = \Psi_D = \Psi_F = \Psi_G = \Psi_H \quad (5.26)$$

where the values of BB' , CC' , and DD' were determined from the FEA.

An amplification ratio is connected to both the geometry and kinematics of a structure in mechanical design. Because of this, we were able to calculate the working amplification ratio of the suggested gripper as:

$$R_a = \frac{2d_o}{d_i} \approx 2 \frac{d_o/dt}{d_i/dt} = \frac{2v_o}{v_i} = \frac{GF \times w_4}{O_1A' \times w_1} \quad (5.27)$$

where d_o and d_i are the displacement of a jaw of the gripper and an input link, respectively.

$$O_1A' = OA + OO_3 = OA + [OB \sin \alpha_0 + (OB \cos \alpha_0) \tan \alpha_0] \cot \alpha_0 \quad (5.28)$$

$$R_a = \left(\frac{GF}{OA + [OB \sin \alpha_0 + OB \cos \alpha_0 \tan \alpha_0] \cot \alpha_0} \right) \times \left(\frac{HE + DE}{GF} \right) \times \left(\frac{O_2D}{ED} \right) \times \left(\frac{OB \sin \alpha_0 + O_2D}{O_2D} \right) \quad (5.29)$$

5.3.3.2. Stiffness analysis

The gripper's stiffness, constant grasping force, resonance frequency, and parasitic motion error were significant performance factors, in addition to the amplification ratio of the working travel. To achieve a large deflection, the flexure beam was combined with a series of middle rigid links. The compliant element was treated as an elastic spring with homogeneous and isotropic properties. A linear connection between strain and stress may be found using Hook's law as follows:

$$\sigma = \varepsilon \times E \quad (5.30)$$

where σ and ε are the stress and strain, respectively.

The Bernoulli-Euler law [16] is a useful tool for calculating the deflection and stress of a flexure beam. In Figure 5. 7, the flexure beam is depicted as a cantilever beam and subjected to a load, F_y , at its free end, serving as a model for analysis.

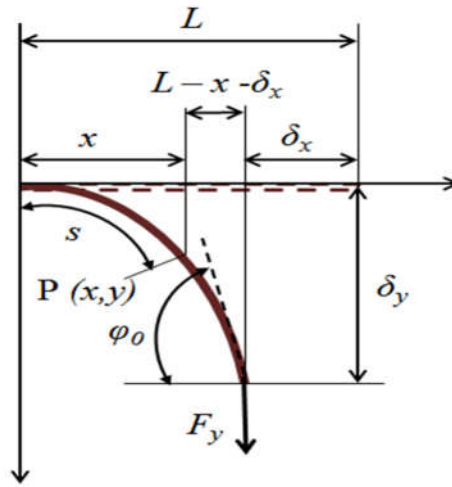


Figure 5. 7: Flexure beam with force at the free end.

On the basis of Bernoulli-theoretical Euler's beams, the relationship between bending moment and beam curvature is as follows:

$$M = EI \frac{d\phi}{ds} \quad (5. 31)$$

where M and $d\phi/ds$ represent the bending moments and the differentiation of deflection concerning the flexion of the beam at any point $P(x,y)$, respectively. The bending rigidity is EI .

Eq. (5. 31) was rewritten using a rectangular coordinate as:

$$M = \frac{EI}{\sqrt{[1 + (dy/dx)^2]^3}} \frac{d^2y}{dx^2} \quad (5. 32)$$

integrating Eq. (5. 32) yielded as:

$$M = EI \frac{dy/dx}{\sqrt{1 + (dy/dx)^2}} + C \quad (5. 33)$$

At the initial boundary condition, at the fixed end $x = 0$, the slope dy/dx is zero, and C will be zero. For a specific case, $dy/dx = \tan\phi$, Eq. (5. 33) is rearranged as:

$$M = EI \sin \varphi \quad (5.34)$$

If a FH achieved a small deflection, i.e. $\varphi \rightarrow 0$ and $\sin \varphi = \varphi$, the deflection angle was defined as:

$$M = EI \varphi \quad (5.35)$$

Assuming that the deflection was small, the $(dy/dx)^2$ was approximately zero, and $[1+(dy/dx)^2]^{3/2}$ was an equal one.

Hence, the equation of the classical beam-moment curvature was as:

$$M = E \frac{d^2 y}{dx^2} \quad (5.36)$$

The moment due to a force at the free end was determined as $M = F(L-x-\delta x)$. When $\delta x \rightarrow 0$ and the maximum deflection occurred when $x \rightarrow L$ and determined. In this structure, the greatest displacement corresponded to the lengthiest flexure beam, and it was assessed to be:

$$\delta_{\max} = \frac{FL^3}{3EI} \quad (5.37)$$

In addition, the stiffness of the flexure beam was measured as follows:

$$k_i = \frac{F}{\delta_i} = \frac{3EI_i}{L_i^3} = \frac{Ew_i t_i^3}{4L_i^3} \quad (5.38)$$

where, $i = AB, OB, CD, EF,$ and GH .

The peaked stress appeared in the beam OB , and its value may be calculated as follows:

$$\sigma_{\max} = \frac{M_{\max} \times t_{OB}}{L} = \frac{3 \times E \times \delta_{OB \max} \times t_{OB}}{2L_{OB}^2} = \frac{3 \times E \times F_i \times f \times t_{OB}}{2} \quad (5.39)$$

To ensure the gripper's safety, the stress value calculated using Eq. (5.39) must be less than the maximum stress the material can withstand. The formula is as follows.

$$\sigma_{\max} \leq \frac{\sigma_y}{n} \quad (5.40)$$

where σ_y represents the yield strength and n is the safety factor. In this investigation, $n = 1.5$ was selected to allow for substantial fatigue life.

5.3.3.3. Static analysis

When slider A is an operation with an input force F_i via PEA, the slider moves an input distance d_i . Regarding the left half of the gripper, the following external work is generated:

$$W = \frac{1}{2} F_i \times x_{in} \quad (5.41)$$

This work is subsequently converted into the elastic potential energies of flexure elements and the dissipation energy of the output force F_o . It was described as follows:

$$E = \sum_{i=A}^H \frac{1}{2} k_i \psi_i + \frac{1}{2} F_o d_o \quad (5.42)$$

The input energy equals to output energy; thus, the input force is recalculated according to the law of energy conservation, $W = E$, as follows:

$$F_i = \frac{1}{x_{in}} \sum_{i=A}^H k_i \psi_i + \frac{1}{2} R_a F_o \quad (5.43)$$

The grasping procedure for the micro-object of the gripper includes the following two phases:

In the initial phase, prior to the hand making touch with the micro-object, the output force is zero. Consequently, the input force is:

$$F_i = \frac{1}{x_{in}} \sum_{i=A}^H k_i \psi_i \quad (5.44)$$

Relationship between the input force and input displacement:

$$F_i = k_{in} x_{in} \quad (5.45)$$

The input stiffness of the gripper was restricted to the beam OB, which was calculated as follows:

$$k_{in} = \frac{1}{x_{in}^2} k_{OB} \psi_o \quad (5.46)$$

During the second phase, when an electric voltage is applied to the PEA, the gripper's output displacement is dependent on the input stiffness and preload for PEA, and can be calculated as follows:

$$\delta_a = \frac{k_{PEA} \Delta l_{nom} - F_{preload}}{k_{PEA} + k_{in}} \times \Delta \quad (5.47)$$

where k_{PEA} , Δl_{nom} , and $F_{preload}$ represent the piezoelectric actuator's stiffness, nominal output displacement, and preload force, correspondingly. Δ is a suitably adjusted deviation between the predicted value and the real one. Eq. (5.46) must be adjusted approximatively to reach a close-to-exact value. In this structure, the suggested value was 39.

Once the gripping hand contacts with the micro-object, the input or output displacement will cease to change. The output force in this scenario is referred to as the reaction force F_r , which is equal to F_o . As a result, the output displacement remains constant and can be computed using the following formula:

$$d_o = \frac{g_o - D_o}{2} \quad (5.48)$$

As follows, the grasping force may be calculated

$$F_g = \frac{2F_i}{R_a} - \frac{2}{g_o - D_o} \times \sum_{i=A}^H k_i \psi_i \quad (5.49)$$

For experimental purposes, a commercialized available PEA (Piezomechanik) with a maximum stroke of 55/40 μm was utilized. It possesses a stiffness $k_{PEA} = 12 \text{ N}/\mu\text{m}$, a length of 46 mm, a nominal output displacement $\Delta l_{nom} = 47.5 \mu\text{m}$, and a resonance frequency of 20 kHz. A maximum load of 800 N.

5.3.3.4. Dynamic analysis

By having a high resonance frequency, the gripper may accomplish a rapid reaction time. When evaluating the dynamic behavior of the gripper, the stiffness and lumped mass of PEA are also taken into account. Using the Lagrangian method, the dynamic equation of the gripper is as follows:

$$M_s \ddot{x}_{in} + K_s x_{in} = F \quad (5.50)$$

where x_{in} and \ddot{x}_{in} represents the input displacement and acceleration of the gripper, correspondingly. M_s and K_s denote the entire mass and stiffness of the gripper, subsequently. F indicates the total force applied on the gripper, which was computed as follows:

$$M_s = m_{in} + m_{OB} + m_1 + m_{CD} + m_2 + m_{EF} + m_3 + m_{GH} + m_{out} \quad (5.51)$$

$$K_s = k_{PEA} + k_{in} \quad (5.52)$$

The frequency of natural resonance was found as:

$$f_{re} = \frac{1}{2\pi} \sqrt{\frac{K_s}{M_s}} \quad (5.53)$$

where f_{re} is the natural resonance frequency of the gripper

5.4. Design optimization of the compliant gripper

5.4.1. Problem statement of optimization design

During the design and optimization process, if data from static and dynamic analysis (mathematical equations describing structural dynamics [145], [176]) are used, unexpected errors are likely to arise as compared to simulation and experiment validations [177]. Because it depends entirely on the experience and knowledge of the designer. Presently, with the development of computational science. Many algorithms have been developed to allow the establishment of virtual mathematical models that describe the relationship between design parameters and the output responses of the problem. ANFIS [178], GRA [152], and ANN [179] are among such tools. From these virtual mathematical models, soft-computing optimization techniques are applied. These techniques allow simpler design and optimization processes, more accurate results, and significantly reduced computation time.

Based on the knowledge presented in Chapter 3, an optimization procedure based

on the combination of ANFIS and Jaya is introduced below. In addition, a CG design and optimization for a mobile phone vibration motor assembly system is considered as a basic example to apply and verify the proposed algorithm.

Optimizing the geometric dimensions of FHs is crucial for improving the proposed CG's sensitivity. Meeting the following essential requirements is necessary for the CG to perform effectively in this system.

- a) A high first natural frequency allows for a large operating bandwidth and prevents resonance with the excitation frequency of actuators.
- b) A large working stroke to allow enough displacement of the jaw;
- c) Small resulting stress to achieve good strength criteria of the gripper.

All in all, these requirements conflicted with one another, leading to the question of how to find a balance. To enhance the gripper's displacement, speed, and stress, the design variables that were taken into consideration were its geometric dimensions.

5.4.1.1. Determination of design variables

The proposed design shown in Figure 5. 2 is influenced by several design parameters, including l_0 , l_i , l_1 , l_2 , l_3 , l_4 , t_1 , t_2 , t_3 , and t_4 , which have a direct impact on the design objective. Figure 5. 3a demonstrates that a conventional lever mechanism is used to achieve a large amplifier design for design. Changing the ratio between l_0 and l_i could lead to alterations in both the amplifier ratio and the structure's stability. To maintain consistency, the l_0 and l_i variables were regarded as design constants in this study. Instead of optimizing the ratio between l_0 and l_i , the study proposed a new CG design with two symmetrically arranged traditional levers to enhance working travel, as depicted in Figure 5. 3b.

In light of the reasons stated earlier, the optimization process selected eight design parameters, encompassing the lengths and thicknesses of FHs as the design variables. These variables were represented as a vector, denoted by $\mathbf{X} = [l_0, l_i, l_1, l_2, l_3, l_4, t_1, t_2, t_3, t_4]^T$. The lower and higher limits for the design variables were established based on the designer's prior experiences, which were as follows:

$$\left\{ \begin{array}{l} 10\text{mm} \leq l_1 \leq 14\text{mm} \\ 20\text{mm} \leq l_2 \leq 24\text{mm} \\ 11\text{mm} \leq l_3 \leq 15\text{mm} \\ 6\text{mm} \leq l_4 \leq 10\text{mm} \\ 0.5\text{mm} \leq t_1 \leq 0.7\text{mm} \\ 0.8\text{mm} \leq t_2 \leq 1.2\text{mm} \\ 0.4\text{mm} \leq t_3 \leq 0.8\text{mm} \\ 0.5\text{mm} \leq t_4 \leq 0.9\text{mm} \end{array} \right. , \quad (5.54)$$

5.4.1.2. Determination of objective functions

To meet the initial design goals, the CG needs to be able to accommodate objects of varying sizes and function effectively in high-speed conditions. Because of this, the optimization problem in this study utilized two objective functions: $f_1(\mathbf{X})$, which describes displacement, and $f_2(\mathbf{X})$, which describes the natural frequency of the CG. ANFIS was used to connect the input and output parameters, allowing for the creation of virtual objective functions for $f_1(\mathbf{X})$ and $f_2(\mathbf{X})$ [134], [180]. Jaya was then employed to optimize both $f_1(\mathbf{X})$ and $f_2(\mathbf{X})$ simultaneously. In conclusion, the optimization issue was explained as follows:

Find design variables $\mathbf{X} = [l_0, l_i, l_1, l_2, l_3, l_4, t_1, t_2, t_3, t_4]^T$.

The combined objective function:

$$f(\mathbf{X}) = -w_1 \times f_1(\mathbf{X}) - w_2 \times f_2(\mathbf{X}), \quad (5.55)$$

where w_1, w_2 are the normalized WFs of displacement and frequency, subsequently. Signal “-” in Eq. (5.55) indicates that the corresponding objective functions were maximized.

5.4.1.3. Determination of constraints

The CG was operating within the elastic limit of Al-7075 and was subject to the following constraints:

$$g(x) = \sigma \leq \frac{\sigma_y}{S}, \quad (5.56)$$

where σ_y denotes the material’s yield strength, and S indicates the safety factor, which is set at 1.5 to ensure the mechanism’s longevity.

5.4.2. Proposed optimization method for the compliant gripper

In this section, the integration of an ANFIS with the Jaya was used to implement the optimization problem. MATLAB R2015b was used to perform the programming. Figure 5. 8 illustrates a flowchart for optimizing process.

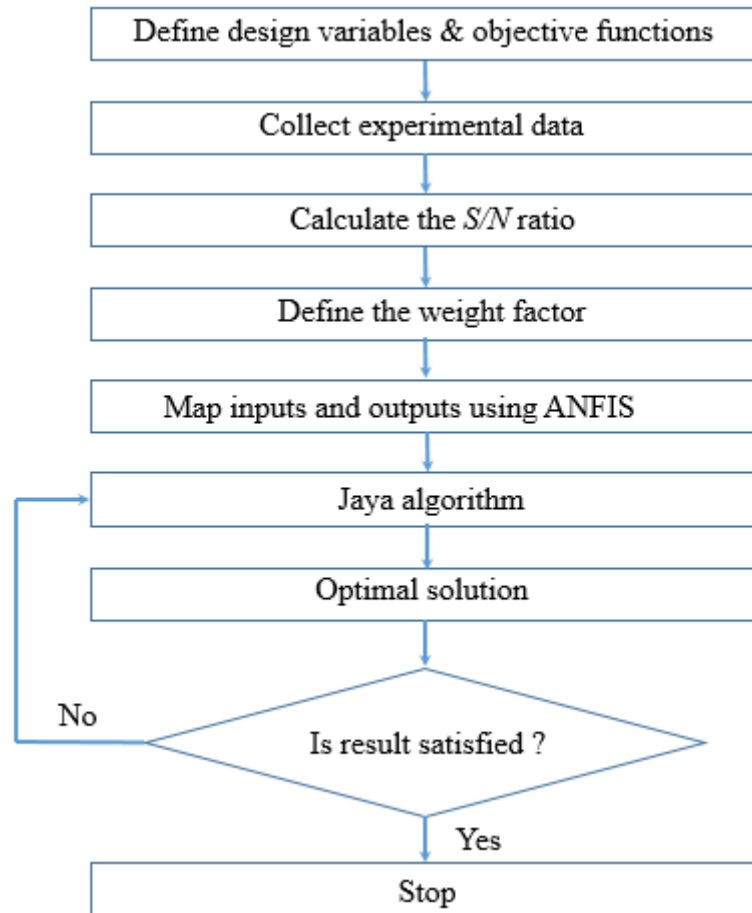


Figure 5. 8: Flowchart of multi-objective optimization by ANFIS-Jaya.

Phase 1: Collect the data

The data collected from the experiment would include both displacement and frequency measurements. To determine the number of experiments, an orthogonal array L_{27} from the TM was utilized.

Phase 2: Determine the weight factor

As previously mentioned, there was a conflict between the displacement, first natural frequency, and gripping effort, and each had a different level of importance. To address this, WF was assigned to each objective function. The calculation procedure followed by the following steps outlined in section 4.4.2.1 is applied to

obtain the precise weight value for each response.

Phase 3: Adaptive neuro-fuzzy inference system

In this phase, the eight design parameters, including the length and thickness of FHs, l_i and t_i with $i = 1,2,3,4$ contributed the largest impact on two quality characteristics, including displacement and frequency. Hence, the structure of ANFIS for the CG was developed according to the theory of ANFIS in section 3.2.2, Chapter 3.

Phase 4: Jaya algorithm

Rao introduced Jaya as a novel population-based optimization algorithm [148]. Unlike other heuristic algorithms, Jaya does not have any specific algorithmic control parameters, and it only requires two ordinary control parameters, namely the population size and the number of generations. This technique's optimization method is based on the premise that the solution selected for a particular issue must go toward the optimal solution and avoid the suboptimal option. According to the above premise, the fundamental Jaya algorithm consists of a single step, making it a straightforward optimization method.

Jaya imitates the survival tactics employed by biological species to thrive in their surroundings. To implement this optimizer, the randomly initial solutions are defined. Each of solution's design variables is then updated by the following formula.

$$U_{a+1,b,c} = U_{a,b,c} + \gamma_{a,b,1} \left(U_{a,b,best} - abs(U_{a,b,best}) \right) - \gamma_{a,b,2} \left(U_{a,b,worst} - abs(U_{a,b,worst}) \right), \quad (5.57)$$

where a , b , c note index of iteration, design variable, and candidate solution, respectively. U is b^{th} design variable of c^{th} candidate in a^{th} iteration. γ , a , b , 1 and γ , a , b , 2 are random numbers in $[0, 1]$. More details about the Jaya algorithm can be read in reference [148].

Due to its fast convergence rate in comparison to metaheuristic optimization algorithms, the Jaya is a more efficient method. As a result, in this thesis, Jaya was employed to optimize both the displacement and frequency of the CG. APPENDIX 2 illustrates the Jaya process.

5.4.3. Optimized results and validations

5.4.3.1. Optimized results

The eight design variables were separated into three levels, as displayed in Table 5. 1. An L_{27} orthogonal array was utilized to collect the experimental data, which is detailed in Table 5. 2.

Table 5. 1: Parameters and their upper and lower limits.

Factor	Symbol	Unit	Levels		
			1	2	3
l_1	A	mm	10	12	14
l_2	B	mm	20	22	24
l_3	C	mm	11	13	15
l_4	D	mm	6	8	10
t_1	E	mm	0.5	0.6	0.7
t_2	F	mm	0.8	1.0	1.2
t_3	G	mm	0.4	0.6	0.8
t_4	H	mm	0.5	0.7	0.9

Table 5. 2: The results of experiments on displacement and frequency.

No.	Displacement (μm)	Frequency (Hz)	No.	Displacement (μm)	Frequency (Hz)
1	2599.6	42.786	15	1147.2	40.659
2	2743.8	45.622	16	2147.2	43.659
3	1633.5	57.927	17	1002.8	49.186
4	1513.9	42.161	18	1220.6	49.322
5	2396.3	45.954	19	1232.6	57.942
6	1731.3	55.492	20	1167.4	57.233
7	3625.0	32.043	21	1401.1	48.485

No.	Displacement (μm)	Frequency (Hz)	No.	Displacement (μm)	Frequency (Hz)
8	2641.3	41.827	22	1201.8	56.782
9	1769.9	54.414	23	1119.6	59.709
10	1601.7	47.321	24	1076.8	36.497
11	1369.5	46.979	25	1029.6	28.044
12	1072.0	55.162	26	1148.0	52.343
13	1587.2	53.803	27	1444.8	48.129
14	1507.5	51.598			

The experimental data were then transferred to the S/N ratios using Eq.(3. 2), as shown in Table 5. 3. Next, the S/N ratios were normalized using Eq.(4. 40), as given in Table 5. 4. In this Table, the normalized S/N ratios for displacement (η_1) and frequency (η_2) were Z_1 and Z_2 , respectively. Using the Eqs. (4. 41) and (4. 42), the WF for the displacement and frequency were computed, as given in Table 5. 5 and Table 5. 6, respectively. The displacement WF had a value of approximately 0.5202, whereas the frequency WF was 0.4789. When the two WF values were added together, the sum equaled one. Normally, each response is assigned a WF of 0.5, this value was deemed inaccurate and could result in an improperly optimized solution. As a result, the dissertation presented a new method for determining precise WF values.

Table 5. 3: The values of S/N ratios.

No.	Displacement (dB)	Frequency (dB)	No.	Displacement (dB)	Frequency (dB)
1	68.29813	32.62603	15	61.19278	32.18313
2	68.76705	33.18349	16	66.63745	32.80148
3	64.26238	35.25762	17	60.02429	33.83683
4	63.60194	32.49822	18	61.73147	33.86081

No.	Displacement (dB)	Frequency (dB)	No.	Displacement (dB)	Frequency (dB)
5	67.59082	33.24647	19	61.81644	35.25987
6	64.76745	34.88461	20	61.34439	35.15293
7	71.18616	30.11466	21	62.92938	33.71215
8	68.43635	32.42913	22	61.59664	35.08421
9	64.95897	34.71421	23	60.98126	35.5208
10	64.09162	33.50108	24	60.64270	31.24514
11	62.73124	33.43808	25	60.25337	28.9568
12	60.6039	34.8328	26	61.19278	32.18313
13	64.01263	34.61613	27	66.63745	32.80148
14	63.56515	34.25266			

Table 5. 4: The normalized S/N ratios (z_i).

No.	Z_1 of η_1	Z_2 of η_2	No.	Z_1 of η_1	Z_2 of η_2
1	0.7413	0.5590	15	0.1047	0.4915
2	0.7833	0.6439	16	0.5925	0.5857
3	0.3797	0.9599	17	0.0000	0.7435
4	0.3205	0.5395	18	0.1529	0.7471
5	0.6779	0.6535	19	0.1606	0.9602
6	0.4249	0.9031	20	0.1183	0.9440
7	1.0000	0.1764	21	0.2603	0.7245
8	0.7536	0.5290	22	0.1409	0.9335
9	0.4421	0.8771	23	0.0857	1.0000
10	0.3644	0.6923	24	0.0554	0.3486
11	0.2425	0.6827	25	0.0205	0.0000

No.	Z_1 of η_1	Z_2 of η_2	No.	Z_1 of η_1	Z_2 of η_2
12	0.0519	0.8952	26	0.1052	0.8258
13	0.3573	0.8622	27	0.2842	0.7147
14	0.3172	0.8068			

Table 5. 5: WF of displacement response

Level	The average of the normalized signal-to-noise ratios for each level							
	A	B	C	D	E	F	G	H
Level 1	0.6137	0.3447	0.3257	0.3437	0.4109	0.2978	0.3579	0.3371
Level 2	0.2426	0.2761	0.2769	0.3009	0.3426	0.4588	0.3163	0.3158
Level 3	0.1368	0.3723	0.3905	0.3485	0.2396	0.2365	0.3189	0.3762
Range r_{ij}	0.4769	0.0963	0.1136	0.0476	0.1713	0.2223	0.0417	0.0604
$w_1 = 0.5202$								

Table 5. 6: WF of frequency response

Level	The average of the normalized signal-to-noise ratios for each level.							
	A	B	C	D	E	F	G	H
Level 1	0.6490	0.7846	0.7246	0.6515	0.5899	0.6865	0.5884	0.6539
Level 2	0.7230	0.7265	0.6563	0.7557	0.7588	0.6394	0.6504	0.7716
Level 3	0.7168	0.5777	0.7080	0.6816	0.7402	0.7630	0.8500	0.6447
Range r_{ij}	0.0739	0.2069	0.0683	0.1041	0.1689	0.1236	0.2616	0.1270
$w_2 = 0.4798$								

ANFIS can be thought of as a black box that maps multiple inputs and outputs. In this particular study, the relationship between the eight design variables with displacement and frequency was challenging to establish and use mathematical modeling because of the potential for inaccurate results. Therefore, ANFIS was deemed a suitable tool for the job. Table 5. 7 displays the automatically generated

parameters of ANFIS, which consisted of 2304 linear parameters and 48 nonlinear parameters. Due to the vast number of parameters, a regression approach would not have accurately defined them. In conclusion, ANFIS was determined to be the best approach for the proposed CG.

Table 5. 7: ANFIS parameters.

ANFIS parameters	
Number of nodes	555
Number of linear parameters	2304
Number of nonlinear parameters	48
Total number of parameters	2352
Number of training data pairs	27
Number of testing data pairs	15
Number of fuzzy rules	256

After determining the *WFs* and the cost functions, Jaya was employed to optimize the CG. Matlab was used to implement the optimal program. The parameters of Jaya were initialized as a population size of 30 and a tolerance of 10^{-6} . The optimal results were generated at the generation of 44. The optimal design results were produced. $x_{val} = [10.0 \ 20.6 \ 11.2 \ 6.0 \ 0.5 \ 0.8 \ 0.4 \ 0.9]$ determined the best design variables. The optimized solutions were corresponding to $l_1 = 10.0$ mm, $l_2 = 20.6$ mm, $l_3 = 11.2$ mm, $l_4 = 6.0$ mm, $t_1 = 0.5$ mm, $t_2 = 0.8$ mm, $t_3 = 0.4$ mm, $t_4 = 0.9$ mm.

In summary, the ideal displacement and frequency were found to be approximately 3260 μm and 61.9 Hz, respectively. To demonstrate that the proposed optimization algorithm had a faster convergence rate than other emerging methods, such as TLBO [181] and NGSA-II [182], a comparison was conducted (refer to Table 5. 8). The results indicated that the optimal solutions were similar, but the Jaya-ANFIS algorithm consumed significantly less time than the other optimization methods. Thus, the Jaya-ANFIS algorithm was demonstrated to be robust in this study. The optimal performance met the actual requirements, and as a result, the

optimization process was concluded.

Table 5. 8: Comparison of several optimization techniques.

Approach	Analysis time (sec)	Generation	Displacement (μm)	Frequency (Hz)
NGSA-II ANFIS	787.3	1000	3260	61.9
TLBO-ANFIS	660	500	3260	61.9
Jaya-ANFIS	30.0	44	3260	61.9

5.4.3.2. Validations

To verify the optimal performances of the proposed CG, both FEA and experimental tests were carried out. The optimal design parameters, including $l_1 = 10.0$ mm, $l_2 = 20.6$ mm, $l_3 = 11.2$ mm, $l_4 = 6.0$ mm, $t_1 = 0.5$ mm, $t_2 = 0.8$ mm, $t_3 = 0.4$ mm, $t_4 = 0.9$ mm, were utilized for 3D modeling and CG fabrication. To ensure that the analysis and experiment results accurately reflected real-world conditions, the deformation along the punch axis due to the F_I force was limited. Based on the design experience, the width of the CG was usually optimized to minimize volume, weight, and operating space. Typically, the width, also known as the out-of-thickness, of grippers was assigned within a range of 1 mm to 15 mm to prevent out-of-plane sagging [183]–[186]. To ensure proper working conditions, a CG with a width of 10 mm was selected to guarantee operational stability and high rigidity, effectively suppressing sagging along the punch axis. After the design process, the overall size of the gripper was determined to be 129 mm in length, 104 mm in width, and 10 mm in thickness.

The study utilized ANSYS 2016 to perform FEA, and a 3D model of CG was constructed in SOLIDWORKS, then imported into ANSYS for simulations. To ensure accurate analysis, it is important to consider the quality of the meshes used. To evaluate mesh quality, Skewness was used as a common measurement concept [187]–[189]. The study actively adjusted the mesh quality based on this standard, ensuring Skewness values were within the range of 0.25 to 0.5, indicating good cell quality. This ensured that the analysis process had converged to a desirable level.

Additionally, the accuracy was improved by refining the FHs.

Following the FEA analysis, an experimental process was carried out to confirm the findings. To experiment, it was necessary to construct a prototype of the gripper. For this study, the gripper prototype was produced using WEDM technology. This method is capable of creating a highly accurate gripper by utilizing wires with a diameter of $\text{Ø}20\ \mu\text{m}$. This allows for achieving a cutoff tolerance of $\pm 5\ \mu\text{m}$, which corresponds to a surface roughness of approximately $0.20\ \mu\text{mRa}$.

Experiments were conducted once the gripper prototype was manufactured, the block diagram of the measuring system was shown in Figure 5. 9, and the experiment was set up as shown in Figure 5. 10.

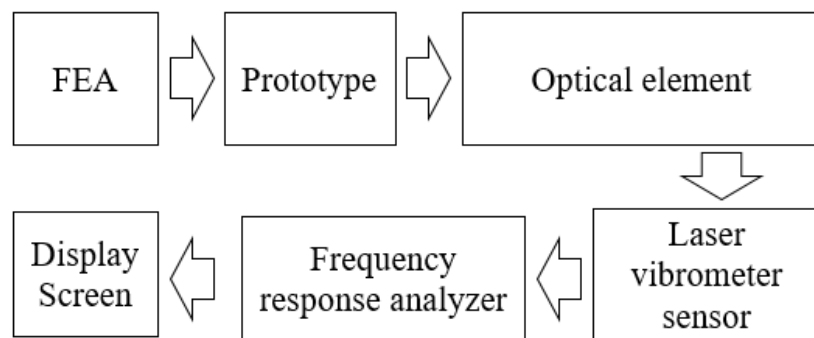


Figure 5. 9: Block diagram of the displacement and frequency measurement system.

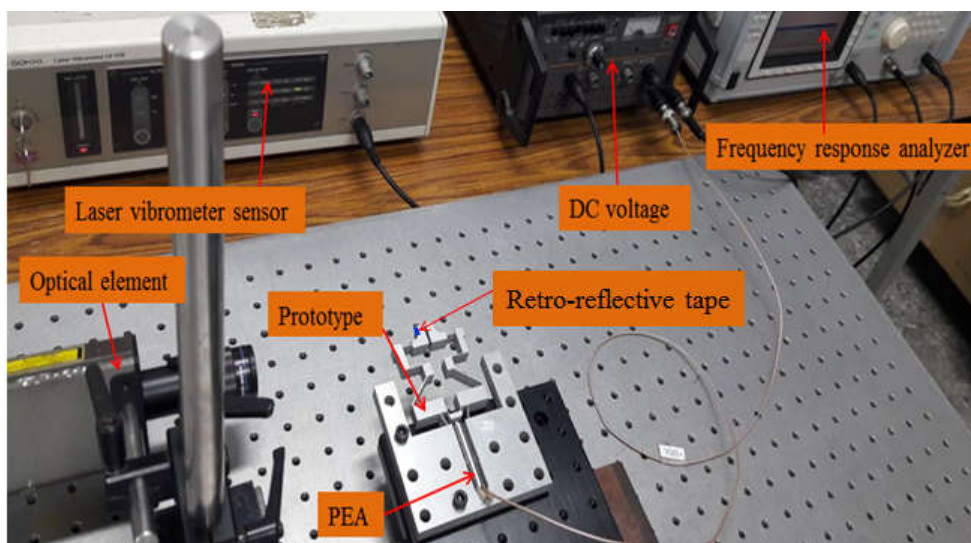


Figure 5. 10: Experiment setup for the prototype.

Figure 5. 10 shows the attachment of CG to the optical table without vibration. To measure the displacement, Retro-reflective tape was affixed to the surface of the left jaw. The PEA with a high-speed bipolar amplifier applied an input force to both the right and left jaws, causing them to move towards and away from each other. The optical element recorded the jaw's motion, which was then transmitted to the laser vibrometer sensor through a technical cable. The jaw's displacement signal was also transmitted to the frequency response analyzer using another engineering cable. The signals were encoded into displacement (μm) and frequency (Hz), and the results were displayed on a monitor. The experiments were performed five times, and the average values were recorded in Table 5. 9.

Table 5. 9: The optimum, FEA and experimental outcomes are compared.

Performances	Optimal results	FEA	Experiment	Errors between optimized and FEA results (%)	Errors between optimized and experimental results (%)
Displacement (μm)	3260	3097	3064	5.26	6.39
Frequency (Hz)	61.9	59.4	58.18	4.16	6.38

Comparative results in Table 5. 9 show that: regarding displacement, the results obtained from the proposed method (3260 μm) are larger than those obtained from experimental (3064 μm) and FEA analysis (3097 μm). The relative error between the obtained optimal results and the experimental results, and the FEA simulation results are 6.39%, and 5.26%, respectively. In terms of frequency, the result obtained from the proposed method is 61.9 Hz, it is larger than the result obtained from the experiment (58.18 Hz) and the simulation result of FEA (59.4 Hz) corresponding to a relative error of 6.38% and 4.16%, respectively. The difference between the best outcomes attained through FEA and the experimental outcomes varied between 4.16% and 6.39%. According to the experience of experts and the results of previous studies in the same field, this is a completely acceptable result [39], [174], [175]. These errors can be improved by improving the mesh quality. These errors can be

improved through improved meshing, manufacturing, and material quality. Consequently, the hybrid optimization algorithm suggested was sturdy and efficient in enhancing the compliant gripper.

In addition, it can also be seen that compared with previous studies, the proposed gripper exhibited superior work travel. However, the stress generated is still under the allowable yield strength. The gripping force of the left and right jaws is similar. These obtained results completely meet the requirements for the cellphone vibration motor assembly. The study's outcomes offer an efficient approach to achieving optimal design for the practical use of a compliant gripper. This facilitates the application of soft computing academic findings in the cell phone industry.

5.5. Summary

In this chapter, a new symmetrical CG has been developed, which was the potential for use in a cylindrical shaft of the DC motor assembly process. Besides, a soft computing-based approach was developed to model and optimize the proposed gripper that was expected to use in the assembly system was presented. In the design stage, to provide for a large working travel, an L-type stroke enlargement mechanism was created. The gripper's form was modeled by the square wave to give a simple construction and high rigidity. Then, the kinematic and dynamic models were analyzed via PRBM and the Lagrange method. Subsequently, multi-criteria optimization was carried out in order to maximize the displacement and the natural resonant frequency. To validate the analytical results, simulations and experiments were conducted.

In the optimization strategy, an intelligent computational technique was proposed to improve effectiveness and accuracy. This technique was a combination of ANFIS with the Jaya. The data was initially collected by the TM. Then, the S/N ratios were computed, and the WF of each cost function was defined by established equations. Subsequently, ANFIS was used to develop a parametric control diagram to establish the relationships between the design parameters and responses. Finally, the MOOP was solved using Jaya. The results of this chapter could be covered as follows:

- The developed CG had a displacement and a frequency are approximately 3260 μm and 61.9 Hz, correspondingly.
- The proposed hybrid optimization algorithm was also robust and effective for the CG as compared with other methods such as NGSA-II ANFIS, and TLBO-ANFIS.
- The error between the results obtained from the proposed optimization method in this dissertation, and the experimental and FEA analysis results were 5.26% and 6.39% for frequencies, correspondingly. 4.16% and 6.38% for displacement, respectively.

The research contents in Chapter 5 have been published by Ho and co-authors [12], [165] in the **Arabian Journal for Science and Engineering** (2018, SCIE – Q1) and **International Journal of Ambient Computing and Intelligence** (2021, SCOPUS)

Chapter 6 CONCLUSIONS AND FUTURE WORKS

In this chapter, the author provides a summary of the results found in this dissertation. In addition, ideas for the next research will be proposed.

6.1. Conclusions

In this dissertation, two types of compliant grippers were developed. One gripper has an asymmetrical structure and integrates displacement sensors, while the other has a symmetrical structure and is designed for assembly. Both are intended to grip small cylinders, such as those used in mobile phone vibration motors.

The first CG is analyzed and optimized in the first part of the study. Strain gauges are used to turn the flexible beams of the gripper into a displacement sensor with a resolution of micrometers. The statistics and dynamic equations of the gripper are developed using the pseudo-rigid-body-model approach and Lagrange's principle. SR is utilized to fill the empty spaces and increase the stiffness of the gripper, thereby improving its frequency. An HTLBO is used to optimize both the displacement and frequency, with the initial populations generated using the Taguchi method. The proposed HTLBO is faster than other optimization algorithms, and the results show a displacement of 1924.15 μm and a frequency of 170.45 Hz.

The second part of the study focuses on designing a CG with two symmetrical jaws for the assembly industry. The kinematic and dynamic models are analyzed using the pseudo-rigid-body model and the Lagrange method, with the displacement and natural resonant frequency of the gripper as the key targets. ANFIS combined with the Jaya algorithm is proposed to improve the output responses of the gripper. Data is collected using the Taguchi method, and the weight factor of each cost function is computed. The results show an optimal displacement of about 3260 μm and a frequency of 61.9 Hz.

Finally, experiments are conducted to evaluate the effectiveness of both compliant grippers, and the results are found to be consistent with the theoretical results.

6.2. Future works

The research process has still a few limitations, especially in the physical experiments. Therefore, in the future, the following points should be done to increase the reliability of the research results.

- (i) The prototype of the displacement sensor will be manufactured. Experimental organization and verification will be performed to evaluate the sensitivity and resolution of the proposed sensor.
- (ii) The proposed displacement sensor will be integrated into the asymmetrical gripper. The stroke of the gripper will be self-measured. The effectiveness of the sensor-integrated gripper will be verified through experimentation.
- (iii) Both the asymmetrical and symmetrical grippers will be manufactured, and they will be attached to a robot arm. Then, the physical assembly process of the DC motor in a cell phone will be conducted to verify the efficiency of the developed grippers.
- (iv) An extra controller will be carried out to examine the precision position and grasping of the jaws of developed grippers.

References

- [1] H. S. Gareth J. Monkman, Stefan Hesse, Ralf Steinmann, *Robot Grippers*. John Wiley & Sons: Weinheim, Germany, 2007.
- [2] “SP Elements– SP Automation & Robotics,” <https://sp-automation.co.uk/sp-elements/sp-elements-case-study/>, 2023.
- [3] “Grippers in Robotics – Types of Grippers used in industrial applications,” <https://learnmech.com/>, 2023.
- [4] “4 Types of robotic grippers and their Pros and Cons,” <https://metapress.com/4-types-of-robotic-grippers-and-their-pros-and-cons/>, 2023.
- [5] “Magnetic Robot End Effector,” <https://blog.robotiq.com/bid/65794/Magnetic-Robot-End-Effector-Top-5-Pros-and-Cons>, 2023.
- [6] K. Tai, A. R. El-Sayed, M. Shahriari, M. Biglarbegian, and S. Mahmud, “State of the art robotic grippers and applications,” *Robotics*, vol. 5, no. 2, 2016, doi: 10.3390/robotics5020011.
- [7] B. Zhang, Y. Xie, J. Zhou, K. Wang, and Z. Zhang, “State-of-the-art robotic grippers, grasping and control strategies, as well as their applications in agricultural robots: A review,” *Comput. Electron. Agric.*, vol. 177, no. August, p. 105694, 2020, doi: 10.1016/j.compag.2020.105694.
- [8] R. A. Romeo, M. Gesino, M. Maggiali, and L. Fiorio, “Combining sensors information to enhance pneumatic grippers performance,” *Sensors*, vol. 21, no. 15, 2021, doi: 10.3390/s21155020.
- [9] S. Noveanu, D. Lates, L. Fusaru, and C. Rusu, “A New Compliant Microgripper and Study for Flexure Hinges Shapes,” *Procedia Manuf.*, vol. 46, pp. 517–524, 2020, doi: <https://doi.org/10.1016/j.promfg.2020.03.074>.
- [10] H. Mehrabi, M. Hamedi, and I. Aminzahed, “A novel design and fabrication of a micro-gripper for manipulation of micro-scale parts actuated by a bending piezoelectric,” *Microsyst. Technol.*, vol. 6, 2019, doi: 10.1007/s00542-019-04696-6.
- [11] T.-P. D. & D.-A. W. Tien-Hoang Ngo, Hong-Van Tran, Thang-An Nguyen,

- “Design and kinetostatic modeling of a compliant gripper for grasp and autonomous release of objects,” *Adv. Robot.*, vol. 32, no. 14, 2018.
- [12] N. Le Chau, N. L. Ho, N. T. Tran, and T.-P. Dao, “Analytical Model and Computing Optimization of a Compliant Gripper for the Assembly System of Mini Direct-Current Motor,” *Int. J. Ambient Comput. Intell.*, vol. 12, no. 1, 2021.
- [13] “<https://www.precisionmicrodrives.com/eccentric-rotating-mass-vibration-motors-erms>,” 2022.
- [14] F. Chen, K. Sekiyama, P. Di, J. Huang, and T. Fukuda, “i-Hand: An Intelligent Robotic Hand for Fast and Accurate Assembly in Electronic Manufacturing,” *2012 IEEE Int. Conf. Robot. Autom.*, pp. 1976–1981, 2012.
- [15] R. H. Burns, “The Kinetostatic Synthesis of Flexible Link Mechanisms,” Yale University, 1964.
- [16] L. L. Howell, *Compliant Mechanisms*. John Wiley & Sons, Ltd, 2011.
- [17] N. Lobontiu, *Compliant mechanisms : design of flexure hinges*. CRC press, 2002.
- [18] L. Zentner and V. Böhm, “On the classification of compliant mechanisms,” *Proceedings of EUCOMES 2008 - The 2nd European Conference on Mechanism Science*. pp. 431–438, 2009. doi: 10.1007/978-1-4020-8915-2_52.
- [19] S. G. B. Pratheek Bagivalu Prasanna, Ashok Midha, “Classification of Compliant Mechanisms and Determination of the Degrees of Freedom Using the Concepts of Compliance Number and Pseudo-Rigid-Body Model,” 2019.
- [20] and Z. H. Heng Wu, Xianmin Zhang, Jinqiang Gan, Hai Li, “High-precision displacement measurement method for three degrees of freedom-compliant mechanisms based on computer micro-vision,” *Appl. Opt.*, vol. 55, no. 10, pp. 2594–2600, 2016.
- [21] J. S. N. Paine and C. F. Hinges, “Corner-Filletted Flexure Hinges,” vol. 123, no. September, pp. 346–352, 2001, doi: 10.1115/1.1372190.
- [22] W. L. Paros M.J., “How to design flexure hinges.pdf.” pp. 151–156, 1965.
- [23] S. T. Smith, V. G. Badami, J. S. Dale, and Y. Xu, “Elliptical flexure hinges,” vol. 68, no. October 1996, pp. 1474–1483, 1997.

- [24] N. Lobontiu and E. Garcia, “Stiffness characterization of corner-filletted flexure hinges,” vol. 75, no. 11, pp. 4896–4905, 2004, doi: 10.1063/1.1806999.
- [25] G. Chen, Y. Ma, and J. Li, “A tensural displacement amplifier employing elliptic-arc flexure hinges,” *Sensors Actuators, A Phys.*, vol. 247, no. October, pp. 307–315, 2016, doi: 10.1016/j.sna.2016.05.015.
- [26] J. Wu, Y. Zhang, S. Cai, and J. Cui, “Modeling and analysis of conical-shaped notch flexure hinges based on NURBS,” *Mech. Mach. Theory*, vol. 128, pp. 560–568, 2018, doi: 10.1016/j.mechmachtheory.2018.07.005.
- [27] L. Li, D. Zhang, S. Guo, and H. Qu, “Design, modeling, and analysis of hybrid flexure hinges,” *Mech. Mach. Theory*, vol. 131, pp. 300–316, 2019, doi: 10.1016/j.mechmachtheory.2018.10.005.
- [28] P. Xu, Y. Jingjun, Z. Guanghua, and B. Shusheng, “The Stiffness Model of Leaf-Type,” vol. 130, no. August 2008, pp. 1–6, 2016, doi: 10.1115/1.2936902.
- [29] P. M. Applicata, “A Design Method for Flexure-Based Compliant Mechanisms on the Basis of Stiffness and Stress Characteristics,” 2012.
- [30] S. Linß, S. Henning, and L. Zentner, “Modeling and Design of Flexure Hinge-Based Compliant Mechanisms,” *Kinemat. - Anal. Appl.*, 2019, doi: 10.5772/intechopen.85224.
- [31] S. Henning, S. Linß, and L. Zentner, “DetasFLEX - A computational design tool for the analysis of various notch flexure hinges based on non-linear modeling,” *Mech. Sci.*, vol. 9, no. 2, pp. 389–404, 2018, doi: 10.5194/ms-9-389-2018.
- [32] Y. Tian, B. Shirinzadeh, D. Zhang, and Y. Zhong, “Three flexure hinges for compliant mechanism designs based on dimensionless graph analysis,” *Precis. Eng.*, vol. 34, no. 1, pp. 92–100, 2010, doi: 10.1016/j.precisioneng.2009.03.004.
- [33] O. Gomis-Bellmunt and L. F. Campanile, “Actuator Principles and Classification,” *Des. Rules Actuators Act. Mech. Syst.*, pp. 3–28, 2010, doi: 10.1007/978-1-84882-614-4_1.
- [34] Piezomechanik GmbH, “Piezo data sheet,” 2021. [Online]. Available: www.piezomechanik.com

- [35] LINAK.COM, “Actuator LA12 - Data sheet,” 2022.
- [36] “Magnetostrictive actuators,” 2022. doi: 10.1115/1.1998-jun-3.
- [37] P. M. Dominik Scholtes, Stefan Seelecke, Gianluca Rizzello, “Design of a Compliant Industrial Gripper Driven by a Bistable Shape Memory Alloy Actuator,” 2020.
- [38] B. G. INC, “Short stroke pneumatic cylinder with non-rotative through hole rod and mounting stud - OFL,” 2022.
- [39] H. G. L. et al. Nhat Linh Ho, Thanh-Phong Dao, “A hybrid amplifying structure for a compliant micro-gripper,” in *Hội nghị Cơ học toàn quốc lần thứ X*, 2017, pp. 807–816.
- [40] X. Y. Hu, J. H. Jia, and S. T. Tu, “Displacement amplifier design for an extensometer in high temperature deformation monitoring,” *Procedia Eng.*, vol. 29, pp. 1872–1876, 2012, doi: 10.1016/j.proeng.2012.01.229.
- [41] Z. Lyu and Q. Xu, “Recent design and development of piezoelectric-actuated compliant microgrippers: A review,” *Sensors Actuators A Phys.*, vol. 331, p. 113002, 2021, doi: 10.1016/j.sna.2021.113002.
- [42] Q. XING and Y. GE, “Parametric study of a novel asymmetric micro-gripper mechanism,” *J. Adv. Mech. Des. Syst. Manuf.*, vol. 9, no. 5, pp. JAMDSM0075–JAMDSM0075, 2015, doi: 10.1299/jamdsm.2015jamdsm0075.
- [43] D. Zhang, Z. Zhang, Q. Gao, D. Xu, and S. Liu, “Development of a monolithic compliant SPCA-driven micro-gripper,” *Mechatronics*, vol. 25, pp. 37–43, 2015, doi: 10.1016/j.mechatronics.2014.11.006.
- [44] K. Lu, J. Zhang, W. Chen, J. Jiang, and W. Chen, “A monolithic microgripper with high efficiency and high accuracy for optical fiber assembly,” *Proc. 2014 9th IEEE Conf. Ind. Electron. Appl. ICIEA 2014*, pp. 1942–1947, 2014, doi: 10.1109/ICIEA.2014.6931486.
- [45] J. L. Ha, Y. S. Kung, S. C. Hu, and R. F. Fung, “Optimal design of a micro-positioning Scott-Russell mechanism by Taguchi method,” *Sensors Actuators, A Phys.*, vol. 125, no. 2, pp. 565–572, 2006, doi: 10.1016/j.sna.2005.06.025.
- [46] X. Sun *et al.*, “A novel flexure-based microgripper with double amplification

- mechanisms for micro / nano manipulation A novel flexure-based microgripper with double amplification mechanisms for micro / nano manipulation,” *Rev. Sci. Instrum.*, vol. 84, no. 8, pp. 1–11, 2013, doi: 10.1063/1.4817695.
- [47] Y. Liu and Q. Xu, “Mechanical design , analysis and testing of a large-range compliant microgripper,” pp. 119–126, 2016, doi: 10.5194/ms-7-119-2016.
- [48] Y. K. Yong, S. O. R. Moheimani, B. J. Kenton, and K. K. Leang, “Invited review article: High-speed flexure-guided nanopositioning: Mechanical design and control issues,” *Rev. Sci. Instrum.*, vol. 83, no. 12, 2012, doi: 10.1063/1.4765048.
- [49] Y. Zhao, X. Huang, Y. Liu, G. Wang, and K. Hong, “Design and control of a piezoelectric-driven microgripper perceiving displacement and gripping force,” *Micromachines*, vol. 11, no. 2, 2020, doi: 10.3390/mi11020121.
- [50] C. Shi, X. Dong, and Z. Yang, “A Microgripper with a Large Magnification Ratio and High Structural Stiffness Based on a Flexure-Enabled Mechanism,” *IEEE/ASME Trans. Mechatronics*, vol. 4435, no. c, 2021, doi: 10.1109/TMECH.2021.3052806.
- [51] X. Chen, Z. Deng, S. Hu, J. Gao, and X. Gao, “Designing a novel model of 2-DOF large displacement with a stepwise piezoelectric-actuated microgripper,” *Microsyst. Technol.*, vol. 26, no. 9, pp. 2809–2816, 2020, doi: 10.1007/s00542-020-04915-5.
- [52] T. K. Das, B. Shirinzadeh, M. Ghafarian, A. Al-Jodah, and J. Pinskiier, “Characterization of a compact piezoelectric actuated microgripper based on double-stair bridge-type mechanism,” *J. Micro-Bio Robot.*, vol. 16, no. 1, pp. 79–92, 2020, doi: 10.1007/s12213-020-00132-5.
- [53] F. Chen, Z. jiang Du, M. Yang, F. Gao, W. Dong, and D. Zhang, “Design and analysis of a three-dimensional bridge-type mechanism based on the stiffness distribution,” *Precis. Eng.*, vol. 51, pp. 48–58, 2018, doi: 10.1016/j.precisioneng.2017.07.010.
- [54] “Optical Displacement Sensor Node _ Senceive.pdf,” *Senceive Ltd*, 2023. <https://www.senceive.com/optical-displacement-sensor-node>
- [55] “Linear Position Sensors,” *AutomationDirect., Ltd*, 2023.

- [56] “Ultrasonic Displacement Sensors,” *KEYENCE CORPORATION*, 2023. <https://www.keyence.com/ss/products/measure/library/type/ultrasonic.jsp>
- [57] Z. Chen, Z. Li, X. Jiang, and X. Zhang, “Strain-based multimode integrating sensing for a bridge-type compliant amplifier,” *Measurement Science and Technology*, vol. 30, no. 10. 2019. doi: 10.1088/1361-6501/ab1984.
- [58] M. Ling, J. Cao, Q. Li, and J. Zhuang, “Design, Pseudostatic Model, and PVDF-Based Motion Sensing of a Piezo-Actuated XYZ Flexure Manipulator,” *IEEE/ASME Trans. Mechatronics*, vol. 23, no. 6, pp. 2837–2848, 2018.
- [59] N. L. Ho, M. P. Dang, and T.-P. Dao, “Design and analysis of a displacement sensor-integrated compliant microgripper based on parallel structure,” *Vietnam J. Mech.*, vol. 42, no. 4, pp. 363–374, 2020, doi: 10.15625/0866-7136/14874.
- [60] C. C. Tsao, Y. C. Tseng, Y. S. Chen, W. H. Chang, and L. T. Huo, “Precision Low-Cost Compact Micro-Displacement Sensors Based on a New Arrangement of Cascaded Levers with Flexural Joints,” *Sensors*, vol. 23, no. 1, 2023, doi: 10.3390/s23010326.
- [61] T.-P. Dao and S.-C. Huang, “Design and analysis of a compliant micro-positioning platform with embedded strain gauges and viscoelastic damper,” *Microsyst. Technol.*, vol. 23, no. 2, pp. 441–456, 2016, doi: 10.1007/s00542-016-3048-3.
- [62] A. N. Reddy, N. Maheshwari, D. K. Sahu, and G. K. Ananthasuresh, “Miniature compliant grippers with vision-based force sensing,” *IEEE Trans. Robot.*, vol. 26, no. 5, pp. 867–877, 2010, doi: 10.1109/TRO.2010.2056210.
- [63] C. Wenjie and L. Wei, “Design of a flexure-based gripper used in optical fiber handling,” in *IEEE Conference on Robotics, Automation and Mechatronics, 2004*, 2004, pp. 83–88.
- [64] A. M. L. L. Howell, “A Method for the Design of Compliant Mechanisms With Small-Length Flexural Pivots,” *J. Mech. Des.*, vol. 116, no. 1, pp. 280–290, 1994.
- [65] K. Lu and S. Kota, “Journal of Intelligent Material Systems and Structures Design of Compliant Mechanisms for Morphing,” *Journal of Intelligent Material Systems and Structures*, vol. 14, no. June. 2003.

- [66] M.-G. H. Yue-Qing Yu, Larry L. Howell, Craig Lusk, Ying Yue, “Dynamic Modeling of Compliant Mechanisms Based on the Pseudo-Rigid-Body Model,” *J. Mech. Des.*, vol. 127, no. 4, pp. 760–765, 2005.
- [67] S. Awtar and S. Sen, “A generalized constraint model for two-dimensional beam flexures: Nonlinear load-displacement formulation,” *J. Mech. Des. Trans. ASME*, vol. 132, no. 8, pp. 0810081–08100811, 2010, doi: 10.1115/1.4002005.
- [68] F. Ma and G. Chen, “Modeling large planar deflections of flexible beams in compliant mechanisms using chained beam-constraint-model,” *J. Mech. Robot.*, vol. 8, no. 2, 2016, doi: 10.1115/1.4031028.
- [69] C. J. K. Joep P. A. Nijssen, Giuseppe Radaelli, Just L. Herder, J. B. Ring, “Spatial Concept Synthesis of Compliant Mechanisms Utilizing Non-Linear Eigentwist Characterization,” 2018.
- [70] W. Z. Guimin Chen, Fulei Ma, Guangbo Hao, “Modeling Large Deflections of Initially Curved Beams in Compliant Mechanisms Using Chained Beam Constraint Model,” *J. Mech. Robot.*, vol. 11, no. 1, 2019.
- [71] C. N. Wang, F. C. Yang, V. T. T. Nguyen, Q. M. Nguyen, N. T. Huynh, and T. T. Huynh, “Optimal design for compliant mechanism flexure hinges: Bridge-type,” *Micromachines*, vol. 12, no. 11. 2021. doi: 10.3390/mi12111304.
- [72] J. Chen, R., Wang, W., Wu, K., Zheng, G., Xu, X., Wang, H., & Luo, “Design and optimization of a novel compliant planar parallelogram mechanism utilizing initially curved beams,” *Mech. Mach. Theory*, vol. 179, 2023.
- [73] B. Zhu *et al.*, “Design of compliant mechanisms using continuum topology optimization: A review,” *Mech. Mach. Theory*, vol. 143, p. 103622, 2020, doi: 10.1016/j.mechmachtheory.2019.103622.
- [74] D. Hujic, E. A. Croft, G. Zak, R. G. Fenton, J. K. Mills, and B. Benhabib, “The robotic interception of moving objects in industrial settings: Strategy development and experiment,” *IEEE/ASME Trans. Mechatronics*, vol. 3, no. 3, pp. 225–239, 1998, doi: 10.1109/3516.712119.
- [75] S. I. Cho, S. J. Chang, Y. Y. Kim, and K. J. An, “Development of a three-degrees-of-freedom robot for harvesting lettuce using machine vision and

- fuzzy logic control,” *Biosyst. Eng.*, vol. 82, no. 2, pp. 143–149, 2002, doi: 10.1006/bioe.2002.0061.
- [76] R. Molfino, R. P. Razzoli, and M. Zoppi, *A low-cost reconfigurable gripper for assembly and disassembly tasks in white industry*, vol. 8, no. PART 1. IFAC, 2006. doi: 10.3182/20060906-3-it-2910.00084.
- [77] G. Mantriota, “Theoretical model of the grasp with vacuum gripper,” *Mech. Mach. Theory*, vol. 42, no. 1, pp. 2–17, 2007, doi: 10.1016/j.mechmachtheory.2006.03.003.
- [78] A. H. Zahraee, J. K. Paik, J. Szewczyk, and G. Morel, “Toward the development of a hand-held surgical robot for laparoscopy,” *IEEE/ASME Trans. Mechatronics*, vol. 15, no. 6, pp. 853–861, 2010, doi: 10.1109/TMECH.2010.2055577.
- [79] F. Chen, K. Sekiyama, P. Di, J. Huang, and T. Fukuda, “i-Hand: An intelligent robotic hand for fast and accurate assembly in electronic manufacturing,” *2012 IEEE Int. Conf. Robot. Autom.*, pp. 1976–1981, 2012.
- [80] F. Cannella, F. Chen, C. Canali, A. Eytan, A. Bottero, and D. Caldwell, “Design of an Industrial Robotic Gripper for Precise Twisting and Positioning in High-Speed Assembly,” *Proc. 2013 IEEE/SICE Int. Symp. Syst. Integr.*, pp. 443–448, 2013.
- [81] G. Tortora, T. Ranzani, I. De Falco, P. Dario, and A. Menciassi, “A miniature robot for retraction tasks under vision assistance in Minimally Invasive Surgery,” *Robotics*, vol. 3, no. 1, pp. 70–82, 2014, doi: 10.3390/robotics3010070.
- [82] M. Zhu, Z. Wang, S. Hirai, and S. Kawamura, “Design and fabrication of a soft-bodied gripper with integrated curvature sensors,” *2017 24th Int. Conf. Mechatronics Mach. Vis. Pract. M2VIP 2017*, vol. 2017-Decem, pp. 1–6, 2017, doi: 10.1109/M2VIP.2017.8211521.
- [83] G. Rosati, S. Minto, and F. Oscari, “Robotics and Computer – Integrated Manufacturing Design and construction of a variable-aperture gripper for flexible automated assembly,” *Robot. Comput. Integr. Manuf.*, vol. 48, no. March, pp. 157–166, 2017, doi: 10.1016/j.rcim.2017.03.010.

- [84] K. Lee, Y. Wang, and C. Zheng, "TWISTER Hand: Underactuated Robotic Gripper Inspired by Origami Twisted Tower," *IEEE Transactions on Robotics*, vol. 36, no. 2, pp. 488–500, 2020. doi: 10.1109/TRO.2019.2956870.
- [85] B. Wen, "Automatic assembly with dual robotic arms based on mutual visual tracking and positioning," vol. 106, no. 2, pp. 1–24, 2023, doi: 10.1177/00368504231172667.
- [86] A. Qiu, C. Young, A. Gunderman, M. Azizkhani, Y. Chen, and A.-P. Hu, "Tendon-Driven Soft Robotic Gripper with Integrated Ripeness Sensing for Blackberry Harvesting," *arXiv Prepr.*, vol. 2302.03099, 2023.
- [87] W. H. Lee *et al.*, "Micropeg manipulation with a compliant microgripper," *Proc. - IEEE Int. Conf. Robot. Autom.*, vol. 3, pp. 3213–3218, 2003, doi: 10.1109/robot.2003.1242085.
- [88] R. K. Jain, S. Datta, S. Majumder, and A. Dutta, "Development of multi micro manipulation system using IPMC micro grippers," *J. Intell. Robot. Syst. Theory Appl.*, vol. 74, no. 3–4, pp. 547–569, 2014, doi: 10.1007/s10846-013-9874-y.
- [89] R. K. Jain, S. Saha, and S. Majumder, "Development of Piezoelectric Actuator Based Compliant Micro Gripper for Robotic Peg-in-hole Assembly," *2013 IEEE Int. Conf. Robot. Biomimetics*, no. December, pp. 1562–1567, 2013.
- [90] R. K. Jain, S. Majumder, B. Ghosh, and S. Saha, "Robotic micro assembly by compliant piezoelectric micro grippers in multi mobile micro manipulation system," *ACM Int. Conf. Proceeding Ser.*, vol. 02-04-July, 2015, doi: 10.1145/2783449.2783452.
- [91] J. Jiang, C. Bian, and Y. Ke, "A new method for automatic shaft-hole assembly of aircraft components," *Assem. Autom.*, vol. 37, no. 1, pp. 64–70, 2017, doi: 10.1108/AA-04-2016-032.
- [92] K. Nie, W. Wan, and K. Harada, "A Hand Combining Two Simple Grippers to Pick Up and Arrange Objects for Assembly," *IEEE Robot. Autom. Lett.*, vol. 4, no. 2, pp. 958–965, 2019, doi: 10.1109/LRA.2019.2893153.
- [93] J. Zhu and G. Hao, "Design and test of a compact compliant gripper using the Scott–Russell mechanism," *Arch. Civ. Mech. Eng.*, vol. 20, no. 3, 2020, doi: 10.1007/s43452-020-00085-3.

- [94] Y. Zhang and P. Yan, “A large range constant force microgripper with a three-stage compliant amplification mechanism,” *IEEE Access*, vol. 10, pp. 1–1, 2022, doi: 10.1109/access.2022.3179588.
- [95] J. Q. P. Yan, “Design and Analysis of a Compliant Micro-gripper with LBL Type Displacement Amplifier,” *2019 IEEE Int. Conf. Manip. Manuf. Meas. Nanoscale*, no. 04-08 August 2019, pp. 112–117, 2019.
- [96] D. Wang, J.-H. Chen, and H.-T. Pham, “A constant-force bistable micromechanism,” *Sensors Actuators A Phys.*, pp. 481–487, 2013, doi: <https://doi.org/10.1016/j.sna.2012.10.042>.
- [97] D. Thanh-phong and S. Huang, “Multi-objective Optimal Design of a 2-DOF Flexure-Based Mechanism Using Hybrid Approach of Grey-Taguchi Coupled Response Surface Methodology and Entropy Measurement,” 2016, doi: 10.1007/s13369-016-2242-z.
- [98] H. Van Tran, T. H. Ngo, N. D. K. Tran, T. N. Dang, T.-P. Dao, and D.-A. Wang, “A threshold accelerometer based on a tristable mechanism,” *Mechatronics*, vol. 53, pp. 39–55, 2018.
- [99] N. VL, N. VK, and P. HH, “Dynamics Study of Compliant Mechanism with Damping,” *J. Appl. Mech. Eng.*, vol. 9, no. 4, 2020.
- [100] V.-K. Nguyen, H.-T. Pham, H.-H. Pham, and Q.-K. Dang, “Optimization design of a compliant linear guide for high-precision feed drive mechanisms,” *Mech. Mach. Theory*, vol. 165, 2021.
- [101] N. Le Chau, N. T. Tran, and T.-P. Dao, “A hybrid computational method for optimization design of bistable compliant mechanism,” *Eng. Comput.*, vol. 38, no. 4, 2020.
- [102] N. D. Anh, L. T. Nhat, and T. V. P. Nhan, “Design and Control Automatic Chess-Playing Robot Arm,” *Recent Adv. Electr. Eng. Relat. Sci. Lect. Notes Electr. Eng.*, vol. 371, 2016, doi: https://doi.org/10.1007/978-3-319-27247-4_41.
- [103] C. A. My, “Inverse kinematics of a serial-parallel robot used in hot forging process,” *Vietnam J. Mech.*, vol. 38, no. 2, pp. 81–88, 2016.
- [104] N. T. Thinh, L. H. Thang, and T. T. Thanh, “Design strategies to improve self-

- feeding device - FeedBot for Parkinson patients,” 2017. doi: 10.1109/ICSSE.2017.8030825.
- [105] N. Hung and H. D. Loc, “Design and Implementation of Welding Mobile Robot Using a Proposed Control Scheme Based On Its Developed Dynamic Modeling for Tracking Desired Welding Trajectory,” in *International Journal of Advanced Engineering Research and Science*, 2017, vol. 4, no. 10. doi: 10.22161/ijaers.4.10.13.
- [106] N. P. T. Anh, S. Hoang, D. Van Tai, and B. L. C. Quoc, “Developing Robotic System for Harvesting Pineapples,” *International Conference on Advanced Mechatronic Systems, ICAMechS*, vol. 2020-Decem. pp. 39–44, 2020. doi: 10.1109/ICAMechS49982.2020.9310079.
- [107] V.-C. Pham, H.-G. Nguyen, T.-K. Doan, and G.-B. Huynh, “A Computer Vision Based Robotic Harvesting System for Lettuce,” *Int. J. Mech. Eng. Robot. Res.*, vol. 19, no. 11, 2020.
- [108] H. M. Dang, C. T. Vo, N. T. Trong, V. D. Nguyen, and V. B. Phung, “Design and development of the soft robotic gripper used for the food packaging system,” *Journal of Mechanical Engineering Research and Developments*, vol. 44, no. 3. pp. 334–345, 2021.
- [109] P. H. Le, T. P. Do, and D. B. Le, “A Soft Pneumatic Finger with Different Patterned Profile,” *International Journal of Mechanical Engineering and Robotics Research*, vol. 10, no. 10. pp. 577–582, 2021. doi: 10.18178/ijmerr.10.10.577-582.
- [110] Pho Van NGUYEN, P. N. NGUYEN, T. NGUYEN, and T. L. LE, “Hybrid robot hand for stably manipulating one group objects,” *Arch. Mech. Eng.*, vol. 6, no. 3, pp. 375–391, 2022.
- [111] T. Nguyen, S. Truong, and H. Hoang, “Proposing a Method to Solve Inverse Kinematics and Dynamics of a Human Upper Limb Rehabilitation Robot,” *Vietnam J. Comput. Sci.*, vol. 9, no. 4, pp. 455–473, 2022, doi: <https://doi.org/10.1142/S2196888822500233>.
- [112] T. Dao, S.-C. Huang, and N. Le Chau, “Robust parameter design for a compliant microgripper based on hybrid Taguchi-differential evolution

- algorithm,” *Microsyst. Technol.*, vol. 24, no. 3, pp. 1461–1477, 2017, doi: 10.1007/s00542-017-3534-2.
- [113] D. B. Lam, N. T. Khoa, N. D. Thuan, and P. H. Phuc, “Modeling and force analysis of an electrothermal micro gripper with amplification compliant mechanism,” *J. Sci. Technol.*, vol. 119, pp. 22–27, 2017, [Online]. Available: <https://jst.hust.edu.vn/journals/jst.119.khcn.2017.27.4.5>
- [114] D. C. Nguyen, T. V. Phan, and H. T. Pham, “Design and Analysis of a Compliant Gripper Integrated with Constant-Force and Static Balanced Mechanism for Micro Manipulation,” in *Proceedings 2018 4th International Conference on Green Technology and Sustainable Development, GTSD 2018*, 2018, pp. 291–295. doi: 10.1109/GTSD.2018.8595638.
- [115] D. N. Nguyen, N. L. Ho, T.-P. Dao, and N. Le Chau, “Multi-objective optimization design for a sand crab-inspired compliant microgripper,” *Microsyst. Technol.*, pp. 1–19, 2019, doi: <https://doi.org/10.1007/s00542-019-04331-4>.
- [116] T. V. T. Nguyen, N. T. Huynh, N. C. Vu, V. N. D. Kieu, and S. C. Huang, “Optimizing compliant gripper mechanism design by employing an effective bi-algorithm: fuzzy logic and ANFIS,” *Microsyst. Technol.*, vol. 27, no. 9, pp. 3389–3412, 2021, doi: 10.1007/s00542-020-05132-w.
- [117] T. T. N. & T.-P. D. Duc Nam Nguyen, Minh Phung Dang, “Intelligent computation modeling and analysis of a gripper for advanced manufacturing application,” *Int. J. Interact. Des. Manuf.*, 2022, doi: <https://doi.org/10.1007/s12008-022-00885-2>.
- [118] R. Davis and P. John, “Application of Taguchi-Based Design of Experiments for Industrial Chemical Processes,” *Stat. Approaches With Emphas. Des. Exp. Appl. to Chem. Process.*, 2018, doi: 10.5772/intechopen.69501.
- [119] R. K. Roy, “Design of experiments using the Taguchi approach : 16 steps to product and process improvement.” p. 538, 2001. doi: DOI: 10.1520/JTE12406J.
- [120] M. S. Said *et al.*, “Comparison between Taguchi Method and Response Surface Methodology (RSM) In Optimizing Machining Condition Department of

- Mechanical & Materials Engineering , Faculty of Engineering and Built Environment ,” *Int. Conf. Robust Qual. Eng.*, pp. 60–64, 2013.
- [121] S. Maghsoodloo and S. Engineering, “Strengths and Limitations of Taguchi ’ s Contributions to Quality , Manufacturing ,” *J. Manuf. Syst.*, vol. 23, no. 2, pp. 73–126, 2004.
- [122] R. Çakiroğlu and A. Acir, “Optimization of cutting parameters on drill bit temperature in drilling by Taguchi method,” *Meas. J. Int. Meas. Confed.*, vol. 46, no. 9, pp. 3525–3531, 2013, doi: 10.1016/j.measurement.2013.06.046.
- [123] C. Lan, “Computational Models for Design and Analysis of Compliant Mechanisms,” Georgia Institute of Technology, 2005.
- [124] Z. Feng, Y. Yu, and W. Wang, “Modeling of large-deflection links for compliant mechanisms,” *Front. Mech. Eng. China*, vol. 5, no. 3, pp. 294–301, 2010, doi: 10.1007/s11465-010-0019-8.
- [125] T. M. Pendleton and B. D. Jensen, “Compliant Wireform Mechanisms,” vol. 130, no. December 2008, pp. 5–10, 2017, doi: 10.1115/1.2991132.
- [126] M. B. Patil and B. B. Deshmukh, “Modelling and Analysis of Flexure based Compliant Microgripper,” no. March, pp. 1–9, 2016.
- [127] C. Lin and C. Shih, “Multiobjective design optimization of flexure micro-compliant mechanisms,” vol. 28, no. 6, pp. 999–1003, 2005, doi: 10.1080/02533839.2005.9671075.
- [128] O. S. Martin Philip Bendsoe, *Topology Optimization: Theory, Methods And Applic.* Springer; 2nd edition (October 4, 2013), 2003.
- [129] O. Kessler, “INTRODUCTION TO THE FINITE ELEMENT METHOD,” *Rev. Int. Stud.*, vol. 38, no. 1, pp. 187–189, 2012, doi: 10.1017/S0260210511000623.
- [130] J. J. Dicker, G. R. Pennock, and J. E. Shigley, *THEORY OF MACHINES AND MECHANISMS*, Third. New York: OXFORD UNIVERSITY PRESS, 2003.
- [131] W. Xu, J. Chen, H. Y. K. Lau, and H. Ren, “Data-driven methods towards learning the highly nonlinear inverse kinematics of tendon-driven surgical manipulators,” *Int. J. Med. Robot. Comput. Assist. Surg.*, vol. 13, no. 3, pp. 1–11, 2017, doi: 10.1002/rcs.1774.

- [132] D. Solomatine, L. M. See, and R. J. Abrahart, “Data-Driven Modelling: Concepts, Approaches and Experiences,” *Pract. Hydroinformatics*, pp. 17–30, 2008, doi: 10.1007/978-3-540-79881-1_2.
- [133] R. Amini and S. C. Ng, “Comparison of Artificial Neural Network, Fuzzy Logic and Adaptive Neuro-Fuzzy Inference System on Air Pollution Prediction,” *J. Eng. Technol. Adv.*, vol. 2, no. 1, pp. 14–22, 2017, doi: 10.35934/segi.v2i1.14.
- [134] J. R. Jang, “ANFIS : Adaptive-Ne twork-Based Fuzzy Inference System,” vol. 23, no. 3, 1993.
- [135] M. Turki, S. Bouzaida, A. Sakly, and F. M’Sahli, “Adaptive control of nonlinear system using neuro-fuzzy learning by PSO algorithm,” *Proc. Mediterr. Electrotech. Conf. - MELECON*, pp. 519–523, 2012, doi: 10.1109/MELCON.2012.6196486.
- [136] M. Bourdeau, X. qiang Zhai, E. Nefzaoui, X. Guo, and P. Chatellier, “Modeling and forecasting building energy consumption: A review of data-driven techniques,” *Sustain. Cities Soc.*, vol. 48, no. April, p. 101533, 2019, doi: 10.1016/j.scs.2019.101533.
- [137] Suraj, R. K. Sinha, and S. Ghosh, “Jaya Based ANFIS for Monitoring of Two Class Motor Imagery Task,” *IEEE Access*, vol. 4, no. April 2017, pp. 9273–9282, 2016, doi: 10.1109/ACCESS.2016.2637401.
- [138] W. Mendenhall, T. Sincich, and M. Danna, *A second course in statistics: regression analysis*. New York: Prentice Hall, 2003.
- [139] R. W. Emerson, “ANOVA and t-tests,” *J. Vis. Impair. Blind.*, vol. 111, no. 2, pp. 193–196, 2017, doi: 10.1177/0145482x1711100214.
- [140] D. Sharpe, “Your chi-square test is statistically significant: Now what?,” *Pract. Assessment, Res. Eval.*, vol. 20, no. 8, pp. 1–10, 2015.
- [141] S. Nikbakt, S. Kamarian, and M. Shakeri, “A review on optimization of composite structures Part I: Laminated composites,” *Compos. Struct.*, vol. 195, no. March, pp. 158–185, 2018, doi: 10.1016/j.compstruct.2018.03.063.
- [142] S. Nikbakt, S. Kamarian, and M. Shakeri, “A review on optimization of composite structures Part I: Laminated composites,” *Compos. Struct.*, vol. 195,

- no. March, pp. 158–185, 2018, doi: 10.1016/j.compstruct.2018.03.063.
- [143] A. Pajares, X. Blasco, J. M. Herrero, and G. Reynoso-meza, “Research Article A Multiobjective Genetic Algorithm for the Localization of Optimal and Nearly Optimal Solutions Which Are Potentially Useful : nevMOGA,” vol. 2018, 2018.
- [144] G. B. Mahanta, A. Rout, B. B. V. L. Deepak, and B. B. Biswal, “Application of meta-heuristic optimization techniques for design optimization of a robotic gripper,” *Int. J. Appl. Metaheuristic Comput.*, vol. 10, no. 3, pp. 107–133, 2019, doi: 10.4018/IJAMC.2019070106.
- [145] Z. Wu and Y. Li, “Optimal design and comparative analysis of a novel microgripper based on matrix method,” *2014 IEEE/ASME Conf. Intell. Mechatronics*, pp. 955–960, 2014, [Online]. Available: http://ieeexplore.ieee.org/xpls/abs_all.jsp?arnumber=6878203
- [146] I. J. Ramirez-Rosado and J. A. Dominguez-Navarro, “New multiobjective Tabu search algorithm for fuzzy optimal planning of power distribution systems,” *IEEE Trans. Power Syst.*, vol. 21, no. 1, pp. 224–233, 2006, doi: 10.1109/TPWRS.2005.860946.
- [147] R. V. Rao, *Teaching Learning Based Optimization Algorithm*. Springer International Publishing Switzerland, 2016. doi: 10.1007/978-3-319-22732-0.
- [148] R. Venkata Rao, “Jaya: A simple and new optimization algorithm for solving constrained and unconstrained optimization problems,” *Int. J. Ind. Eng. Comput.*, vol. 7, no. 1, pp. 19–34, 2016, doi: 10.5267/j.ijiec.2015.8.004.
- [149] N. T. Huynh and Q. M. Nguyen, “Application of Grey Relational Approach and Artificial Neural Network to Optimise Design Parameters of Bridge-Type Compliant Mechanism Flexure Hinge,” *Int. J. Automot. Mech. Eng.*, vol. 18, no. 1, pp. 8505 – 8522, 2021.
- [150] T.-P. Dao and S.-C. Huang, “Optimization of a two degrees of freedom compliant mechanism using Taguchi method-based grey relational analysis,” *Microsyst. Technol.*, 2017, doi: 10.1007/s00542-017-3292-1.
- [151] W. Ai and Q. Xu, “New Structural Design of a Compliant Gripper Based on the Scott-Russell Mechanism,” 2014, doi: 10.5772/59655.

- [152] N. Le Chau, N. L. Ho, T. T. Vinh Chung, S. C. Huang, and T. P. Dao, “Computing optimization of a parallel structure-based monolithic gripper for manipulation using weight method-based grey relational analysis,” *Int. J. Ambient Comput. Intell.*, vol. 12, no. 3, pp. 39–74, 2021, doi: 10.4018/IJACI.2021070103.
- [153] R. V. Rao and G. G. Waghmare, “Multi-objective design optimization of a plate-fin heat sink using a teaching-learning-based optimization algorithm,” *Appl. Therm. Eng.*, vol. 76, pp. 521–529, 2015, doi: 10.1016/j.applthermaleng.2014.11.052.
- [154] C. L. Liu, Y. S. Chiu, Y. H. Liu, Y. H. Ho, and S. S. Huang, “Optimization of a fuzzy-logic-control-based five-stage battery charger using a fuzzy-based taguchi method,” *Energies*, vol. 6, no. 7, pp. 3528–3547, 2013, doi: 10.3390/en6073528.
- [155] M. Phung, D. Hieu, G. Le, N. Le, C. Thanh, and P. Dao, *A multi - objective optimization design for a new linear compliant mechanism*, no. 0123456789. Springer US, 2019. doi: 10.1007/s11081-019-09469-8.
- [156] H. An, S. Chen, and H. Huang, “Multi-objective optimization of a composite stiffened panel for hybrid design of stiffener layout and laminate stacking sequence,” *Struct. Multidiscip. Optim.*, vol. 57, no. 4, pp. 1411–1426, 2018, doi: 10.1007/s00158-018-1918-2.
- [157] Z. Li and X. Zhang, “Multiobjective topology optimization of compliant microgripper with geometrically nonlinearity,” *Proc. Int. Conf. Integr. Commer. Micro Nanosyst. 2007*, vol. A, pp. 1–7, 2007, doi: 10.1115/MNC2007-21294.
- [158] Q. Lu, Z. Cui, and X. Chen, “Fuzzy multi-objective optimization for movement performance of deep-notch elliptical flexure hinges,” vol. 065005, pp. 1–9, 2015.
- [159] M. Meinhardt, M. Fink, and H. Tünschel, “Landslide susceptibility analysis in central Vietnam based on an incomplete landslide inventory: Comparison of a new method to calculate weighting factors by means of bivariate statistics,” *Geomorphology*, vol. 234, no. 2015, pp. 80–97, 2015, doi:

10.1016/j.geomorph.2014.12.042.

- [160] T.-P. Dao, Nhat Linh Ho, Hieu Giang Le, and Tan Thang Nguyen, “Analysis and optimization of a micro - displacement sensor for compliant microgripper,” *Microsyst. Technol.*, vol. 23, no. 12, pp. 5375–5395, 2017, doi: 10.1007/s00542-017-3378-9.
- [161] M. N. Mohd Zubir and B. Shirinzadeh, “Development of a high precision flexure-based microgripper,” *Precis. Eng.*, vol. 33, no. 4, pp. 362–370, 2009, doi: 10.1016/j.precisioneng.2008.10.003.
- [162] Q. Zhang, J. Zhao, Y. Peng, H. Pu, and Y. Yang, “A novel amplification ratio model of a decoupled XY precision positioning stage combined with elastic beam theory and Castigliano’s second theorem considering the exact loading force,” *Mech. Syst. Signal Process.*, vol. 136, p. 106473, 2020, doi: 10.1016/j.ymsp.2019.106473.
- [163] T. P. Dao *et al.*, “Analysis and optimization of a micro-displacement sensor for compliant microgripper,” *Microsyst. Technol.*, vol. 23, no. 12, pp. 5375–5395, 2017, doi: 10.1007/s00542-017-3378-9.
- [164] N. L. Ho, M. P. Dang, and T.-P. Dao, “Design and analysis of a displacement sensor-integrated compliant microgripper based on parallel structure,” *Vietnam J. Mech. Vietnam Acad. Sci. Technol.*, pp. 1–12, 2020, [Online]. Available: <http://dx.doi.org/10.1016/j.aquaculture.2013.03.019>
- [165] N. L. Ho, T. Dao, H. G. Le, and N. Le Chau, “Optimal Design of a Compliant Microgripper for Assemble System of Cell Phone Vibration Motor Using a Hybrid Approach of ANFIS and Jaya,” *Arab. J. Sci. Eng.*, vol. 44, no. 2, pp. 1205–1220, 2019, doi: <https://doi.org/10.1007/s13369-018-3445-2>.
- [166] J. Shigley and C. Mischke, *Shigley’s Mechanical Engineering Design*. 1989.
- [167] G. Wang, Y. Yan, J. Ma, and J. Cui, “Design, test and control of a compact piezoelectric scanner based on a compound compliant amplification mechanism,” *Mech. Mach. Theory*, vol. 139, pp. 460–475, 2019, doi: 10.1016/j.mechmachtheory.2019.05.009.
- [168] N. L. C. & S.-C. H. Nhat Linh Ho, Thanh-Phong Dao, “Multi-objective optimization design of a compliant microgripper based on hybrid teaching

- learning-based optimization algorithm,” *Microsyst. Technol.*, 2018.
- [169] W. Stadler, “A survey of multicriteria optimization or the vector maximum problem, part I: 1776-1960,” *J. Optim. Theory Appl.*, vol. 29, no. 1, pp. 1–52, 1979, doi: 10.1007/BF00932634.
- [170] D. C. Du, H. H. Vinh, V. D. Trung, N. T. Hong Quyen, and N. T. Trung, “Efficiency of Jaya algorithm for solving the optimization-based structural damage identification problem based on a hybrid objective function,” *Eng. Optim.*, vol. 50, no. 8, pp. 1233–1251, 2018, doi: 10.1080/0305215X.2017.1367392.
- [171] F. O. Castillo, L. Trujillo, and P. Melin, “Multiple Objective Genetic Algorithms for Path-planning Optimization in Autonomous Mobile Robots,” *Soft Comput.*, vol. 11, no. 3, pp. 269–279, 2007, doi: 10.1007/s00500-006-0068-4.
- [172] M. P. Aghababa, “Optimal design of fractional-order PID controller for five bar linkage robot using a new particle swarm optimization algorithm,” *Soft Comput.*, 2015, doi: 10.1007/s00500-015-1741-2.
- [173] N. L. C. Thanh-Phong Dao, Shyh-Chour Huang, “Robust parameter design for a compliant microgripper based on hybrid Taguchi-differential evolution algorithm,” *Microsyst. Technol.*, vol. 24, no. March 2018, pp. 1461–1477, 2017, doi: 10.1007/s00542-017-3534-2.
- [174] W. Ai and Q. Xu, “New Structural Design of a Compliant Gripper Based on the Scott-Russell Mechanism,” *Int. J. Adv. Robot. Syst.*, vol. 11, no. 12, pp. 1–10, 2014, doi: <https://doi.org/10.5772/59655>.
- [175] G. Hao and J. Zhu, “Design of a Monolithic Double-Slider Based Compliant Gripper with Large Displacement and Anti-Buckling Ability,” *Micromachines*, vol. 10, no. 10, 2019.
- [176] S. Zhang and G. Chen, “Design of Compliant Bistable Mechanism for Rear Trunk Lid of Cars,” *Int. Conf. Intell. Robot. Appl.*, vol. 7101, pp. 291–292, 2011.
- [177] S.-C. Huang and T.-P. Dao, “Design and computational optimization of a flexure-based XY positioning platform using FEA-based response surface

- methodology,” *Int. J. Precis. Eng. Manuf.*, vol. 17, no. 8, pp. 1035–1048, 2016, doi: 10.1007/s12541-016-0126-5.
- [178] T. V. T. Nguyen, N. T. Huynh, N. C. Vu, V. N. D. Kieu, and S. C. Huang, “Optimizing compliant gripper mechanism design by employing an effective bi-algorithm: fuzzy logic and ANFIS,” *Microsyst. Technol.*, vol. 27, no. 9, pp. 3389–3412, 2021, doi: 10.1007/s00542-020-05132-w.
- [179] N. Le Chau, T. P. Dao, and V. T. Tien Nguyen, “An efficient hybrid approach of finite element method, artificial neural network-based multiobjective genetic algorithm for computational optimization of a linear compliant mechanism of nanoindentation tester,” *Math. Probl. Eng.*, vol. 2018, 2018, doi: 10.1155/2018/7070868.
- [180] A. M. Zaki and A. M. Soliman, “High Performance Robotic Gripper Based on Choice of Feedback Variables,” pp. 54–59, 2010.
- [181] D. Yu, J. Hong, J. Zhang, and Q. Niu, “Multi-Objective Individualized-Instruction Teaching-Learning-Based Optimization Algorithm,” *Appl. Soft Comput. J.*, no. 28, pp. 1–73, doi: 10.1016/j.asoc.2017.08.056.
- [182] Y. Zhu, J. Liang, J. Chen, and Z. Ming, “PT US CR,” *Knowledge-Based Syst.*, doi: 10.1016/j.knosys.2016.10.030.
- [183] M. Helal, A. A. Alshennawy, and A. Alogla, “Optimal Design of a Positioning Flexible Hinge Compliant Micro-Gripper Mechanism with Parallel Movement Arms,” *Int. J. Eng. Res. Technol.*, vol. 10, no. 2, pp. 105–128, 2017.
- [184] N. L. Ho, T. Dao, S. Huang, and H. G. Le, “Design and Optimization for a Compliant Gripper with Force Regulation Mechanism,” vol. 10, no. 12, pp. 1969–1975, 2016.
- [185] Y. Jia, X. Zhang, and Q. Xu, “Design and Optimization of a Dual-Axis PZT Actuation Gripper,” in *2014 IEEE International Conference on Robotics and Biomimetics (ROBIO 2014)*, 2014, no. 1, pp. 321–325.
- [186] C. Liang *et al.*, “Design and control of a novel asymmetrical piezoelectric actuated microgripper for micromanipulation,” *Sensors Actuators, A Phys.*, vol. 269, pp. 227–237, 2018, doi: 10.1016/j.sna.2017.11.027.
- [187] I. ANSYS, “ANSYS Workbench,” vol. Release 16.

- [188] N. Le Chau, N. T. Tran, and T. P. Dao, “A multi-response optimal design of bistable compliant mechanism using efficient approach of desirability, fuzzy logic, ANFIS and LAPO algorithm,” *Appl. Soft Comput. J.*, vol. 94, p. 106486, 2020, doi: 10.1016/j.asoc.2020.106486.
- [189] D. N. Nguyen, N. L. Ho, T. P. Dao, and N. Le Chau, “Multi-objective optimization design for a sand crab-inspired compliant microgripper,” *Microsyst. Technol.*, vol. 25, no. 10, pp. 3991–4009, 2019, doi: 10.1007/s00542-019-04331-4.

LIST OF AUTHOR'S PUBLICATIONS

A. The research results are used in the dissertation

1. **Nhat Linh Ho**, Thanh-Phong Dao, Hieu Giang Le, Ngoc Le Chau (2019). “Optimal Design of a Compliant Microgripper for Assemble System of Cell Phone Vibration Motor Using a Hybrid Approach of ANFIS and Jaya”. *Arabian Journal for Science and Engineering*, 44, 1205–1220. <https://doi.org/10.1007/s13369-018-3445-2>. (SCIE - Q1).
2. **Nhat Linh Ho**, Thanh-Phong Dao, Ngoc Le Chau, Shyh-Chour Huang (2019). “Multi-objective optimization design of a compliant micro-gripper based on hybrid teaching learning-based optimization algorithm”, *Microsystem Technologies*, 25, 2067–2083. <https://doi.org/10.1007/s00542-018-4222-6> (SCIE - Q2).
3. Thanh-Phong Dao, **Nhat Linh Ho**, Tan Thang Nguyen, Hieu Giang Le, Pham Toan Thang, Huy-Tuan Pham, Hoang-Thinh Do, Minh-Duc Tran, Trung Thang Nguyen (2017). “Analysis and optimization of a micro - displacement sensor for compliant micro-gripper”, *Microsystem Technologies*, 23, 5375–5395. <https://doi.org/10.1007/s00542-017-3378-9> (SCIE - Q2).
4. Ngoc Le Chau, **Nhat Linh Ho**, Ngoc Thoai Tran, Thanh-Phong Dao (2021). “Analytical Model and Computing Optimization of a Compliant Gripper for the Assembly System of Mini Direct-Current Motor”. *International Journal of Ambient Computing and Intelligence*, 12(1), <https://doi.org/10.4018/IJACI.2021010101>. (SCOPUS - Q2)
5. **Nhat Linh Ho**, Minh Phung Dang, Thanh-Phong Dao (2020). “Design and analysis of a displacement sensor-integrated compliant micro-gripper based on parallel structure”, *Vietnam Journal of Mechanics*, 42 (4), 363–374. <https://doi.org/10.15625/0866-7136/14874> (ACI)
6. Ngoc Le Chau, **Nhat Linh Ho**, Tran The Vinh Chung, Shyh-Chour Huang, **Thanh-Phong Dao** (2021). “Computing Optimization of a Parallel Structure-Based Monolithic Gripper for Manipulation Using Weight Method Based Grey Relational Analysis”. *International Journal of Ambient Computing and*

Intelligence, 12(3), <https://doi.org/10.4018/IJACI.2021070103>. (**SCOPUS - Q2**)

7. **Nhat Linh Ho**, Minh Phung Dang, Ngoc Le Chau, Thanh-Phong Dao, Hieu Giang Le (2017). “A hybrid amplifying structure for a compliant micro-gripper”, The 10th National Conference on Mechanics, Ha Noi 12/2017, 42. (**National Conference**).

B. Other published

1. Duc Nam Nguyen, **Nhat Linh Ho**, **Thanh-Phong Dao**, Ngoc Le Chau (2019). “Multi-objective optimization design for a sand crab-inspired compliant microgripper”, *Microsystem Technologies*, 25, 3991–4009. <https://doi.org/10.1007/s00542-019-04331-4> (**SCI - Q2**)
2. **Nhat Linh Ho**, **Thanh-Phong Dao**, Shyh-Chour Huang, **Hieu Giang Le** (2016). “Design and Optimization for a Compliant Gripper with Force Regulation Mechanism, *International Journal of Mechanical*”, *International Journal of Mechanical, Industrial and Aerospace Sciences*, 10.0(12). <https://doi.org/10.5281/zenodo.1339720> (**International Journal**)
3. **Nhat Linh Ho**, Thanh Phong Dao, Hieu Giang Le (2017). “Analysis of sensitivity of a compliant micro-gripper”, *Journal of Technical Education Science*, 42, 53-61. (**UTE – HCMC, Domestic Journal**)

APPENDIX

APPENDIX 1 LIST OF DEVICES ARE USED IN THE THESIS.

No.	Equipment name	Model	Producer	Spec
1	Force gage	NF-9500	Lutron, Taiwan	Maximum 196, DC 9V Resolution: 0.05N
2	Sensor gauge			An excitation voltage of 2.5 V
3	CPU (computer processing unit)		ASUS	
4	DAQ (data acquisition)		National Instruments, Japan	
5	Monitor screen		ASUS	
6	A laser displacement sensor		Keyence, Japan	Resolution: 0.1 μ m
7	Piezoelectric actuator (PEA)	150/5/40 VS10	Piezomechanik GmbH	
8	A modal hammer	9722A2000- SN 2116555	Kistler	
9	An accelerator	4744892	Kistler	
10	A modal analyzer	NI USB 9162	National Instruments	
11	A high-speed bipolar amplifier	HAS 4011	NF Corporation	
12	Retro- reflective tape		Ono Sokki	

No.	Equipment name	Model	Producer	Spec
13	A laser vibrometer sensor	LV-170	Ono Sokki	Resolution: 0.1μm
14	A frequency response analyzer	FRA 5097	NF Corporation	
15	A sensor gauge	KFG 5-120-C1-11L1M2R	KYOWA, Japan	Gauge factor: 2.07 Resistance: 120.4ohms Excitation voltage: 2.5 V

APPENDIX 2 PROCEDURE OF THE JAYA ALGORITHM [184].

